

STATISTICAL MECHANICS OF SIMPLE COULOMB SYSTEMS

Marc BAUS

*Université Libre de Bruxelles, C.P. 231,
B-1050 Bruxelles, Belgium*

and

Jean-Pierre HANSEN

*Laboratoire de Physique Théorique des Liquides, Université Pierre et Marie Curie,
75230 Paris Cedex 05, France*



NORTH-HOLLAND PUBLISHING COMPANY – AMSTERDAM

STATISTICAL MECHANICS OF SIMPLE COULOMB SYSTEMS

Marc BAUS*

*Université Libre de Bruxelles**, C.P. 231, B-1050 Bruxelles, Belgium*

and

Jean-Pierre HANSEN

*Laboratoire de Physique Théorique des Liquides***, Université Pierre et Marie Curie,
75230 Paris Cedex 05, France*

Received March 1979

Contents:

1. Introduction	3	4.4. The hydrodynamic limit	43
1.1. Physical systems	4	4.5. Computer "experiments"	45
1.2. Some important parameters	4	4.6. Approximate theoretical results	52
2. The stability of Coulomb systems	7	5. An outlook on further Coulomb systems	61
2.1. Overview of basic results	7	5.1. Corrections to the classical OCP-model: contact with the real world	62
2.2. The stability of the OCP	9	5.2. The classical electron layer: a 2-D OCP	65
3. The static properties of the OCP	12	5.3. Binary ionic mixtures	69
3.1. Thermodynamics	12	5.4. An OCP with hard cores	76
3.2. Correlations and fluctuations	14	5.5. More complex ionic systems	80
3.3. Asymptotic behaviour	16	6. Conclusions and perspectives	85
3.4. "Exact" numerical results	19	Appendix 1: Fourier and Laplace transforms	86
3.5. Weak coupling theories	25	Appendix 2: The Debye–Hückel theory and the non- linear Poisson–Boltzmann equation	87
3.6. Intermediate coupling theories	27	Appendix 3: Chemical potential in the HNC approxima- tion	88
3.7. Strong coupling theories	30	References	89
4. The dynamic properties of the OCP	35		
4.1. Time-dependent equilibrium correlation functions	35		
4.2. Short-time behaviour	39		
4.3. The long-wavelength behaviour	41		

Single orders for this issue

PHYSICS REPORTS (Review Section of Physics Letters) 59, No. 1 (1980) 1–94.

Copies of this issue may be obtained at the price given below. All orders should be sent directly to the Publisher. Orders must be accompanied by check.

Single issue price Dfl. 39.00, postage included.

* Chercheur Qualifié du Fonds National Belge de la Recherche Scientifique.

** Association Euratom-Etat Belge.

*** Equipe Associée au C.N.R.S.

Abstract:

We critically review the rapidly growing number of studies devoted to classical fluids of charged particles. The main emphasis is on the simplest such fluid, the so-called one-component plasma (OCP). Both theoretical results and numerical experiments are considered. We also explicate the basic differences between charged and ordinary fluids and draw attention to those questions which in our opinion have not yet received a satisfactory answer.

1. Introduction

Since the classic work of Debye and Hückel on electrolyte solutions, the study of systems composed of charged particles has grown into a major area of Statistical Mechanics. In recent years, the main theoretical effort has shifted from the study of dilute, weakly coupled Coulomb systems (like low density plasmas or low-concentration electrolytes) to the investigation of strongly correlated ionic systems (like highly-compressed or turbulent plasmas and ionic melts); such systems are generally characterized by a ratio of potential (Coulomb) to kinetic (thermal) energy which is of the order of, or greater than one. Such a change in emphasis is reminiscent of a similar evolution in the field of uncharged fluids, where the main interest has shifted from the gas phase to the statistical mechanics of the liquid state. In fact, many of the theoretical techniques developed over the last two decades in the latter field [1.1, 1.2] can, and have been successfully applied to strongly coupled Coulomb systems.

The present review is devoted to the statistical mechanics of some simple models for classical ionic fluids. The simplest model of a Coulomb system is the so-called one-component plasma (OCP), a system of identical point ions, interacting exclusively through the Coulomb potential, and which are immersed in a rigid, uniform background of opposite charge to ensure overall charge neutrality. Although this model is an over-simplification, it serves as a prototype for more “realistic” systems and can in fact be considered as a limiting case of real matter under extreme conditions. The physical relevance of the model will be discussed in the following sections. Section 2 will deal with the important problem of the stability of Coulomb systems in general, and of the OCP in particular. Section 3 will be devoted to the static properties (thermodynamics and equal time correlation functions) of the OCP, while section 4 will be concerned with the dynamics (time-dependent properties) of the model. In section 5, it will be shown how the OCP model can be generalized to make contact with the real world, and some other simple models (charged hard spheres) will be briefly considered, mainly to illustrate how the theoretical concepts introduced for the OCP carry over rather naturally to more complex ionic systems.

To limit the size of the review, we shall only consider strongly coupled classical systems in or near thermodynamic equilibrium. This excludes the more classic field of traditional low density plasmas, quantum-mechanical systems like the low temperature electron gas (although reference to this fluid will sometimes be unavoidable), as well as the study of systems far from equilibrium, including such an active field as plasma turbulence. Most of the general background material can be found in references [1.1–1.4] and some of the topics covered by this review are more thoroughly exposed in ref. [1.5]. The list of references, although not pretending to be exhaustive, covers the field until January 1979.

1.1. Physical systems

In this subsection we list some of the most important ionic systems encountered in nature and their relationship to the simple models discussed in this review.

Most of astrophysics is concerned with ionized matter, usually under rather extreme physical conditions. The interior of stars, especially of white dwarfs, can usually be described in a first approximation as a one-component plasma of nuclei embedded in an almost uniform sea of electrons [1.5, 1.6].

The domain of plasma physics [1.4], with its recent evolution towards fusion problems [1.5], did in fact start from the study of the most simple plasma, the OCP, which consequently played an important role in the elaboration of most of the concepts used in this important field of physics.

The quantum-mechanical equivalent of the OCP is the electron gas (or “jellium”) which is a first approximation to the electron fluid in metals ignoring the details of the underlying ionic lattice which is “smeared out” to form a uniform positive background [1.7]. Note that the respective roles of ions (or nuclei) and electrons are inverted in going from the classical OCP to the electron gas of solid state physics. A related two component system is the electron-hole “liquid” in semiconductors.

Liquid metals which are fundamentally ionic liquids [1.1] are also describable, to lowest order, as an OCP in a polarizable background of degenerate electrons.

The two-dimensional equivalent of the OCP is an excellent first approximation for the description of electron layers bound to the surface of liquid dielectrics [1.8] and of inversion layers in semi-conductor physics.

The classical two-component systems which will be briefly examined in section 5 fall mostly into the realm of chemical physics; they include electrolytes [1.9], molten salts [1.10] and superionic conductors [1.11]. The corresponding basic theoretical model is that of charged hard spheres (the so-called “primitive model” of electrolytes).

Very recently, it has been argued that it should be possible experimentally to confine an unneutralized electron gas by a strong magnetic field which acts essentially like a neutralizing background [1.12]. If cooled sufficiently, this pure electron plasma will constitute the closest laboratory analogue of the strongly coupled (three-dimensional) OCP, so that further experimental work in this direction is highly desirable.

1.2. Some important parameters

Since we shall be mostly concerned with the simplest charged fluid, the OCP, we define in this subsection the basic parameters which characterize this model, and then go on to show under which limiting conditions this model yields a good description of real matter.

A convenient length scale for the OCP is the “ion-sphere” radius, a , defined by:

$$n = \left(\frac{4}{3}\pi a^3\right)^{-1} \quad (1.1)$$

where $n = N/\Omega$ is the number density, i.e., the number of point ions per unit volume; a is the radius of a sphere containing on the average one ion and is hence of the order of the mean interionic spacing.

A natural time scale is the inverse of the plasma frequency ω_p defined by:

$$\omega_p^2 = 4\pi(Ze)^2 n/m \quad (1.2)$$

where Ze is the ionic charge (e is the elementary proton charge) and m the ionic mass.

If $\beta = (k_B T)^{-1}$ is the inverse temperature in energy units, a widely used dimensionless coupling parameter is the ratio of the Landau length:

$$l = \beta(Ze)^2$$

over the ion sphere radius; this ratio is usually denoted by Γ :

$$\Gamma = l/a = \beta(Ze)^2/a. \quad (1.3)$$

Note that the Landau length is roughly equal to the classical distance of closest approach, while Γ is also the ratio of the Coulomb energy of a pair of ions separated by a , over the mean kinetic (thermal) energy $k_B T$. Hence the strong coupling regime corresponds to $\Gamma \gtrsim 1$, where the interaction energy dominates the kinetic energy of the ions, while in the weak coupling limit ($\Gamma \ll 1$) the latter dominates the former. This review is essentially devoted to strong coupling situations.

We now consider fully ionized matter made up of N ions of charge Ze and NZ electrons in a volume Ω and ask the question: under which conditions is the classical OCP a reasonable model to describe such a situation. The electron gas is characterized by the usual dimensionless length parameter:

$$r_s = \frac{a}{Z^{1/3}a_0} \quad (1.4)$$

where $a_0 = \hbar^2/m_e e^2$ is the electron Bohr radius, and $a/Z^{1/3}$ is the radius of a sphere containing on the average one electron.

Quantum effects are very different for the ions and the electrons because the mass ratio m/m_e is of the order of 2×10^3 or larger. If T is the temperature of the plasma, the degree of quanticity of the ionic component is characterized by the ratio of the thermal de Broglie wavelength Λ over the ion-sphere radius:

$$\frac{\Lambda}{a} = \frac{[h/(2\pi m k_B T)^{1/2}]}{a} = \left(\frac{2\pi\Gamma}{r_s} \cdot \frac{m_e}{m} \cdot \frac{1}{Z^{7/3}} \right)^{1/2}. \quad (1.5)$$

If $\Lambda/a \ll 1$ (a *high* temperature requirement!), the ions can essentially be treated classically. Quantum diffraction effects at short distances will only be negligible if $\Lambda/l \ll 1$ (a *low* temperature requirement!); these questions will be examined in section 5.

On the other hand, in many astrophysical situations, T will be less than the Fermi temperature

$$T_F = \frac{\hbar^2(3\pi^2 n Z)^{2/3}}{2k_B m_e} \quad (1.6)$$

of the electrons, so that the electron gas will be highly degenerate. The condition $T \ll T_F$ is equivalent to:

$$T \ll 10^6/r_s^2$$

which is easily satisfied, even for very high temperatures, if the density is sufficiently high, i.e. if $r_s \ll 1$. This highly degenerate electron gas can be considered as a *rigid* uniform background, if the Thomas–Fermi screening length

$$\lambda_{TF} = a \left(\frac{\pi}{12Z} \right)^{1/3} r_s^{-1/2} \quad (1.7)$$

is much larger than the ion-sphere radius a , i.e. for $r_s \ll 1$. Note that for $r_s \lesssim 10^{-2}$, the kinetic energy of an electron is of the order of its rest mass energy $m_e c^2$, so that the electrons behave then as a relativistic ideal Fermi gas. Finally the transverse electromagnetic interactions between ions will be negligible for non-relativistic thermal velocities

$$v_0^2 = (m\beta)^{-1} \ll c^2. \quad (1.8)$$

The neglect of nuclear interactions puts some further constraints on the ionic density and temperature.

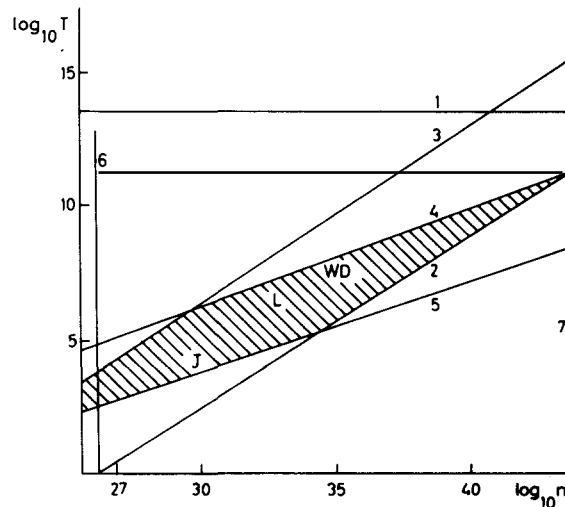


Fig. 1. Different domains in the temperature T (K)-number density $n(m^{-3})$ plane for the particular case of helium (after [4.15]). The straight lines correspond to: 1. The upper limit in temperature of the non-relativistic zone for the ions; 2. The lower limit in T of the classical zone for the ions; 3. The lower limit in T of the electrons; 4. The upper limit in T of the strong coupling zone ($\Gamma = 1$); 5. The lower limit in T of the fluid zone ($\Gamma = 155$); 6. The lower limit in density of the weak electronic screening zone; 7. The upper limit in density for the neglect of the nuclear core. The points corresponding to the interior of Jupiter (J), the white dwarfs (WD) and laser experiments (L) are also indicated.

Table 1
Strongly coupled OCP in some typical astrophysical situations. Z is the charge of the dominant nuclear species

	Jupiter (interior)	White dwarf	Neutron star crust
Z	1 (H)	6 (C)	26 (Fe)
ρ_m (g/cm ³)	10	10^8	10^{10}
n (nuclei/cm ³)	6×10^{24}	5×10^{30}	10^{32}
a (A)	0.34	0.36×10^{-2}	1.3×10^{-3}
r_s	0.65	0.4×10^{-2}	0.8×10^{-3}
T (K)	10^4	10^8	10^8
Γ	50	17	870
Λ/a	0.5	0.1	0.1
$k_B T_F$ (MeV)	10^{-4}	3	80
T/T_F	7×10^{-3}	3×10^{-3}	10^{-4}
λ_{TF}/a	0.8	5.6	7.6
ω_p (sec ⁻¹)	3×10^{15}	5×10^{18}	5×10^{19}

To summarize this discussion, we see that a plasma of point ions and electrons is well modeled by the OCP in the limit $r_s \rightarrow 0$ and $\Lambda/a \rightarrow 0$. The situation is most easily visualized in the T - n plane as shown in fig. 1. Table 1 lists some astrophysical situations where the limiting conditions on density and temperature are fairly well satisfied.

2. The stability of Coulomb systems

A basic and unavoidable pre-requisite for the use of statistical mechanics stems from the observation that although all experiments, be it in the laboratory or on a computer, are always performed on a finite-volume system, we nevertheless always assume that the system's bulk-properties will not depend on the applied boundary conditions. If this is so and as long as the experimental results are also claimed to be independent of the boundary conditions, e.g. the shape and size of the system, then it is also reasonable to consider all bulk-properties (pressure, ...) in the so-called thermodynamic limit where the number of particles N and the system's volume Ω tend to infinity at fixed number density $n = N/\Omega$. Only in this limit can one justify the use of many of the calculational techniques of statistical mechanics. For instance, in this limit the results of our calculations will no longer depend on the ensemble which was used to compute them nor will they depend on the size and shape of the system. It is interesting to observe here that for dipole-dipole interactions the existence of the thermodynamic limit has not yet been shown while precisely in this system many physical results appear to depend on the sample's shape.

2.1. Overview of basic results

During the last decade a number of studies have been devoted to the very question whether one could prove *mathematically* whether equilibrium statistical mechanics gives unique answers. Very soon it became clear that this was the case only if the potential energy satisfies two basic conditions. If we consider a simple fluid with only binary interactions described by the two-body potential $v(\mathbf{r})$ then v has to satisfy: 1) the condition of stability:

$$V_N = \frac{1}{2} \sum_{\substack{i,j=1 \\ i \neq j}}^N v(\mathbf{r}_i - \mathbf{r}_j) \geq -AN; \quad A \geq 0 \quad (2.1)$$

which states that the total potential energy V_N has to be bounded from below by an *extensive* lower bound, and 2) the condition of weak tempering:

$$v(\mathbf{r}) \leq B/|\mathbf{r}|^{3+\varepsilon} \quad \text{for } |\mathbf{r}| \geq R, \quad \varepsilon > 0, \quad B \geq 0 \quad (2.2)$$

which states that the potential cannot be too repulsive at large interparticle distances. In eqs. (2.1–2) A , B , R and ε are constants. More refined statements can be found in Ruelle's book [2.1]. For ordinary simple fluids interacting by short ranged forces, typically a hard-core or Lennard-Jones potential, these two conditions, eqs. (2.1–2), are satisfied. On this basis one can show: 1) the existence of the thermodynamic limit, 2) the equivalence of the various ensembles and 3) the consistency of the statistical mechanical and the thermodynamic results including the thermodynamic stability conditions and the possibility of phase transitions. On the contrary, for charged fluids interacting with Coulomb forces both conditions, eqs. (2.1–2), are violated! This is a rather uncomfortable position as the Coulomb potential is the basic potential as far as the atomic proper-

ties of matter are concerned. In fact two important properties of the Coulomb potential are showing up here. The violation of condition (2.1) by the Coulomb potential is related to the short-distance singularity of the Coulomb interaction between particles of opposite charges. Indeed, the condition (2.1) will clearly be violated if we consider the configuration in which the oppositely charged particles stay arbitrarily close together while the particles with like charge stay well separated, i.e. if the system behaves as composed of collapsing atoms. The fact that Coulomb systems do not collapse and hence that our real world exists, i.e. is stable in the sense of condition (2.1), although evident experimentally, is very difficult to show from first principles. In order to prove this Dyson and Lenard [2.2] have shown that one has to invoke quantum mechanics. One can say that the Heisenberg uncertainty principle prevents unlike charges from collapsing, but more surprisingly also the Pauli exclusion principle is necessary in order to prevent the like charges from collapsing. For the latter condition the fact that at least one of the charged species are fermions is crucial or more concretely, if electrons were bosons ionized helium would collapse! Moreover one also has to add the positive contribution coming from the total kinetic energy, because in this case only does the total energy have an extensive lower bound. Condition (2.1) has thus to be replaced by the so-called condition of H -stability: $H_N \geq -AN$, H_N being the total Hamiltonian of a system of N particles. For a detailed account and the original references concerning this fundamental problem of physics one should consult the review article by Lieb [2.3]. For the Coulomb system of our major concern here, the one-component plasma (OCP), the situation is much simpler as there is no possibility for atomic collapse and one can prove that the H -stability condition is in fact fulfilled *classically*. The proof of condition (2.1) for the classical OCP was given recently by Lieb and Narnhofer [2.4] following an idea due to Onsager [2.5]. The extension of this proof to the d -dimensional OCP was given by Sari and Merlini [2.6]. We cannot resist repeating this proof in some detail in subsection 2.2 because of its intrinsic beauty, being at the same time mathematically simple, physically transparent and nevertheless “exact”. It moreover turns out that the Lieb–Narnhofer lower bound to the potential energy is extremely accurate.

The violation of condition (2.2) by the Coulomb potential stems in turn from the long range of the Coulomb forces as they clearly correspond to eq. (2.2) with $\varepsilon = -2$ which is excluded by the restriction $\varepsilon > 0$. The distinction between short- and long-range potentials can be simply formulated by saying that a short-range potential is integrable at large distances, i.e. $\int_{r>R} dr v(r) < \infty$. The violation of this condition by the Coulomb potential, $v(r) = Z^2 e^2 / |r|$, is equivalent to the observation that its Fourier transform, $v(\mathbf{k}) = 4\pi Z^2 e^2 / k^2$, diverges for small wavenumbers k ; this observation will be the “leitmotiv” of many of the subsequent subsections. Here quantum mechanics is of no help and the violation of condition (2.2) also persists for the classical OCP. In fact the difficulty with (2.2) is worst for the OCP. Indeed, the condition (2.2) can be replaced by a weaker one (see [2.1]) on the mutual potential energy of separated groups of particles:

$$V_{N_1+N_2} - V_{N_1} - V_{N_2} \leq N_1 N_2 B' / R^{3+\varepsilon}; \quad \varepsilon > 0 \quad (2.3)$$

where $|\mathbf{r}_i - \mathbf{r}_j| \geq R$ for all pairs (i, j) while V_N is defined in eq. (2.1). The condition (2.3) is necessary for preventing the system from exploding. This explosion problem is clearly more stringent for the OCP where all particles are repelling each other. The way out of this difficulty clearly requires the introduction of some kind of screening mechanism at the *mechanical* level. This was done with a lot of ingenuity, by Lebowitz and Lieb [2.7] who proved the so-called “cheese theorem” stating that a Coulomb system can be built up with non-overlapping closely packed electrically neutral balls which no longer interact by virtue of Newton’s theorem. For the OCP a separate proof was however

necessary which was given by Lieb and Narnhofer [2.4]. As these proofs are rather technical we will not go into details but merely summarize the results of interest to us. One can show [2.4] for the classical OCP that: 1) notwithstanding all the difficulties just mentioned the free energy density and the energy density have a thermodynamic limit which is both continuous and uniform, 2) the micro-canonical and canonical ensemble averages are well behaved and equivalent, 3) the grand-canonical averages diverge if overall electroneutrality is imposed for each N , it gives finite results only if electroneutrality is imposed on the average, 4) the free energy is *not* a convex function of the density and hence both the pressure and the isothermal compressibility can become negative. A less rigorous but more physical approach to the latter property has been given recently by Baus [3.7] (see also subsection 3.3 below).

2.2. The stability of the OCP

We will now show *explicitly* that the energy per particle of the classical OCP has a thermodynamic limit which is bounded from below and hence that the system will not collapse (*H-stability*). Although this result is evident from the physical point of view its proof provides us with an interesting value of the lower bound to the energy of the OCP. The present proof is adapted from the appendix to Lieb and Narnhofer's paper [2.4] and from Choquard's review article [2.10]. Let us start from the Hamiltonian of a system of N point particles immersed into a uniform and inert neutralising background

$$H_N(\Omega) = \sum_{j=1}^N \frac{\mathbf{p}_j^2}{2m} + \frac{1}{2} \int_{\Omega} d\mathbf{r} \int_{\Omega} d\mathbf{r}' \frac{1}{|\mathbf{r} - \mathbf{r}'|} \left[\rho(\mathbf{r})\rho(\mathbf{r}') - Z^2 e^2 \delta(\mathbf{r} - \mathbf{r}') \sum_{j=1}^N \delta(\mathbf{r} - \mathbf{r}_j) \right]$$

where m is the mass and Ze the charge of the mobile particles having at the instant $t = 0$ positions \mathbf{r}_j and momenta \mathbf{p}_j ($j = 1, \dots, N$), the system being completely enclosed in a spatial region of volume Ω . Moreover, $\rho(\mathbf{r})$ represents the *total* charge density:

$$\rho(\mathbf{r}) = \sum_{j=1}^N Ze\delta(\mathbf{r} - \mathbf{r}_j) - Zen \quad (2.4)$$

n being the background density which, because of the overall electroneutrality requirement, has to be fixed at $n = N/\Omega$. As we are interested in a lower bound to H_N we can omit the kinetic term which is always positive and fix our attention to the potential energy term V_N , i.e. the electrostatic energy of the *total* charge distribution of eq. (2.4) *minus* its self-energy. We can rewrite V_N as:

$$\begin{aligned} V_N(\Omega) &= \frac{1}{2} \sum_{\substack{i,j=1 \\ i \neq j}}^N \frac{Z^2 e^2}{|\mathbf{r}_i - \mathbf{r}_j|} - \sum_{j=1}^N n \int_{\Omega} d\mathbf{r} \frac{Z^2 e^2}{|\mathbf{r} - \mathbf{r}_j|} + \frac{n^2}{2} \int_{\Omega} d\mathbf{r} \int_{\Omega} d\mathbf{r}' \frac{Z^2 e^2}{|\mathbf{r} - \mathbf{r}'|} \\ &\equiv \sum_{i < j} V_{ij} - \sum_j V_j + V_0 \end{aligned} \quad (2.5)$$

which differs from eq. (2.1) by background contributions. To proceed we consider, following hereby an idea which goes back to Onsager [2.5], a different system consisting of N balls centered at the positions of the original point particles but having each a charge Ze smeared out over the interior of the ball. The *total* electrostatic energy of this ball-system can be written:

$$V'_N(\Omega) = \frac{1}{2} \int_{\Omega} d\mathbf{r} \int_{\Omega} d\mathbf{r}' \frac{\rho'(\mathbf{r})\rho'(\mathbf{r}')}{|\mathbf{r} - \mathbf{r}'|} \equiv \frac{1}{2} \sum_{i,j} V'_{ij} \quad (2.6)$$

where $\rho'(\mathbf{r}) = (Ze/\Omega') \sum_{j=1}^N \theta(\mathbf{r} - \mathbf{r}_j)$, $\theta(\mathbf{r} - \mathbf{r}_j)$ being the characteristic function of the ball centered at \mathbf{r}_j , i.e. $\theta(\mathbf{r} - \mathbf{r}_j)$ equals one when \mathbf{r} belongs to the ball centered at \mathbf{r}_j and zero otherwise, whereas Ω' is the volume of each ball. Similarly, the electrostatic energy of the interaction between the balls and the background can be written:

$$V''_{\Omega}(\Omega) = -Zen \int_{\Omega} d\mathbf{r} \int_{\Omega} d\mathbf{r}' \frac{\rho'(\mathbf{r})}{|\mathbf{r} - \mathbf{r}'|} \equiv -\sum_j V''_j. \quad (2.7)$$

Adding and subtracting $V'_N + V''_{\Omega}$ to V_N and re-arranging terms we obtain:

$$V_N(\Omega) = \frac{1}{2} \int_{\Omega} d\mathbf{r} \int_{\Omega} d\mathbf{r}' \frac{(\rho'(\mathbf{r}) - Zen)(\rho'(\mathbf{r}') - Zen)}{|\mathbf{r} - \mathbf{r}'|} + \sum_{i < j} (V_{ij} - V'_{ij}) - \frac{1}{2} \sum_j V'_{jj} - \sum_j (V_j - V''_j). \quad (2.8)$$

Let us analyse now each term of eq. (2.8) separately. The first term in the r.h.s. of eq. (2.8) is the *total* electrostatic energy of the ball plus background system. This term can also be written as the volume integral (over a sufficiently large volume so that surface contributions can be neglected) of the energy density of the electric field produced by this system and is thus positive. For the next term we consider $V_{ij} - V'_{ij}$ which we can write as:

$$V_{ij} - V'_{ij} = \frac{Z^2 e^2}{\Omega'^2} \int_{\Omega'} d\mathbf{r} \int_{\Omega'} d\mathbf{r}' \left[\frac{1}{|\mathbf{r}_i - \mathbf{r}_j|} - \frac{1}{|\mathbf{r} - \mathbf{r}' + \mathbf{r}_i - \mathbf{r}_j|} \right]. \quad (2.9)$$

If for simplicity we take spherical balls, i.e. $\Omega' = \frac{4}{3}\pi R^3$, then because of the rotational invariance of the domain the r.h.s. of eq. (2.9) cannot depend on the orientation of $\mathbf{r}_i - \mathbf{r}_j$ and we can as well integrate this angular dependence out by operating with $\int d(\hat{\mathbf{r}}_i - \hat{\mathbf{r}}_j)/4\pi$ on eq. (2.9) leaving us with:

$$V_{ij} - V'_{ij} = \frac{Z^2 e^2}{\Omega'^2} \int_{\Omega'} d\mathbf{r} \int_{\Omega'} d\mathbf{r}' \left[\frac{1}{|\mathbf{r}_i - \mathbf{r}_j|} - \frac{1}{\max(|\mathbf{r} - \mathbf{r}'|, |\mathbf{r}_i - \mathbf{r}_j|)} \right] \geq 0. \quad (2.10)$$

Notice that the equality sign holds only when $|\mathbf{r}_i - \mathbf{r}_j| \geq |\mathbf{r} - \mathbf{r}'|$ which is always achieved when $|\mathbf{r}_i - \mathbf{r}_j| \geq 2R$ in which case eq. (2.10) states that the charge of non-overlapping spheres can be put at their centre (Newton's theorem). To obtain the r.h.s. of eq. (2.10) we have used the following elementary result which will be used repeatedly below ($d\hat{\mathbf{r}}$ denotes the angular part of $d\mathbf{r}$):

$$\int \frac{d\hat{\mathbf{r}}}{4\pi} \frac{1}{|\mathbf{r} - \mathbf{a}|} = \frac{r + a - |\mathbf{r} - \mathbf{a}|}{2\bar{a}r} \equiv \frac{1}{\max(a, r)}. \quad (2.11)$$

As we are interested here only in a lower bound to V_N we can drop the positive terms from eq. (2.8) and write:

$$V_N(\Omega) \geq - \sum_j (V_j - V''_j + \frac{1}{2} V'_{jj}). \quad (2.12)$$

From eqs. (2.6) and (2.11) we have for the self-energy of a ball:

$$\begin{aligned} V'_{jj} &= \frac{Z^2 e^2}{\Omega'^2} \int_{\Omega'} d\mathbf{r} \int_{\Omega'} d\mathbf{r}' \frac{1}{|\mathbf{r} - \mathbf{r}'|} = \frac{Z^2 e^2}{\Omega'^2} \int_{\Omega'} d\mathbf{r} \int_0^R d\mathbf{r}' r'^2 \frac{4\pi}{\max(r, r')} = \frac{Z^2 e^2}{\Omega'^2} \int_{\Omega'} d\mathbf{r} 4\pi \left(\frac{R^2}{2} - \frac{r^2}{6} \right) \\ &= \frac{6}{5} \frac{Z^2 e^2}{R}. \end{aligned} \quad (2.13)$$

From eqs. (2.5) and (2.7) we have for $V_j - V''_j$:

$$V_j - V''_j = Z^2 e^2 n \int_{\Omega'} d\mathbf{r} \left[\frac{1}{|\mathbf{r} - \mathbf{r}_j|} - \frac{1}{\Omega'} \int_{\Omega'} d\mathbf{r}' \frac{1}{|\mathbf{r} - \mathbf{r}' - \mathbf{r}_j|} \right]. \quad (2.14)$$

Using eq. (2.11) we see that the integrand of eq. (2.14) vanishes unless $|\mathbf{r} - \mathbf{r}_j| < r'$. Putting $\mathbf{y} = \mathbf{r} - \mathbf{r}_j$ we obtain thus for (2.14):

$$\begin{aligned} V_j - V''_j &= Z^2 e^2 n \int_{\Omega'} d\mathbf{y} \left[\frac{1}{|\mathbf{y}|} - \frac{1}{\Omega'} \int_{\Omega'} d\mathbf{r}' \frac{1}{|\mathbf{y} - \mathbf{r}'|} \right] \\ &= Z^2 e^2 n \int_{\Omega'} d\mathbf{y} \frac{1}{|\mathbf{y}|} - n\Omega' V'_{jj} = n\Omega' \cdot \frac{Z^2 e^2}{R} \cdot \frac{3}{10} \end{aligned} \quad (2.15)$$

where we have used eq. (2.13). We now observe from eqs. (2.13) and (2.15) that both $V_j - V''_j$ and V'_{jj} are independent of \mathbf{r}_j and hence eq. (2.12) provides an *extensive* lower bound:

$$V_N(\Omega) \geq -N \cdot \frac{Z^2 e^2}{R} \cdot \left(\frac{6}{10} + \frac{3}{10} n\Omega' \right). \quad (2.16)$$

We are still free to choose the radius R of the balls such as to optimize the lower bound given by eq. (2.16). The best lower bound is obtained when $n\Omega' = 1$ with $\Omega' = \frac{4}{3}\pi R^3$. Eq. (2.16) reduces then to:

$$V_N(\Omega)/N \geq -\frac{9}{10} Z^2 e^2 / a \quad (2.17)$$

where a is the so-called ion-sphere radius, $n^{-1} = \frac{4}{3}\pi a^3$ being the average volume per particle. This result, eq. (2.17), which is due to Lieb and Narnhofer [2.4], has a very simple physical interpretation. Indeed we can imagine that the lower bound of the OCP will be attained by forming some kind of Wigner solid in which each particle is surrounded by a ball of background which precisely neutralises its charge. If these balls do not overlap then by virtue of Newton's theorem the total energy of the system will be N times the electrostatic energy of one-particle-ball system which equals:

$$\frac{n^2}{2} \int_{\Omega'} d\mathbf{r} \int_{\Omega'} d\mathbf{r}' \frac{Z^2 e^2}{|\mathbf{r} - \mathbf{r}'|} - n \int_{\Omega'} d\mathbf{r} \frac{Z^2 e^2}{|\mathbf{r}|} = \frac{(n\Omega')^2}{2} \cdot \frac{Z^2 e^2}{a} \cdot \frac{6}{5} - (n\Omega') \cdot \frac{Z^2 e^2}{a} \cdot \frac{3}{2} = -\frac{9}{10} \cdot \frac{Z^2 e^2}{a} \quad (2.18)$$

where we have used eqs. (2.13) and (2.15) and the fact that here by definition $\Omega' n = 1$. Hence this Wigner solid picture reproduces exactly the equality in eq. (2.17). This picture is known in the

literature as the ion-sphere model [2.11]. These arguments become even more appealing if we report that the binding energy per particle in a static Wigner crystal has been estimated [2.8] to be, $-0.8800Z^2e^2/a$, $-0.8959Z^2e^2/a$ and $-0.8958Z^2e^2/a$ for respectively a simple, body centered and face centered cubic crystal. More precise values can be found in [2.12]. Hence the lower bound $-0.9Z^2e^2/a$ given in eq. (2.17) appears to be extremely accurate. Before closing this section let us recall the lower bound derived by Mermin [2.9] from the Bogoliubov inequality [1.3]. He found that the Debye–Hückel approximation always constitutes a lower bound to the *average* potential energy per particle:

$$\left\langle \frac{V_N}{N} \right\rangle \geq - \frac{Z^2 e^2}{a} \cdot (3\Gamma)^{1/2}. \quad (2.19)$$

For dilute systems, i.e. $(3\Gamma)^{1/2} < 0.9$, this lower bound is the best whereas eq. (2.17) yields the best bound for dense systems.

More details about the rigorous results for Coulomb systems can be found in a recent review by Choquard [2.10] and in the original literature cited above.

3. The static properties of the OCP

This section is entirely devoted to a summary of the theoretical and numerical results for the static (time-independent) equilibrium properties of the one-component plasma (OCP); we recall that this is a model system of mobile point charges in an inert neutralising background of opposite charge. As explained in section 2, this system is, even when considered classically, “well behaved”, i.e. it does not explode or collapse and it has a thermodynamic limit. Although the model has some pathology in it, it does exhibit most of the characteristics which distinguish charged from neutral fluids. Because of its intrinsic simplicity the OCP is in some sense the analogue of the hard sphere model of non-ionized matter. Since most of the peculiar features of charged particle fluids can be traced back to their statics, we first review the known results for the thermodynamics and the static correlation functions of the OCP.

3.1. Thermodynamics

According to the rigorous results summarized in section 2 a statistical mechanics description of the equilibrium properties of the OCP adopting Gibb’s canonical ensemble, with H_N of eq. (2.4) as Hamiltonian, is a well defined problem. The N -body probability density reads [3.1]:

$$\rho_N(\mathbf{r}^N, \mathbf{p}^N) = \frac{1}{h^{3N} N!} \frac{\exp \{-\beta H_N(\mathbf{r}^N, \mathbf{p}^N; \Omega)\}}{Q_N(\Omega, \beta)} \quad (3.1)$$

where $Q_N(\Omega, \beta)$ is the canonical partition function:

$$Q_N(\Omega, \beta) = \frac{1}{h^{3N} N!} \int d\mathbf{r}^N d\mathbf{p}^N \exp \{-\beta H_N(\mathbf{r}^N, \mathbf{p}^N; \Omega)\} \quad (3.2)$$

for a system of N charges enclosed in a volume Ω ; here h is Planck’s constant and $\beta = (k_B T)^{-1}$ the inverse temperature in energy units. The appropriate thermodynamic potential, from which

all the OCP thermodynamics can be derived, is the Helmholtz free energy $F_N(\Omega, \beta)$ defined by:

$$Q_N(\Omega, \beta) = \exp \{ -\beta F_N(\Omega, \beta) \}. \quad (3.3)$$

This relation establishes the required contact between thermodynamics and equilibrium statistical mechanics. From the thermodynamic potential F_N one can obtain all thermodynamic properties: the pressure P , the internal energy U and the three independent thermodynamic response functions: the isothermal compressibility χ_T , the specific heat at constant volume C_v and the coefficient of thermal expansion α_T . It is convenient to introduce excess quantities by separating off the ideal gas values according to:

$$Q_N(\Omega, \beta) = Q_N^0(\Omega, \beta) Z_N(\Omega, \beta) \quad (3.4)$$

where Q_N^0 is the ideal gas partition function:

$$Q_N^0(\Omega, \beta) = \frac{\Omega^N}{h^{3N} N!} (2\pi m k_B T)^{3N/2},$$

m being the mass of the mobile charges, and where Z_N is the dimensionless configuration integral:

$$Z_N(\Omega, \beta) = \int \frac{d\mathbf{r}^N}{\Omega^N} \exp \{ -\beta V_N(\mathbf{r}^N, \Omega) \}, \quad (3.5)$$

V_N being the potential energy part, eq. (2.5), of the Hamiltonian H_N .

It is readily seen from eqs. (2.5) and (3.5) that Z_N depends on β and on the interactions only through the dimensionless combination $\beta Z^2 e^2 / l$, where l is some characteristic length*. Different choices of l have been used in the literature. Most of the theoretical studies have used the Debye length λ_D , whereas most of the numerical data are given with $l = a$, a being the ion-sphere radius defined by eq. (1.1). The most common “plasma parameters” (or “coupling constant”) are thus with their standard notation:

$$\begin{aligned} \Gamma &= \beta Z^2 e^2 / a; & a &= (\frac{4}{3}\pi n)^{-1/3} \\ \varepsilon &= \beta Z^2 e^2 / \lambda_D; & \lambda_D &= (4\pi Z^2 e^2 n \beta)^{-1/2}. \end{aligned} \quad (3.6)$$

A frequently used alternative expression of ε is $\lambda = 4\pi\varepsilon \equiv (n\lambda_D^3)^{-1}$ which is the inverse of the number of particles in a “Debye cube”. The following relations between these parameters and length scales will be frequently used:

$$\varepsilon = \frac{\lambda}{4\pi} = \sqrt{3} \Gamma^{3/2}; \quad \frac{a}{\lambda_D} = (3\Gamma)^{1/2}. \quad (3.7)$$

Gathering some of the above results we may now state that: 1°) the existence of intensive variables in the thermodynamic limit implies that $\ln Z_N(\Omega, \beta)/N$ depends on N and Ω only through the ratio $n = N/\Omega$, and 2°) because of the inverse power property of the Coulomb potential, this limiting value will depend on n and β only through the dimensionless combination Γ (or ε), i.e.:

$$\lim_{\substack{N, \Omega \rightarrow \infty \\ N/\Omega = n}} -\frac{1}{N} \ln Z_N(\Omega, \beta) = f(n, \beta) \equiv f(\Gamma). \quad (3.8)$$

* A similar property holds for all inverse power potentials $v(r) = ar^{-b}$ [3.2].

Hence we reach the important conclusion that all dimensionless excess thermodynamic properties will depend on a single parameter. We now list the essential thermodynamic quantities:

$$P = - \left. \frac{\partial F_N}{\partial \Omega} \right|_{\beta} = P^0 \left(1 + n \frac{\partial f}{\partial n} \right); \quad P^0 = \frac{n}{\beta} \quad (3.9a)$$

$$U = \left. \frac{\partial \beta F_N}{\partial \beta} \right|_{\Omega} = \frac{2}{3} U^0 \left(\frac{3}{2} + \beta \frac{\partial f}{\partial \beta} \right); \quad U^0 = \frac{3}{2} \frac{N}{\beta} \quad (3.9b)$$

$$\chi_T^{-1} = -\Omega \left. \frac{\partial P}{\partial \Omega} \right|_{\beta} = n \left. \frac{\partial P}{\partial n} \right|_{\beta} = (\chi_T^0)^{-1} \left[1 + n \frac{\partial f}{\partial n} + \left(n \frac{\partial}{\partial n} \right)^2 f \right]; \quad \chi_T^0 = \frac{\beta}{n} \quad (3.9c)$$

$$C_v = \left. \frac{\partial U}{\partial T} \right|_{\Omega} = -\beta^2 k_B \left. \frac{\partial U}{\partial \beta} \right|_n = \frac{2}{3} C_v^0 \left[\frac{3}{2} + \beta \frac{\partial f}{\partial \beta} - \left(\beta \frac{\partial}{\partial \beta} \right)^2 f \right]; \quad C_v^0 = \frac{3}{2} N k_B \quad (3.9d)$$

where, for each item, the first line gives the standard thermodynamic definition, while in the second line we have gone to the thermodynamic limit, using eq. (3.8), and split off the ideal-gas values (indicated by a superscript zero). The above relations can be rewritten in terms of Γ or ε with the help of the following operational relations:

$$3n\partial f/\partial n = \beta\partial f/\partial \beta = \Gamma\partial f/\partial \Gamma = \frac{3}{2}\varepsilon\partial f/\partial \varepsilon, \quad (3.10)$$

which follow from eqs. (3.6) and (3.8). Using eq. (3.10) and comparing eqs. (3.9a) and (3.9b), we obtain:

$$\frac{P}{P^0} = 1 + \frac{1}{2} \frac{U - U^0}{U^0} = 1 + \frac{1}{3} \frac{\beta(U - U^0)}{N} \quad (3.11)$$

which is the particular form taken by the virial theorem for the Coulomb potential*.

3.2. Correlations and fluctuations

The transition from the mechanical properties described by the Hamiltonian H_N of eq. (2.4) to the thermodynamics embodied in $f(\Gamma)$ of eq. (3.8) represents a drastic reduction in the number of independent variables. In practice it is often useful to stop at some intermediate level and relate the thermodynamics to the two-body equilibrium distribution function F_2 defined from eq. (3.1) by:

$$n^2 F_2(\mathbf{r}_1, \mathbf{p}_1; \mathbf{r}_2, \mathbf{p}_2) = \frac{N!}{(N-2)!} \int d\mathbf{r}^{N-2} d\mathbf{p}^{N-2} \rho_N(\mathbf{r}^N, \mathbf{p}^N) = n^2 \varphi(\mathbf{p}_1) \varphi(\mathbf{p}_2) g(|\mathbf{r}_1 - \mathbf{r}_2|) \quad (3.12)$$

where, in the second line, we have taken into account that in a fluid and in the thermodynamic limit the radial distribution function g depends only on the distance $|\mathbf{r}_1 - \mathbf{r}_2|$ between the two particles; $\varphi(\mathbf{p})$ is the normalized Maxwellian:

$$\varphi(\mathbf{p}) = \frac{\exp \{-\beta p^2/2m\}}{(2\pi m/\beta)^{3/2}}. \quad (3.13)$$

* Similar relations between P and U exist for all inverse power potentials [3.2].

We also introduce the (total) correlation function $h(r)$:

$$h(r) = g(r) - 1. \quad (3.14)$$

Two related functions which will be of interest are:

$$S(\mathbf{r}) = \delta(\mathbf{r}) + nh(r) \quad (3.15)$$

where $\delta(\mathbf{r})$ is the Dirac delta function, and the direct correlation function $c(r)$ which is defined such that $S^{-1}(\mathbf{r}) = \delta(\mathbf{r}) - nc(r)$ is the inverse of $S(\mathbf{r})$, i.e.:

$$\int d\mathbf{r} S^{-1}(\mathbf{r}_1 - \mathbf{r}) S(\mathbf{r} - \mathbf{r}_2) = \delta(\mathbf{r}_1 - \mathbf{r}_2). \quad (3.16)$$

Eq. (3.16) is just an alternative form of the Ornstein–Zernike relation [3.1]:

$$h(r) = c(r) + n \int d\mathbf{r}' c(|\mathbf{r} - \mathbf{r}'|) h(\mathbf{r}'). \quad (3.17)$$

The link between the correlation function language, embodied in $g(r)$ and $c(r)$, and the fluctuation language embodied in $S(\mathbf{r})$ is most easily established in Fourier space. Let us therefore introduce spatial Fourier transforms as defined in appendix 1. The Fourier transform of $S(\mathbf{r})$ is the static structure factor $S(k)$ which is also the spectrum of the number density fluctuations:

$$S(k) = \frac{1}{N} \langle \delta n(\mathbf{k}) \delta n(-\mathbf{k}) \rangle_{\Omega} = \frac{1}{n} \langle |\delta n(\mathbf{k})|^2 \rangle \quad (3.18)$$

where $\langle \dots \rangle_{\Omega}$ denotes the canonical equilibrium average taken with ρ_N of eq. (3.1), while $\langle \dots \rangle$ denotes the thermodynamic limit of $\langle \dots \rangle_{\Omega}/\Omega$; $\delta n(\mathbf{k})$, defined by:

$$\delta n(\mathbf{k}) = n(\mathbf{k}) - \langle n(\mathbf{k}) \rangle_{\Omega} = \sum_{j=1}^N \exp \{i\mathbf{k} \cdot \mathbf{r}_j\} - N\delta_k^{kr} \quad (3.19)$$

denotes the Fourier transformed number density fluctuation. Eqs. (3.15)–(3.17) are most conveniently rewritten in Fourier space as:

$$S(k) = 1 + \hat{h}(k) = [1 - \hat{c}(k)]^{-1} \quad (3.20)$$

where $\hat{h}(k) = nh(k)$ and $\hat{c}(k) = nc(k)$ are the *dimensionless* Fourier transformed total and direct correlation functions.

Finally the relation between the correlation function language and thermodynamics is established by noting that the excess internal energy is just the canonical average of the potential energy (2.5). Using (3.12) and going to the thermodynamic limit leads immediately to:

$$\frac{U - U^0}{N} = \frac{n}{2} \int d\mathbf{r} v(r) [g(r) - 1] = \frac{1}{2} \int \frac{d\mathbf{k}}{(2\pi)^3} v(k) [S(k) - 1]. \quad (3.21)$$

From (3.11) and (3.21) we derive the equation of state:

$$\frac{P - P^0}{P^0} = \frac{n\beta}{6} \int d\mathbf{r} v(r) [g(r) - 1] = \frac{\beta}{6} \int \frac{d\mathbf{k}}{(2\pi)^3} v(k) [S(k) - 1] \quad (3.22)$$

where $v(r) = Z^2 e^2 / r$, $v(k) = 4\pi(Ze)^2 / k^2$. It will often be useful to use dimensionless integration variables $x = r/a$, $y = r/\lambda_D$, $q = ak$ and $l = \lambda_D k$, transforming for instance eq. (3.22) into:

$$\frac{P - P^0}{P^0} = \frac{1}{6} \int_0^\infty dy y [g(y) - 1] = \frac{\Gamma}{2} \int_0^\infty dx x [g(x) - 1] \quad (3.23)$$

$$= \frac{\varepsilon}{3\pi} \int_0^\infty dl l [S(l) - 1] = \frac{\Gamma}{3\pi} \int_0^\infty dq q [S(q) - 1]. \quad (3.24)$$

Before closing these introductory subsections let us summarize those features which are valid only for the particular fluid under consideration. All the relations used in this section are of general validity for a one component fluid except for two points: 1°) in eqs. (3.8)–(3.11) explicit use was made of the inverse power nature of the Coulomb potential, and 2°) the Hamiltonian used in eq. (3.1) contains explicitly background contributions not found in other fluids. This latter point explains the departure of the relations (3.21) and (3.22) from the standard form for neutral fluids [3.1] where $g(r) - 1$ is replaced by $g(r)$.

3.3. Asymptotic behaviour

Much of the information on the statics of fluid systems can be derived from a knowledge of $g(r)$ or $S(k)$. We summarize here some important constraints on these functions, against which theoretical and numerical results can be tested. From their definitions (3.12) and (3.19) both these functions are obviously non-negative. Moreover as the repulsion between a pair of ions becomes infinite as their mutual distance r goes to zero, $g(r)$ must vanish in that limit, while the same function goes to one for very large separations. As will be discussed in subsection 3.6 a major difficulty met by approximate theories of the OCP statics has been to avoid negative values of $g(r)$ for small r . In order to inquire about the asymptotic behaviour of $S(k)$ we use eqs. (3.14)–(3.15) to write:

$$S(k) = 1 + n \int dr e^{-ik \cdot r} [g(r) - 1]. \quad (3.25)$$

Under very weak conditions, related to the existence of the Fourier transform of $h(r) = g(r) - 1$, we see from eq. (3.25) that $S(k)$ has to go to one for large k values. The behaviour of $S(k)$ for small k is not obvious from eq. (3.25), except that $S(k=0)$ should be finite if $g(r) - 1$ is integrable as expected. The precise behaviour of $S(k)$ for small k is however the most characteristic feature of the OCP statics. To obtain this important information various independent routes have been followed by different authors [3.3–3.5]. The easiest way is to invoke a general property of the direct correlation function $\hat{c}(k)$ defined in eq. (3.20):

$$\hat{c}(k) = -\beta \hat{v}(k) \quad \text{for } k \rightarrow 0 \quad (3.26)$$

where $\hat{v}(k)$ is the dimensionless Fourier transform of the interaction potential. The physical content of eq. (3.26) is very simple if we observe that $-\beta \hat{v}(k)$ is also the weak-coupling limit of $\hat{c}(k)$ and hence that eq. (3.26) states that at large distances ($k \rightarrow 0$) particles can only be weakly coupled. The precise status of eq. (3.26) is however still that of a basic “belief” which underlies many approximate results in the theory of fluids; no rigorous proof is as yet available. The general validity of eq. (3.26) has

been discussed by Stell [3.6] in a diagrammatic context. Now when eq. (3.26) is used for the OCP, where $v(k) = 4\pi Z^2 e^2 / k^2$, we reach the conclusion that the direct correlation function of the OCP is singular for small k , $\hat{c}(k) = O(k^{-2})$. This singular behaviour reflects the long (non-integrable) range of the Coulomb potential. For any potential which is integrable at large distances the r.h.s. of eq. (3.26) would be finite for small k . Nevertheless this equation remains extremely useful for the OCP in the following form. We just split $\hat{c}(k)$ into a singular term, $c^S(k) = -\beta \hat{v}(k) = -k_D^2/k^2$ (where $k_D = \lambda_D^{-1}$ is the inverse Debye length), and a regular term $c^R(k)$:

$$\hat{c}(k) \equiv c^S(k) + c^R(k) = -k_D^2/k^2 + c^R(k) \quad (3.27a)$$

and assume that $c^R(k)$ can be expanded as:

$$c^R(k) = c^R(0) + O(k^2) \quad (3.27b)$$

i.e. the remainder $c^R(k)$, once the singular term $c^S(k)$ has been extracted from $\hat{c}(k)$, is short ranged. This assumption is equivalent [3.7] to the assumption of perfect screening used in the past [3.3–3.5]. Indeed the latter assumption states that the charge, $\rho^{ind}(k)$, induced by an external charge distribution, $\rho^{ext}(k)$, exactly cancels the latter in the limit $k \rightarrow 0$. Since both charge distributions are linked by the static dielectric function $\epsilon(k)$ through the defining relation:

$$\rho^{ind}(k) = [1/\epsilon(k) - 1]\rho^{ext}(k) \quad (3.28)$$

the condition $\rho^{ind}(k) + \rho^{ext}(k) \rightarrow 0$ as $k \rightarrow 0$ implies that $1/\epsilon(k)$ vanishes for small k . But $\epsilon(k)$, which measures the linear response of the charged fluid to an external charge, is related to $S(k)$ through the fluctuation dissipation theorem [3.3]:

$$S(k) = \frac{k^2}{k_D^2} \left[1 - \frac{1}{\epsilon(k)} \right]. \quad (3.29)$$

If we expect $\epsilon(k)$ to behave as $1 + k_s^2/k^2$ for small k , where k_s is an inverse screening length, then the perfect screening condition is equivalent to eq. (3.27b) if $k_D^2/k_s^2 = 1 - c^R(0)$. This is immediately seen by substituting eqs. (3.27a) and (3.27b) into (3.20) and comparing with the leading terms in (3.29). In summary the small k expansion of $S(k)$ reads:

$$S(k) = \frac{k^2}{k_D^2} + \frac{k^4}{k_D^4} [c^R(0) - 1] + O(k^6) \quad (3.30)$$

i.e. $S(k)$ vanishes with k . This is a typical OCP feature not encountered in ordinary fluids where both $S(k)$ and $c(k)$ tend to a finite non-zero value for small k . Comparing now eq. (3.30) with eq. (3.25) we obtain under very weak conditions on the integral in eq. (3.25), a number of sum rules to be satisfied by $g(r)$:

$$n \int d\mathbf{r} [g(r) - 1] = -1 \quad (3.31a)$$

$$n \int d\mathbf{r} r^2 [g(r) - 1] = -6/k_D^2 \quad (3.31b)$$

$$n \int d\mathbf{r} r^4 [g(r) - 1] = \frac{120}{k_D^4} [c^R(0) - 1]. \quad (3.31c)$$

The first sum-rule expresses just overall electroneutrality, while the second was first proposed by Stillinger and Lovett [3.8] on the basis of a perfect screening argument. Eq. (3.31c) is the OCP equivalent of the compressibility sum-rule. We recall that for an ordinary fluid the isothermal compressibility χ_T (see eq. (3.9c)) is given by:

$$\chi_T/\chi_T^0 = S(k=0) = 1 + n \int d\mathbf{r} [g(r) - 1] = [1 - \hat{c}(k=0)]^{-1}. \quad (3.32)$$

Because of the singular behavior of $\hat{c}(k)$ this relation does not hold for the OCP. It must be replaced by (3.3–3.5]:

$$\chi_T/\chi_T^0 = [1 - c^R(k=0)]^{-1} \quad (3.33)$$

in which case eq. (3.31c) becomes the OCP equivalent of eq. (3.32). In fact eq. (3.33), but in the form (see eqs. (3.20) and (3.27a)):

$$S(k) = [k_D^2/k^2 + \chi_T^0/\chi_T]^{-1} \quad \text{for } k \rightarrow 0 \quad (3.34)$$

has also been derived by Vieillefosse and Hansen [3.9] from a macroscopic fluctuation calculation. Recently it has been shown [3.7] from first principles that if eq. (3.33) is considered as the *definition* of χ_T , then this compressibility is consistent with the thermodynamic definition (3.9c), provided eq. (3.22) is adopted as equation of state. However, contrary to what happens for ordinary fluids, the OCP compressibility χ_T is not a positive definite quantity [3.9] in agreement with the rigorous result of section 2 that the free energy of the OCP, $F_N(\Omega, \beta)$, is not a convex function of the volume Ω .

Before closing this subsection on the asymptotic properties of the various correlation functions, let us mention some recent theoretical work on the behaviour of $g(r)$ for small r which is essential for the prediction of nuclear reaction rates in dense stellar interiors [3.10]. At the short distances involved in such reactions, $g(r)$ is in fact dominated by quantum tunnelling effects, which will be briefly examined in subsection 5.1. For the classical OCP, Jancovici [3.11] obtained the small r behaviour by separating the singular Coulomb potential $(Ze)^2/r_{12}$ between a given pair of particles (labeled 1 and 2) from the remaining total potential energy $W_N = V_N - (Ze)^2/r_{12}$, and by Taylor expanding W_N (which is regular as $r_{12} \rightarrow 0$) in powers of \mathbf{r}_1 and \mathbf{r}_2 . The calculation yields, to order $r^2 = r_{12}^2$:

$$g(r) = \exp \left\{ -\Gamma \frac{a}{r} + C - \frac{\Gamma}{4} \frac{r^2}{a^2} + \dots \right\}. \quad (3.35)$$

The positive constant C , which characterizes the enhancement of $g(r)$, as $r \rightarrow 0$, over its zero-density limit $\exp \{-\Gamma a/r\}$, due to screening, is given by:

$$C = \beta[F(0, N) - F(1, N - 2)] \quad (3.36a)$$

where $F(M, N)$ is the excess Helmholtz free energy of a mixture of M particles of charge $2Ze$ and N particles of charge Ze . In section 5 it will be shown that $F(M, N)$ can be expressed to a high degree of accuracy, in terms of the excess free energy of the OCP. Using the notation of eq. (3.8), C can be cast in the form:

$$C = 2f(\Gamma) - f(2^{5/3}\Gamma). \quad (3.36b)$$

The same problem was also considered, from a less rigorous point of view, by Itoh et al. [3.12].

For intermediate r values the transition region from eq. (3.35) to the first peak of $g(r)$ (see subsection 3.4) appears to contain an approximately linear region [3.10]:

$$g(r) \approx \exp \{ -\Gamma a/r + C_1 - C_2 r/a \}.$$

A theoretical model for this behaviour has been proposed recently [3.13].

3.4. "Exact" numerical results

Before reviewing the various approximate theories of the OCP statics, we present in this subsection a summary of the "exact" results on the thermodynamics and structural properties of this model which have been obtained by numerical simulation techniques, the so-called computer "experiments". These techniques were originally designed to improve our understanding of dense, neutral fluids and liquids, but over the last decade or so they have also proved to be very powerful in the study of Coulomb systems. The theoretical importance of these computer "experiments" lies in the fact that they yield essentially exact numerical results for various statistical mechanical averages, against which approximate theories can be tested. Since the numerical simulations and the approximate theories can both be made for exactly the same model, i.e. for systems of particles interacting through prescribed force laws under identical conditions, the comparison is particularly stringent, since it avoids all the uncertainties linked to a comparison with true laboratory experiments, which arise e.g. from our incomplete knowledge of inter-atomic or inter-ionic forces. In the case of the OCP the simulation results are particularly important: indeed they represent the only measure against which theories can be tested, since this model is too idealized to be directly relevant for any physical system, at least under conditions which are easily accessible in a laboratory experiment.

Two rather distinct computer simulation techniques are by now standard in Statistical Mechanics: the Monte Carlo (MC) method, due to Metropolis et al. [3.14], which allows the computation of static properties of classical and quantum-mechanical many-particle systems, and the Molecular Dynamics method, invented by Alder and Wainwright [3.15], which is more specifically designed for the computation of dynamical properties of classical systems; the latter will be introduced in section 4. We present here a summary of the thermodynamic and structural properties of the OCP obtained by a series of MC computations. The Monte Carlo method is thoroughly described in a number of review articles and books [3.16], so that there is no need to go into details in this review. We only briefly recall that in a classical Monte Carlo simulation, a large number of configurations (typically 10^5 – 10^6) are generated for systems of $N = 10^2$ – 10^4 particles interacting via a prescribed pair potential. The Metropolis algorithm [3.14] is set up so that the configurations are generated with a probability which is proportional to the Boltzmann factor $e^{-\beta V_N}$, where $V_N(r^N)$ is the total potential energy of the system in a given configuration. Normalized canonical ensemble averages for a given temperature and density $n = N/\Omega$ are then estimated by averaging any function of the coordinates over the total number of configurations generated in a run. Because this number is finite, the averages are affected by statistical uncertainties which decrease roughly with the square root of the number of configurations. In order to eliminate surface effects, which would be severe for such small systems, periodic boundary conditions are imposed.

The great success of the MC method lies in the fact that systems of a few hundred particles have generally proved sufficient to yield results which are very close to their values in the thermodynamic limit! In other words, beyond $N \simeq 10^2$, the N -dependence of the statistical averages is very weak.

For Coulomb systems a special problem arises in the MC simulations, because of the long range of the potential. In the case of short range potentials one generally uses the “nearest-image” convention: each particle in the basic cell interacts only with the *nearest* periodic image of each of the $N - 1$ other particles of the system; this means that for a cubic box of length $L = \Omega^{1/3}$, interactions between particles do not extend beyond $r = L/2$, where they are generally negligible anyway. In the case of the Coulomb potential this truncation is of course highly unsatisfactory and leads to unphysical results for the OCP in the strong coupling limit ($\Gamma \gg 1$) [3.17]. Two very different procedures have been proposed to overcome this difficulty and to take proper account of the long range of the Coulomb potential.

The first procedure, due to Barker [3.18] and to Brush et al. [3.17] generalizes the “nearest image” convention by letting each particle in the basic cell interact not only with the *nearest* image of each of the other particles, but also with *all* the other images in the infinite array of periodic replicas of the system. Taking due account of the electrostatic interaction with the neutralizing background, the resulting infinite sums are handled by an Ewald transformation [3.19]. As a result the bare Coulomb potential between ions is replaced by a short range effective pair potential which is no longer spherically symmetric, but reflects the cubic symmetry of the simulated system. For computational purpose the effective Ewald potential can be approximated by an expansion in Kubic harmonics [3.20]; the leading term is then spherically symmetric and represents the dominant contribution for most relative positions of a pair of ions.

A second procedure for treating the long range of the Coulomb potential has been exploited by Ceperley and Chester [3.21]. It is based on a separation of the potential into short range and long range parts:

$$v(r) = v_0(r) + w(r). \quad (3.37)$$

The short range reference potential $v_0(r)$ is chosen such that it behaves like the full Coulomb potential at $r \rightarrow 0$, and such that its range is shorter than the dimension of the simulated sample. MC computations are then carried out for a system of particles interacting through the reference potential $v_0(r)$ which can be properly handled by the simple “nearest image” convention. These computations yield, in particular, the reference system pair distribution function $g_0(r)$. The pair distribution of the OCP, i.e. of a system of particles interacting through the *full* potential $v(r)$, is then obtained by a perturbation method due to Lado [3.22], and based on the HNC theory which will be introduced in subsection 3.7. Lado’s method is quite general and can be used whenever the pair potential is split into a reference part $v_0(r)$ and a perturbation $w(r)$; the method will be described in a somewhat different context in subsection 5.4.

In practice, Ceperley and Chester chose:

$$\beta v_0(x) = \frac{\Gamma}{x} \operatorname{erfc}\left(\frac{x}{\sigma}\right) \quad (3.38)$$

where $x = r/a$, and erfc is the complementary error function; σ is an adjustable range parameter. This choice of v_0 coincides with the spherically symmetric part of the Ewald potential. MC computations were done for $\Gamma = 50, 75, 100, 120$ and 140 , with values of σ ranging between 0.8 and 1.5 , and for systems of 128 and 256 particles. The resulting pair distribution functions and thermodynamics of the OCP turn out to be in excellent agreement with those obtained by the Ewald procedure [3.17, 3.20], provided the range parameter is chosen to be sufficiently large ($\sigma \simeq 1.5$). The differences between the two sets of results are less than the statistical uncertainties of the

MC computations and can hence be regarded, with a high degree of confidence, as essentially exact.

The remainder of this subsection is devoted to a presentation of the MC results for the thermodynamics and structure of the OCP obtained by the Ewald procedure [3.17, 3.20, 3.23]. The properties which were directly computed in the MC computations are essentially the excess internal energy per particle, $u = \beta U^{\text{ex}}/N$ and the radial distribution function $g(r)$. The other thermodynamic properties can be derived from u through the usual thermodynamic relations; in particular the equation of state follows from eq. (3.11). The structure factor $S(k)$ is calculated by numerical Fourier transformation of the MC results for $g(r)$ and the direct correlation function $c(r)$ follows from the Ornstein–Zernike relation (3.17); the isothermal compressibility can then be obtained from eq. (3.33).

The MC results show that for sufficiently strong coupling, i.e. for very high values of Γ , the crystalline phase of the OCP is stable [3.23]. The distinction between fluid and solid phases is relatively easy if the r.m.s. displacement σ of the particles from their initial positions is monitored as a function of the number of configurations generated in a MC run. If the initial positions of the particles coincide with the sites \mathbf{R}_i of a perfect lattice, σ is defined as:

$$\sigma = \left\{ \frac{1}{N} \sum_{i=1}^N \langle (\mathbf{r}_i - \mathbf{R}_i)^2 \rangle \right\}^{1/2} \quad (3.39)$$

where \mathbf{r}_i is the position of the i th particle. In the case where the solid is stable, the particles are localized around their lattice sites; as a result σ remains finite and fluctuates around a well-defined value, whatever the length of the run. On the other hand, if σ increases steadily with the number of generated configurations, this means that the particles diffuse away from their initial positions and the system is in a fluid state. The MC simulations of Pollock and Hansen [3.23] indicate that the solid phase is stable for $\Gamma \gtrsim 140$. The criterion described above yields of course only a lower limit for *mechanical* stability and does not distinguish between *thermodynamically* stable states and metastable states of the solid phase. The value of Γ beyond which the solid is thermodynamically stable can only be determined by comparing the Helmholtz free energies of the fluid and solid phases. We shall return to this point shortly.

The MC computations of Brush et al. [3.17] cover the fluid phase in the range $0.05 \leq \Gamma \leq 100$, for systems of $32 \leq N \leq 500$ ions, whereas the calculations of Hansen [3.20] cover fluid states with $1 \leq \Gamma \leq 160$, and systems of size $16 \leq N \leq 250$. The latter results are probably more reliable since averages were taken over considerably more configurations (about 5×10^5 per run, compared to about 10^5 in [3.17]) and because the Ewald potential was approximated with a higher degree of accuracy in Hansen's work. Nevertheless the two sets of results for the OCP statics are in excellent agreement, except at the highest values of Γ , and are practically independent of system size for $N \gtrsim 10^2$. The computations of Pollock and Hansen [3.23] cover the solid phase in the range $140 \leq \Gamma \leq 300$, for systems of 128 and 250 particles.

We first summarize the fluid phase data. Rather than presenting a detailed table of the MC results for the OCP thermodynamics [3.17, 3.20] it seems more useful to reproduce here the very accurate and simple functional fit to Hansen's data obtained by De Witt [3.24]. Observing that $u = \beta U^{\text{ex}}/N$ varies essentially linearly with Γ in the strong coupling regime ($\Gamma > 1$), De Witt proposed the very simple form:

$$u(\Gamma) = a\Gamma + b\Gamma^s + c. \quad (3.40)$$

The dominant linear term is termed “static”, in analogy with the energy of a static perfect lattice, because the optimum coefficient a for the fluid turns out to be very close to the Madelung constant for cubic lattices, of which the BCC structure yields the lowest energy:

$$a_{\text{BCC}} = -0.895929. \quad (3.41)$$

The remainder in the r.h.s. of eq. (3.40) is called the “thermal” part; a careful numerical analysis of the MC data shows that the optimum fit is achieved for the exponent $s = 1/4$. This simple function must be regarded as a strong coupling asymptotic form which breaks down in the weak coupling regime ($\Gamma < 1$), since it obviously does not reduce to the limiting Debye–Hückel form $u = -(\sqrt{3}/2)\Gamma^{3/2}$ when $\Gamma \rightarrow 0$ (subsection 3.5). The optimum values of the constants a , b and c , as determined from a least squares fit to the MC data over the entire fluid range $1 \leq \Gamma \leq 160$, are:

$$a = -0.89643; \quad b = 0.86185; \quad c = -0.5551. \quad (3.42)$$

The corresponding standard deviation is of the order of 0.01, which is a reasonable estimate of the statistical uncertainties of the MC results. The MC energies for $\Gamma \leq 40$ can be fitted by the expression (3.40) with slightly different values of the coefficients ($a = -0.89461$; $b = 0.8165$; $c = -0.5012$), resulting in a standard deviation which is down by an order of magnitude. The results for $\Gamma \gtrsim 50$ may be slightly more N -dependent, because the spatial correlations extend over distances which become larger than the system size, as is evident from the slower decay of the oscillations in $g(r)$ (see fig. 2).

From eq. (3.40) and the relations (3.9)–(3.11), the other excess thermodynamic quantities are easily derived:

$$\frac{\beta F^{\text{ex}}}{N} = f(\Gamma) = f(\Gamma_1) + \int_{\Gamma_1}^{\Gamma} \frac{u(\Gamma')}{\Gamma'} d\Gamma' = a\Gamma + 4b\Gamma^{1/4} + c \ln \Gamma + d \quad (3.43a)$$

$$\frac{C_V}{Nk_B} - 1 = c_V(\Gamma) = -\Gamma^2 \frac{d}{d\Gamma} \left[\frac{u(\Gamma)}{\Gamma} \right] = \frac{3}{4}b\Gamma^{1/4} + c \quad (3.43b)$$

$$\frac{\chi_T^0}{\chi_T} = 1 + \frac{u(\Gamma)}{3} + \frac{\Gamma}{9} \frac{d}{d\Gamma} u(\Gamma) = 1 + \frac{4a}{9}\Gamma + \frac{13b}{36}\Gamma^{1/4} + \frac{c}{3}. \quad (3.43c)$$

In (3.43a) the additive constant d has been determined from the free energy calculated by the most accurate theory (i.e. HNC theory exposed in subsection 3.7) at $\Gamma = 1$; in conjunction with the parameter values given in eq. (3.42), d takes the value -2.996 .

Inspection of formulae (3.40)–(3.43) calls for the following remarks:

- a) The “thermal” contribution to the excess energies, pressure and compressibility is less than 3% for $\Gamma \gtrsim 100$.
- b) The “static” term does not contribute to the excess specific heat at constant volume, which behaves essentially as $T^{3/4}$.
- c) In the limit of very strong coupling ($\Gamma \gtrsim 100$) the MC results for the excess internal energy lie only about 2% above the lower bound (2.17), which lies itself only 0.5% below the Madelung energy of a BCC lattice.
- d) The inverse isothermal compressibility (3.43c) becomes *negative* for $\Gamma \gtrsim 3$. In a neutral fluid this would correspond to thermodynamic instability against spontaneous density fluctuations,

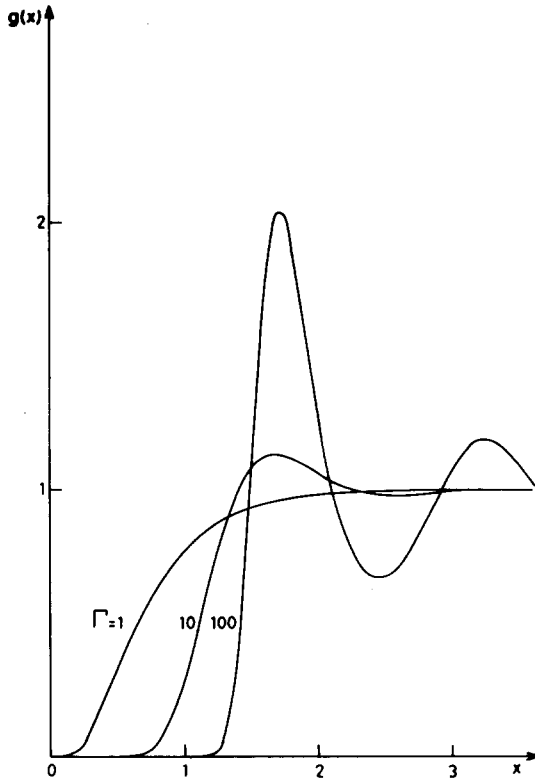


Fig. 2. OCP pair distribution function $g(x)$ versus $x = r/a$, for $\Gamma = 1, 10$ and 100 ; from the MC computations of Hansen [3.20].

but for the OCP a negative compressibility has no particular meaning, as emphasized in the previous subsection.

The other important quantity which is directly determined by the MC simulations is the radial distribution function $g(r)$; this is tabulated for several values of Γ in [3.17] and [3.20] and three examples are shown in fig. 2. For $\Gamma < 3$, $g(r)$ increases monotonously from 0 to its asymptotic value 1 in qualitative agreement with the simple non-linear Debye–Hückel form (3.52) (see subsection 3.5). For $\Gamma \gtrsim 3$, $g(r)$ exhibits oscillations which are characteristic of short range order. As Γ increases, the oscillations become more and more pronounced and extend further out while an effective “hard core” (where $g(r) \simeq 0$) builds up at short distances.

The structure factor $S(k)$ is calculated from eq. (3.25) by numerical Fourier transformation of $g(r)$. Since $g(r)$ is known only for $r < L/2$ from the MC computations, it must first be suitably extrapolated to larger distances [3.25, 3.21] in order to avoid spurious truncation errors in $S(k)$. Structure factors for $2 \leq \Gamma \leq 160$ are tabulated in [3.25]. The variation of $S(k)$ with Γ is illustrated in fig. 3.

The Fourier transform $\hat{c}(k)$ of the direct correlation function is easily determined from $S(k)$ using (3.20). The resulting $c(r)$ approaches its asymptotic form $-\Gamma a/r$ rapidly beyond $r \simeq a$, but goes to a finite limit as $r \rightarrow 0$, with zero slope. For $\Gamma \gtrsim 10$, $c(r)/\Gamma$ is nearly a universal function of $x = r/a$; in particular $c(0)/\Gamma$ is practically independent of Γ , and close to $-4/3$.

Figure 4 shows the inverse static dielectric constant $\epsilon(k)^{-1}$ defined by (3.29) for $\Gamma = 1$ and 100 .

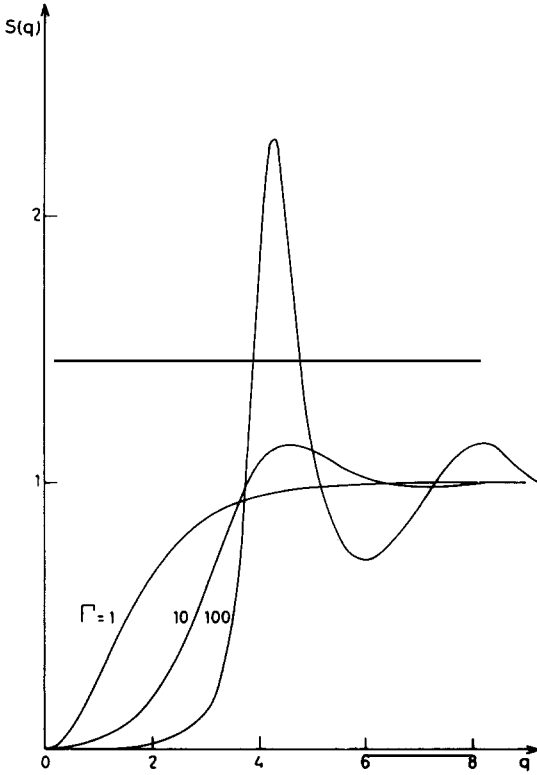


Fig. 3. OCP static structure factor $S(q)$ versus $q = ak$, for $\Gamma = 1, 10$ and 100 [3.20, 3.25].

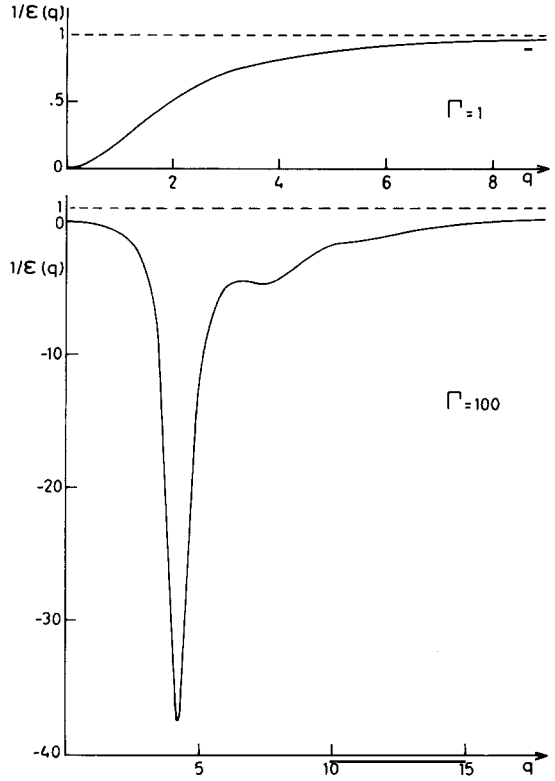


Fig. 4. Inverse of OCP static dielectric function, $\epsilon(q)^{-1}$, versus $q = ak$, for $\Gamma = 1$ and 100 ; based on the MC data of Hansen [3.20, 3.25].

$\epsilon(k)^{-1}$ exhibit a negative portion for small k at the higher Γ value. From (3.29) and (3.34) negative values of $\epsilon(k)$ are directly linked to the negative compressibility of the OCP for $\Gamma > 3$.

The MC computations in the solid phase of the OCP [3.23] were done for a BCC lattice which has the lowest static energy. The excess internal energy is the sum of this static contribution and of a thermal contribution; in the harmonic phonon approximation this thermal contribution is just $k_B T/2$ per degree of freedom. The anharmonic contributions, as determined by the MC computations, turn out to be fairly small, even close to melting. A simple calculation [3.23] shows that the dominant anharmonic contribution to the energy should be positive and quadratic, rather than linear, in T . In summary the excess internal energy of the OCP solid is well represented by

$$\beta U^{\text{ex}}/N = u(\Gamma) = a_{\text{BCC}}\Gamma + \frac{3}{2} + b/\Gamma^2 = -0.895929\Gamma + 1.5 + 3500/\Gamma^2 \quad (3.44)$$

where the coefficient b has been determined by a least squares fit to the MC data. The Helmholtz free energy is again obtained by integrating $u(\Gamma)$; the additive constant is determined by a harmonic phonon calculation which is exact in the $\Gamma \rightarrow \infty$ limit [3.23].

The free energy versus Γ curves of the fluid and solid phases intersect at $\Gamma \approx 155$. This value is very sensitive to small errors in the computed values of the free energies. The entropy change on melting $\Delta S/Nk_B \approx 0.8$, and the “Lindemann ratio” at melting $\sigma/d \approx 0.17$ (where σ is the r.m.s.

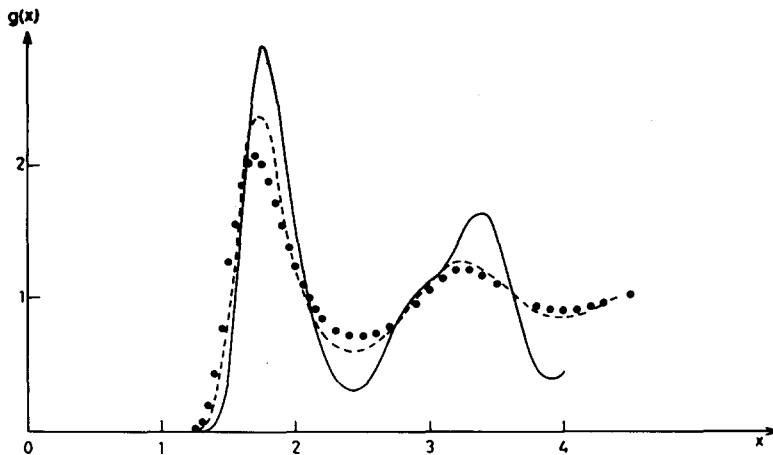


Fig. 5. OCP pair distribution function $g(x)$ versus $x = r/a$, for $\Gamma = 160$. Full curve: solid phase MC results [3.23]; dashed curve: fluid phase MC results [3.20]; circles: fluid phase HNC results [3.53].

displacement defined in eq. (3.39) and d is the nearest neighbour distance) are close to the corresponding values observed for simple neutral systems [3.26], but the relative volume change on melting is much smaller in the case of the OCP [3.23]. A comparison between the pair distribution functions of the fluid and the solid at $\Gamma = 160$ is made in fig. 5.

3.5. Weak coupling theories

It is the purpose of any theory of the OCP statics to provide an approximate calculational device from which the equilibrium properties summarized in subsections 3.1–3.3 can be computed and compared with the numerical results presented in subsection 3.4. We first consider the weak coupling theories which rely on expansions in powers of the coupling parameter ε for small values of this parameter ($\varepsilon < 1$, or $\Gamma < 3^{-1/3}$). For $\varepsilon \ll 1$ any such theory should reduce to the celebrated Debye–Hückel theory which amounts to replacing $\hat{c}(k)$, for all k , by its asymptotic form (3.27). The various correlation functions introduced in subsection 3.2 become then, in the conventional notations of eqs. (3.6), (3.23) and (3.24):

$$g_{\text{DH}}(r) = 1 - \frac{\varepsilon}{y} e^{-y} = 1 - \frac{\Gamma}{x} \exp \{ -(3\Gamma)^{1/2} x \} \quad (3.45a)$$

$$S_{\text{DH}}(k) = l^2/(l^2 + 1) = q^2/(q^2 + 3\Gamma) \quad (3.45b)$$

$$c_{\text{DH}}(r) = -\varepsilon/y = -\Gamma/x \quad (3.46a)$$

$$\hat{c}_{\text{DH}}(k) = -1/l^2 = -3\Gamma/q^2. \quad (3.46b)$$

According to (3.21) and (3.45a) the resulting internal energy is

$$\frac{\beta U}{N} = \frac{3}{2} - \frac{\varepsilon}{2} = \frac{3}{2} - \frac{\sqrt{3}}{2} \Gamma^{3/2}. \quad (3.47)$$

The DH theory is what we call in modern terms a mean field theory, and as such it has played a very important role in statistical physics [3.28]. A careful analysis of the standard derivation of $g_{\text{DH}}(r)$ from the Poisson–Boltzmann equation (see appendix 2) reveals that it is a good approximation to the exact $g(r)$ for $\varepsilon \ll 1$ only in the range of r values corresponding to $\varepsilon < k_{\text{D}}r < 1$. Undue extrapolation of $g_{\text{DH}}(r)$ to very short or very large distances is bound to run into difficulties even for very weak couplings. Several theories have been proposed to 1°) compute higher order terms ($\sim \varepsilon^n$, $n > 1$) in the small ε expansion of the thermodynamic properties, and 2°) correct $g_{\text{DH}}(r)$ for short and large distances. The main feature of these results has been the emergence of a bewildering variety of non-analytic expressions. As such these Coulomb non-analyticities have played the role of prototypes for a number of other non-analyticities discovered in other areas of statistical physics [3.29]. Gathering the currently known results for the limiting behaviour ($\varepsilon \rightarrow 0$) of the thermodynamics, we have the following expression for the internal energy:

$$\frac{\beta U}{N} = \frac{3}{2} - \frac{\varepsilon}{2} - \left(\frac{\varepsilon}{2}\right)^2 \left[\ln \varepsilon + \ln 3 + 2\gamma - \frac{4}{3} \right] - \left(\frac{\varepsilon}{2}\right)^3 [3 \ln \varepsilon - c] + \dots \quad (3.48)$$

where $c = 2.0224 \pm 0.0032$ and γ is Euler's constant. The first two terms ($O(\varepsilon^0)$ and $O(\varepsilon)$) reproduce the DH result (3.47). The third term ($O(\varepsilon^2)$) was first obtained by Abe [3.30] who adapted the Mayer cluster expansion to the Coulomb case; this implies partial resummations of the Mayer diagrams culminating in the so-called nodal expansion [3.31]. The last term ($O(\varepsilon^3)$) was obtained by Cohen and Murphy [3.32] after further resummations. It is however not clear how this series could be extended. As such the series of eq. (3.48) does reveal the presence of non-analytic ($\sim \ln \varepsilon$) terms, but it should be remembered that ε itself is already non-analytic with respect to the bare coupling constant e^2 , since $\varepsilon \sim (e^2)^{3/2}$.

Instead of directly computing the thermodynamic properties one can also solve the equilibrium BBGKY hierarchy for $g(r)$ [3.1] approximately and substitute the result into eq. (3.22). If we call h_3 the triplet correlation function, obtained from a cluster expansion of the three-body distribution function, then the appropriate hierarchy equations, neglecting four-body correlations, read in the dimensionless notation of eq. (3.23):

$$\frac{d^2 h(y_{12})}{dy_{12}^2} + \left(\frac{2}{y_{12}} - \frac{\varepsilon}{y_{12}^2} \right) \frac{dh(y_{12})}{dy_{12}} - h(y_{12}) = \frac{1}{4\pi} \frac{\partial}{\partial y_1} \int dy_3 \frac{y_{13}}{y_{13}^3} h_3(y_{12}, y_{23}, y_{31}) \quad (3.49a)$$

$$\begin{aligned} \frac{dh_3}{dy_{12}}(y_{12}, y_{23}, y_{31}) - \frac{1}{4\pi} \int dy_4 \frac{y_{12} \cdot y_{14}}{y_{12} y_{14}^3} h_3(y_{23}, y_{34}, y_{42}) - \frac{\varepsilon}{y_{12}^2} h_3(y_{12}, y_{23}, y_{31}) \\ = \frac{\varepsilon}{y_{12}^2} [h(y_{12}) + h(y_{23})] + \frac{1}{4\pi} \int dy_4 \frac{y_{12} \cdot y_{14}}{y_{12} y_{14}^3} h(y_{13})h(y_{24}) \end{aligned} \quad (3.49b)$$

where $y_{ij} = y_i - y_j$, $y_{ij} = |y_{ij}|$, $y_i = r_i/\lambda_{\text{D}}$. This procedure was followed by a series of authors [3.33]. The resulting U is always equivalent to eq. (3.48), except for the last term ($O(\varepsilon^3)$) which would have required consideration of the four particle correlations neglected in eq. (3.49b).

The situation is less clear as far as the large r behaviour of $g(r)$ is concerned, since the cluster expansion and hierarchy methods have led to conflicting expressions [3.33]. The generally accepted large r behaviour of $g(r)$ for small ε is [3.32]:

$$\begin{aligned}
g(r) &= \exp \left\{ -C_1 \frac{\varepsilon}{y} \exp [-C_2 y] \right\}, \quad \text{as } y = k_D r \rightarrow \infty \\
C_1 &= 1 + \varepsilon \left(\frac{3}{8} \ln 3 + \frac{1}{6} \right) + \dots \\
C_2 &= 1 + \frac{\varepsilon}{8} \ln 3 + \dots
\end{aligned} \tag{3.50}$$

It is interesting to compare eq. (3.50) with the DH result of eq. (3.46a). Clearly, for a given value of y and for small ε , we can expand the exponential in eq. (3.50) and to lowest order in ε , recover the DH result. Such an expansion is however not uniform with respect to y and when extrapolated to small y values will lead to negative values of $g(r)$. This difficulty is well known from DH theory and a glance at eq. (3.49a) shows that for small y and given ε one should expect:

$$g(r) = \exp(-\varepsilon/y), \quad \text{as } y \rightarrow 0. \tag{3.51}$$

One is tempted to reconcile $g_{\text{DH}}(r)$ with eqs. (3.50) and (3.51) by exponentiating the DH result (3.46a), introducing hereby the nonlinear DH result:

$$g_{\text{DH}}^{\text{NL}}(r) = \exp \left\{ -\frac{\varepsilon}{y} \exp(-y) \right\}. \tag{3.52}$$

Although eq. (3.52) agrees with eq. (3.51) for small y , it differs from eq. (3.50) by $O(\varepsilon^2)$ terms. Hence eq. (3.52), when used for all y values and keeping higher orders of ε , is inconsistent with eq. (3.48). An alternative approach to a non-linear DH theory is sketched in appendix 2.

Still further resummations of diagrams, in an attempt to cover the intermediate coupling regime, have indicated that the long range behaviour of $g(r)$ can change from the form given in eq. (3.50) to an oscillatory form [3.34, 3.35, 3.36]:

$$g(r) = \exp \left\{ -\frac{a}{y} \cos(by + c) \exp(-dy) \right\} \tag{3.53}$$

when the coupling exceeds a critical value (in eq. (3.53) a, b, c and d are functions of ε). This behaviour of $g(r)$ is in qualitative agreement with the onset of “short range order” revealed by the MC data discussed in subsection 3.4. The critical value of the coupling parameter, say ε_0 , for the onset of oscillations in $g(r)$ predicted by these theories ($\varepsilon_0 \approx 4$) lies somewhat below the value $\varepsilon_0 \approx 9$ estimated from the MC data. In view of the uncertainties affecting the precise location of ε_0 by the MC computations, a better candidate for a test of the analytical theories is the value $\varepsilon_c \approx 9$ at which the inverse compressibility vanishes (see eq. (3.43c)). The critical values ε_0 and ε_c are clearly closely related since eq. (3.34), which is valid only for small k , predicts oscillations in $g(r)$ for $\varepsilon > \varepsilon_c$ [3.9], a value which for finite k could be shifted somewhat. It should be stressed however that there is no compelling reason why this “transition” to short range order could not be continuous. In any case in order to predict such a transition point with any degree of confidence, theories not relying on expansions are required, and we now turn our attention to such theories.

3.6. Intermediate coupling theories

It is clear that theories based on diagrammatic expansions cannot produce a reliable description of the OCP in the strong coupling regime ($\Gamma > 1$), but can at best produce results for intermediate

couplings ($\Gamma \lesssim 1$). For $\Gamma > 1$ a new, non-perturbative approach is necessary. Before reviewing such theories, let us enumerate a few criteria against which they can be tested.

A major role in the whole development has been played by the observation that $g_{\text{DH}}(r)$ becomes negative for small r , typically for $k_{\text{D}}r < \varepsilon$. This is easily understood since for small r the particles are always strongly correlated; such an effect is outside the scope of a mean field theory. Therefore, as a first criterion, we require that any reasonable approximation to $g(r)$ should produce only non-negative values of $g(r)$; more precisely, $g(r)$ should be compatible with eq. (3.51) for small r . At the other extreme, for large r , $g(r)$ should be compatible with the position-space sum rules of eqs. (3.31). Via eq. (3.25) the latter can be translated into conditions on the static structure factors $S(k)$ for small k . With the help of eq. (3.30) we obtain:

$$\lim_{k \rightarrow 0} S(k) = 0 \quad (3.54a)$$

$$\lim_{k \rightarrow 0} \frac{k_{\text{D}}^2}{k^2} S(k) = 1 \quad (3.54b)$$

$$\lim_{k \rightarrow 0} \left[\frac{1}{S(k)} - \frac{k_{\text{D}}^2}{k^2} \right] = \frac{\chi_T^0}{\chi_T}. \quad (3.54c)$$

Finally, as a last criterion, we should require any approximate $g(r)$ to reproduce the exact expansion of eq. (3.48) for small ε , while for large ε this $g(r)$ should be compatible with the MC data discussed in subsection 3.4.

The existing strong coupling theories of the OCP statics can be most conveniently subdivided into extended mean-field theories, and the standard theories of ordinary liquids applied to the OCP. In this subsection we shall review the former, leaving the latter for the next subsection.

The large variety of approximations grouped here under the heading of extended mean field (EMF) theories all find their origin in the study of electron correlations at metallic densities. Although these theories are essentially concerned with the quantum version of the OCP, they also have a classical counterpart. Many of these theories have moreover both dynamic and static aspects; here we shall concentrate on the latter, leaving the former aspects for section 4. The starting point of these “extended” MF theories stems from the observation that dramatic errors are introduced into the calculations of the cohesion energy of metals by the incorrect short distance behaviour ($g(r=0) < 0!$) of the correlation functions obtained from the “ordinary” MF theory which in this context is usually referred to as the random phase approximation (RPA) whose classical static version is the DH theory. The first proposal to remedy for this defect was made by Hubbard [3.37]. His theory and its subsequent developments all amount to changing the bare potential appearing in the ordinary MF equations into some effective potential. These theories are therefore often referred to as a RPA with local field corrections. For the sake of clarity we shall not return to the original derivations, but present them from a unified point of view. If we recall that the static dielectric function $\varepsilon(k)$, defined by eq. (3.29), reads in the MF or DH approximation $\varepsilon_{\text{DH}}(k) = 1 + k_{\text{D}}^2/k^2$, we can introduce herein a local field correction, say $t(k)$, most conveniently defined by:

$$\varepsilon(k) = 1 + \frac{k_{\text{D}}^2}{k^2[1 - t(k)]}. \quad (3.55)$$

Returning to eq. (3.29) we see that eq. (3.55) implies that:

$$S(k) = [1 + k_{\text{D}}^2/k^2 - t(k)]^{-1} \quad (3.56)$$

and from eq. (3.20) we see that:

$$\hat{c}(k) = -k_D^2/k^2 + t(k) \quad (3.57)$$

i.e. the local field correction, $t(k)$, is nothing but the “regular” part, $c^R(k)$, of the direct correlation function defined in eq. (3.27). Any relation which expresses the local field correction $t(k)$ in terms of $S(k)$ and/or $\epsilon(k)$ will close the system of defining equations (3.20), (3.29) and (3.55)–(3.57), and produce hereby an (integral) equation which will be the basis of the corresponding EMF theory.

Hubbard’s proposal amounts to replacing in the MF equations the bare Coulomb potential by a phenomenological effective potential $v_{\text{eff}}(r)$ defined by the following force equation:

$$-\nabla v_{\text{eff}}(r) = -g(r)\nabla(Z^2e^2/r). \quad (3.58)$$

The corresponding local field correction reads [3.38]:

$$t(k) = 1 - \left[1 + \frac{1}{n} \int \frac{d\mathbf{k}'}{(2\pi)^3} \frac{\mathbf{k} \cdot \mathbf{k}'}{k'^2} S(\mathbf{k} - \mathbf{k}') \right]^{-1}. \quad (3.59)$$

This correction term leads to some improvement over the RPA values of $g(r)$ for small r . However, since from eq. (3.59) we see that $t(k=0)=0$, whereas the exact result is $t(k=0)=O(\epsilon)$, this proposal clearly leads to an incorrect small ϵ expansion of the thermodynamic properties. At about the same time Singwi et al. [3.39] proposed to close the first BBGKY equation by assuming that the pair correlations are at equilibrium; this ansatz led them to:

$$t(k) = -\frac{1}{n} \frac{k_D^2}{k^2} \int \frac{d\mathbf{k}'}{(2\pi)^3} \frac{\mathbf{k} \cdot \mathbf{k}'}{k'^2} [S(\mathbf{k} - \mathbf{k}') - 1]. \quad (3.60)$$

Eq. (3.60) clearly implies $t(k=0) \neq 0$ and hence leads to corrections to the DH theory; these do not however reproduce eq. (3.48). This defect was corrected in a later proposal [3.40] which reeds:

$$t(k) = -\frac{1}{n} \frac{k_D^2}{k^2} \int \frac{d\mathbf{k}'}{(2\pi)^3} \frac{\mathbf{k} \cdot \mathbf{k}'}{k'^2} \frac{[S(\mathbf{k} - \mathbf{k}') - 1]}{\epsilon(k')}. \quad (3.61)$$

A thorough numerical analysis of this theory has been performed by Berggren [3.41]. Although eq. (3.61) considerably improves the RPA results, many difficulties, such as negative values of $g(r=0)$, remain especially for strong coupling ($\Gamma > 1$). Later improvements of eq. (3.61) by Schneider [3.42] and by Vashista and Singwi [3.43] have focused on the compressibility sum rule (see eq. (3.33)) by replacing $t(k)$ of eq. (3.61) by $t(k) + \frac{1}{2}n\partial t(k)/\partial n$, but these theories run into difficulties with the $O(\epsilon^2 \ln \epsilon)$ term of the compressibility.

A somewhat different approach was put forward by Ichimaru [3.44] who introduced a closure ansatz for the BBGKY hierarchy on the triplet instead of the pair correlations. The ansatz which amounts to writing the triplet correlations as a convolution of the pair correlation functions leads to:

$$t(k) = -\frac{1}{n} \frac{k_D^2}{k^2} \int \frac{d\mathbf{k}'}{(2\pi)^3} \frac{\mathbf{k} \cdot \mathbf{k}'}{k'^2} S(k') [S(\mathbf{k} - \mathbf{k}') - 1]. \quad (3.62)$$

A thorough analysis of eq. (3.62) by Totsuji and Ichimaru [3.45] indicates that $g(r=0)$ is still negative for $\epsilon > 5$, while the $O(\epsilon^2)$ term of the compressibility is incorrect.

Finally, in order to get around the small r problem, Abramo and Tosi [3.46] proposed to meet the small and large r requirements separately by combining the convolution term of the previous authors with the well-known Kirkwood superposition approximation for the triplet correlations which should improve the small r behaviour. This approach leads to the following form for $t(k)$:

$$t(k) = -\frac{1}{n} \frac{k_D^2}{k^2} \int \frac{d\mathbf{k}'}{(2\pi)^3} \frac{\mathbf{k} \cdot \mathbf{k}'}{k'^2} \left\{ S(k') [S(\mathbf{k} - \mathbf{k}') - 1] + \frac{1}{n} \int \frac{d\mathbf{k}''}{(2\pi)^3} [S(\mathbf{k} - \mathbf{k}'') - 1] \right. \\ \left. \times [S(\mathbf{k}' - \mathbf{k}'') - 1] [S(k'') - 1] \right\}. \quad (3.63)$$

Also this attempt fails to meet the basic requirements in a completely satisfactory manner. These authors propose therefore to match the small and large r solution order by order, which is a rather difficult task.

Still another approach was proposed by Golden et al. [3.47]. Instead of looking for an ansatz relating the triplet correlation function to the pair correlations, these authors try to relate the linear and quadratic polarizabilities (in our notation the linear polarizability is just $\epsilon(k) - 1$). Such a relation, together with the quadratic fluctuation-dissipation theorem [3.48] leads to a non-linear equation for the linear polarizability. This method, although shifting the attention from the correlation functions to the polarizabilities, is in fact closely related to the previously discussed EMF theories. Indeed, the contents of the linear and quadratic fluctuation-dissipation theorems is equivalent to, respectively, the first and second equations of the equilibrium BBGKY hierarchy. Relating the quadratic and linear polarizabilities is hence equivalent to relating the triplet and pair correlations. The original closure ansatz between the polarizabilities [3.47] can be written in our notations as:

$$t(k) = 1 - \left[1 - \frac{1}{n} \frac{k_D^2}{k^2} \int \frac{d\mathbf{k}'}{(2\pi)^3} \frac{\mathbf{k} \cdot \mathbf{k}'}{k'^2} \frac{1}{\epsilon(k')} \frac{1}{\epsilon(\mathbf{k} - \mathbf{k}')} \right]^{-1}. \quad (3.64)$$

Attempting to incorporate more and more terms of the limiting weak coupling expansion, these authors have modified their original proposal of eq. (3.64) into a much more complicated one [3.49]. As yet, no numerical investigations have been published for this theory, and hence it is quite impossible to compare it to the previous theories and to draw any definite conclusion.

Although all of the above EMF theories improve in various manners the RPA, it is clear by now that none of them solves in a satisfactory manner the original objectives summarized at the beginning of this section. It is therefore of interest to enquire for alternative theories.

3.7. Strong coupling theories

For many years a number of investigators have tried to apply to the OCP some of the well-known integral equations originally designed to describe the statics of ordinary liquids [3.1]. Various attempts in this direction have been based on the Born–Green–Yvon equation [3.50], the Percus–Yevick (PY) equation [3.51, 3.52], the hypernetted chain (HNC) equation [3.51, 3.52, 3.53] and modifications thereof [3.54]. It soon became clear [3.52, 3.53] that the ordinary HNC equation is by far the most adequate when applied to Coulomb systems. The other integral equations yield poor results when applied to the OCP. In particular the solutions of the PY equation do not satisfy the long wave-length limit (3.34) of the structure factor, since they lead to a k^3 term

in the small k expansion [3.53]. As moreover the HNC equation appears to be superior to the theories discussed in the previous section, we shall discuss it in some detail.

A convenient starting point is the following exact relation for the pair distribution function:

$$g(r) = \exp \{ -\beta v(r) + N(r) + B(r) \} \quad (3.65)$$

where $N(r)$ denotes the sum of nodal diagrams in the Mayer cluster expansion of $g(r)$, and $B(r)$ is the sum of all bridge diagrams [3.1]. The sum of all nodal diagrams can be written as:

$$N(r) = h(r) - c(r) = n \int d\mathbf{r}' c(|\mathbf{r} - \mathbf{r}'|) h(\mathbf{r}') \quad (3.66)$$

where the total (h) and direct (c) correlation functions have been defined in eqs. (3.14–3.17). The HNC approximation amounts to neglecting the contribution of the bridge diagrams in eq. (3.65), so that the HNC equation reads:

$$g(r) = 1 + h(r) = \exp \{ -\beta v(r) + h(r) - c(r) \}. \quad (3.67)$$

Eq. (3.67) together with the Ornstein–Zernike (OZ) relation (3.17) form now a closed set of equations for $h(r)$ and $c(r)$ in terms of the potential $v(r)$, the inverse temperature β and the number density n .

Before discussing the properties of the HNC equation, let us briefly indicate alternative forms. In principle one can eliminate $c(r)$ between eqs. (3.67) and (3.17) by taking the logarithm of both sides of eq. (3.67). This leads to a relatively complicated integral equation for $h(r)$ and in practice one prefers to first compute the Fourier transform $\hat{h}(k)$ and then compute $c(r)$ using the Fourier transform (3.20) of the O.Z. relation:

$$c(r) = \int \frac{d\mathbf{k}}{(2\pi)^3} \frac{\hat{h}(k)}{1 + \hat{h}(k)} e^{i\mathbf{k} \cdot \mathbf{r}} \quad (3.68)$$

and finally substitute this result back into eq. (3.67). Starting from some initial guess for $h(r)$ (or for $c(r)$), a solution can thus be obtained iteratively; but the use of two Fourier transforms at each iteration is one of the major sources of error in the numerical treatment of the HNC equation. For this reason, but also for the purpose of studying the analytic properties of the HNC equation, it is useful to cast it in the following alternative form [3.55]:

$$\hat{c}(k) = -\phi(k) + \frac{1}{n} \int \frac{d\mathbf{k}'}{(2\pi)^3} \frac{\mathbf{k} \cdot \mathbf{k}'}{k'^2} \frac{\hat{c}(\mathbf{k} - \mathbf{k}')}{[1 - \hat{c}(\mathbf{k} - \mathbf{k}')]^2} \frac{[\hat{c}(k')(\phi(k') + \hat{c}(k')) - \phi(k)]}{[1 - \hat{c}(k')]} \quad (3.69)$$

which is a closed relation for $\hat{c}(k) = nc(k)$ in terms of $\phi(k) = \beta\hat{v}(k)$. Equation (3.69) can be easily derived by taking the gradient of both sides of eq. (3.67). We are now in a position to study the properties of solutions of the HNC equation for the OCP:

1) In view of the criteria listed in the previous subsection which should be satisfied by a theory of the OCP statics, it is important to notice that eq. (3.67) implies a non-negative $g(r)$ for all r . We thereby overcome at once the major difficulty encountered by the theories discussed in subsection 3.6.

2) As we expect $c(r = 0)$ and $h(r = 0)$ to be finite, we deduce from eq. (3.58) that:

$$g(r) \simeq \exp \{ -\beta v(r) + h(0) - c(0) \} \quad \text{as } r \rightarrow 0 \quad (3.70)$$

which agrees with the small r behaviour in eq. (3.51).

3) From eq. (3.69) we see that

$$\hat{c}(k) \simeq -\phi(k) \quad \text{as } k \rightarrow 0 \quad (3.71)$$

in agreement with eq. (3.27).

4) Observing that

$$\frac{1}{n} \int \frac{d\mathbf{k}'}{(2\pi)^3} \equiv \varepsilon \int \frac{d\mathbf{k}'}{2\pi^2 k_D^3}$$

we see from eq. (3.69) that the second term in the r.h.s. vanishes with ε , so that we recover the correct Debye–Hückel result:

$$\lim_{\varepsilon \rightarrow 0} \hat{c}(k) = -\phi(k).$$

5) For larger values of ε , eq. (3.69) has to be solved self-consistently and corresponds, in the language of the EMF theories discussed in subsection 3.6, to a local field correction $t(k)$ of the form:

$$t(k) = -\frac{1}{n} \frac{k_D^2}{k^2} \int \frac{d\mathbf{k}'}{(2\pi)^3} \frac{\mathbf{k} \cdot \mathbf{k}'}{k'^2} [S(\mathbf{k} - \mathbf{k}') - 1] S(k') + \frac{1}{n} \int \frac{d\mathbf{k}'}{(2\pi)^3} \frac{\mathbf{k} \cdot \mathbf{k}'}{k^2} h(\mathbf{k} - \mathbf{k}') h(k') t(k') \quad (3.72)$$

where eqs. (3.57) and (3.20) have been used. To lowest order in $\varepsilon (\sim n^{-1})$ we can drop the second term in the r.h.s. of eq. (3.72) which is then seen to reduce to eq. (3.62). Hence the theory proposed by Ichimaru corresponds to the lowest order iterative solution of the self-consistent equation (3.72) characterizing the HNC theory, a result also obtained by Choquard with the aid of field-theoretic methods [3.56]. Hence for small ε , eq. (3.72) will lead to the same small- ε expansion as eq. (3.62), which was shown to agree with eq. (3.48); notice in passing the power raising property, i.e. the $O(\varepsilon^n)$ terms of eq. (3.72) determine the $O(\varepsilon^{n+1})$ thermodynamic properties.

6) It can be shown that the HNC $h(k)$ and the regular part, $c^R(k)$, of $c(k)$ (cf. eq. (3.27)) can be expanded in even powers of k around $k = 0$ [3.53]. Hence $h(r)$ and $c^R(r)$ fall off exponentially as $r \rightarrow \infty$.

From the above discussion we see that the qualitative properties of the HNC equation are quite satisfactory, so that we can now inquire for its quantitative behaviour. Early numerical solutions of the HNC equation for the OCP in the range $\Gamma \leq 2.5$ [3.51] are unreliable because the long range part of the Coulomb potential was not treated correctly. The numerical problems linked to the large- r behaviour were elegantly solved by Springer et al. [3.52] and by Ng [3.53] who split the potential and the direct correlation function into short range and long range parts; only the short range parts occur in the numerical Fourier transforms, avoiding any serious truncation errors. Using this procedure, Springer et al. [3.52] calculated the pair distribution function and the excess internal energy in the range $0.05 \leq \Gamma \leq 50$, whereas Ng obtained extremely accurate solutions in the range $20 \leq \Gamma \leq 7000$; most of Ng's calculations hence cover the metastable fluid phase ($\Gamma \geq 160$). None of the previous investigators apparently realized that the chemical potential, and hence the free energy, are expressible in terms of $g(r)$ in the framework of HNC theory. For the OCP, the formula for the excess chemical potential reads:

$$\beta\mu^{\text{ex}} = \frac{3}{2} \int_0^\infty h(x) N(x) x^2 dx - c^R(k=0) \quad (3.73)$$

where $x = r/a$; $N(x)$ and $c^R(k)$ are defined by eqs. (3.66) and (3.27) respectively. The relation (3.73) is proved in appendix 3. The excess Helmholtz free energy follows from the standard thermodynamic relation:

$$f(\Gamma) = \beta F^{\text{ex}}/N = \beta\mu^{\text{ex}} + \beta P^{\text{ex}}/n = \beta\mu^{\text{ex}} + \frac{1}{3}u. \quad (3.74)$$

Since the free energy calculated in this way is consistent with the HNC equation of state calculated via eq. (3.22) [3.57], the use of eqs. (3.73) and (3.74) avoids the more cumbersome and less accurate calculation via thermodynamic integration.

The HNC results for the internal energy have been fitted by De Witt [3.24] in the range $\Gamma > 1$ with the simple function:

$$\beta U^{\text{ex}}/N = u(\Gamma) = a\Gamma + b\Gamma^{1/2} + c \ln \Gamma + d. \quad (3.75)$$

In view of the high numerical accuracy of the HNC results (eight significant digits in Ng's work!), the functional form (3.75), which leads to a very small standard deviation, can be trusted with a high degree of confidence. The least squares fit leads to the following values of the coefficients:

$$\begin{aligned} a &= -0.900470 ; & b &= 0.2688263 \\ c &= 0.0719925; & d &= 0.0537919. \end{aligned}$$

The asymptotic form (3.75) breaks down for $\Gamma < 1$. Comparison with the expression (3.40) which represents the Monte Carlo result for $\Gamma \gtrsim 1$ calls for the following remarks:

1) Quantitatively the MC and HNC internal energies agree to better than 1% over the whole fluid range. This is essentially due to the predominance of the "static" contribution (linear in Γ) in both cases, the coefficients a differing by less than 0.5%!

2) The "thermal" part of the internal energy varies essentially as $\Gamma^{1/2}$ in the HNC theory, while the "exact" MC results are compatible with a $\Gamma^{1/4}$ behaviour. This explains why the excess specific heat computed from the HNC results differs relatively more from the MC values (as much as 20%) than the internal energy.

3) In the very strong coupling limit ($\Gamma \gg 100$), the HNC excess internal energies violate the Lieb–Narnhofer lower bound $u = -0.9\Gamma$. This occurs however only very far inside the metastable region.

The HNC radial distribution functions agree fairly well with the MC results: they exhibit short range order beyond $\Gamma \approx 3$ and the oscillations are in phase with the "exact" results at all values of Γ . Only the amplitudes of the oscillations are underestimated by HNC theory. The situation is pictured in fig. 5 for $\Gamma = 160$. The HNC direct correlation function also closely resembles its MC counterpart, although, for a given value of Γ , it lies systematically above the MC results, as illustrated in fig. 6; in particular $c(0)/\Gamma \approx -1.22$ for $\Gamma \gtrsim 50$, compared to the "exact" value ≈ -1.33 .

A restricted semi-analytic solution of the HNC equations has been obtained in [3.55].

Despite its great success, the HNC equation applied to the OCP suffers from an internal inconsistency. Indeed the isothermal compressibilities calculated either by differentiating the equation of state (3.75) according to eq. (3.9c), or from the long wave-length limit of $c^R(k)$ (see eq. (3.33)) differ significantly (by as much as 30%!) for all values of Γ , even in the weak coupling limit. Only the "virial" compressibility, calculated by differentiating eq. (3.75), is in good agreement with the "exact" results. Very recently Rosenfeld and Ashcroft [3.58] have made a semi-empirical proposal

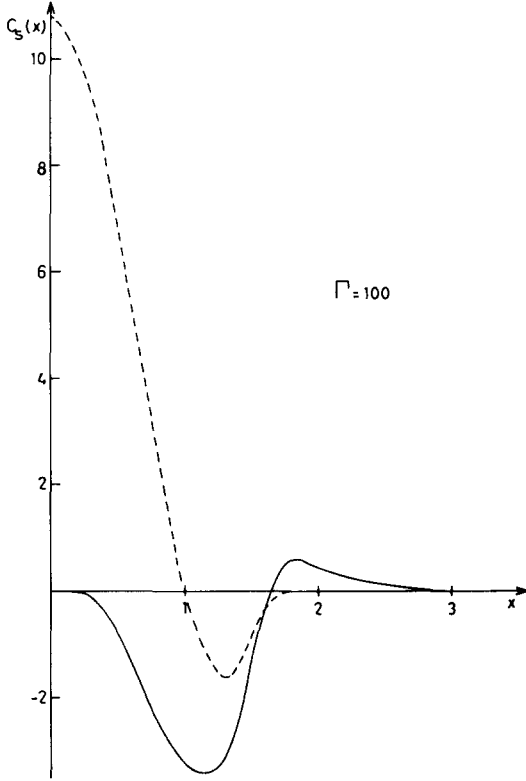


Fig. 6. OCP direct correlation function $c(x)$ versus $x = r/a$. Full curve: $c_s(x) = c(x) + \Gamma \operatorname{erfc}(\alpha x)/x$ from MC data [3.20]; dashed curve: $c_s(x)$ based on HNC results [3.53]. α has been adjusted so that $c_s(x = 0) = 0$ for the MC data ($\alpha = 1.1741$).

to overcome this inconsistency. They have modified the HNC equation (3.67) by approximately including the contribution from the bridge diagrams, $B(r)$ (see eq. (3.65)). The function $B(r)$ is chosen to be of the form valid for a hard sphere (HS) fluid; the packing fraction $\eta = \pi n d^3/6$ (where d is the HS diameter) of the “equivalent” HS fluid is determined by a thermodynamic consistency requirement. The resulting thermodynamics and pair distribution functions are nearly indistinguishable from the “exact” results.

The description of an alternative strong coupling theory based on the “mean spherical approximation” [3.59] is postponed until subsection 5.4.

Before closing this subsection we briefly mention some theoretical work dealing with the solid phase of the O.C.P. In a crystal at low temperature or under high compression (i.e. at high Γ), the particles undergo only small amplitude vibrations. The theory of harmonic lattice dynamics amounts to expanding the total potential energy to second order in the small displacements of the particles from their equilibrium lattice positions. The resulting hamiltonian can be diagonalized by introducing $3N$ normal modes. The corresponding frequencies depend on the wave-vector \mathbf{k} and the polarization and must be computed numerically. For an OCP crystal they satisfy, for every \mathbf{k} , the so-called Kohn sum rule:

$$\sum_{v=1}^3 \omega_v^2(\mathbf{k}) = \omega_p^2 \quad (3.76)$$

where $\omega_p = [4\pi(Ze)^2 n/m]^{1/2}$ is the plasma frequency. Once the normal mode frequencies are known, thermodynamic and other properties can be easily calculated either for the quantum or the classical solid, at any temperature and density. In particular the Helmholtz free energy can be calculated by the standard formula [3.60]:

$$\frac{\beta F}{N} = \frac{1}{N} \sum_{\mathbf{k}}' \sum_{\nu} \ln \left[2 \sinh \frac{\hbar \omega_{\nu}(\mathbf{k})}{2k_B T} \right]. \quad (3.77)$$

The normal mode frequency distribution has been calculated by several authors [2.8, 3.61, 3.23]. Anharmonic corrections have been considered both at zero temperature [3.62, 3.63] and in the classical limit [3.23]. It is interesting to note that the harmonic approximation predicts r.m.s. displacements (see eq. (3.29)) which agree well with the MC results in the classical limit [3.23]. Advantage has been taken of this good agreement to construct the fluid-solid coexistence curve of the OCP in the whole $(n-T)$ plane, including the quantum region, on the assumption of the validity of the Lindemann melting criterion [3.64, 3.23].

4. The dynamic properties of the OCP

As we have seen in section 3, the static properties of the OCP have a very characteristic long-wavelength behaviour which is easily traced back to the infinite range of the Coulomb potential. The dynamical or time-dependent properties of charged fluids can also be expected to exhibit some typical features not encountered in ordinary fluids. This will be especially so when considering the collective modes. Indeed here, any charge imbalance will lead to a dynamic response known as the plasma oscillations. For long wavelengths these typical plasma modes become well-defined and their precise status as compared to the hydrodynamical modes of ordinary fluid systems is one of the most challenging problems in this field. As has become familiar from the study of liquids, the dynamical properties of fluid systems are most conveniently studied via the time-dependent equilibrium correlation functions. For real systems, they provide a direct link between theory and experiment. Here we will therefore limit ourselves to those dynamical properties of the OCP which can be verified at least by numerical experiments. We do start, however, with a few definitions.

4.1. Time-dependent equilibrium correlation functions

Although this topic has been considered many times in the literature, we briefly re-consider it here mainly because we want to establish contact between the usual space-time correlation functions and the less well-known momentum-dependent correlation functions used in the kinetic theories discussed below. We have, however, tried to avoid repeated definitions by gathering the main items here including those requiring a multi-species notation which will be used mainly in subsection 5.3 devoted to the ionic mixtures. For the OCP one should simply drop all species labels while for the single-particle motions of the OCP one can consider the tagged particle as being the unique member of a separate but otherwise undistinguished species. The latter case will be indicated by a subscript “s”.

Coming back to the physics we will study the *collective* (resp. *single particle*) motions by producing a space- and time-dependent fluctuation in a collective (resp. single particle) variable,

i.e. a variable depending on all (resp. one) particles, of a system which is otherwise in equilibrium. If this variable is moreover chosen to be a *conserved* variable then the decay of such a fluctuation will reveal the system's *macroscopic* properties. The most frequently studied variables are the one-body additive variables. The case of the (potential) energy which is two-body additive is discussed in [4.1–2] and will, for simplicity, not be considered here. All one-body additive variables can be obtained from the following one-body phase-space density:

$$f_\sigma(\mathbf{r}pt; \Gamma) = a_\sigma \sum_{j=1}^{N_\sigma} \delta(\mathbf{r} - \mathbf{r}_j(t))\delta(\mathbf{p} - \mathbf{p}_j(t)) \quad (4.1)$$

of the N_σ particles of positions $\mathbf{r}_j(t)$, momenta $\mathbf{p}_j(t)$ and type σ characterised by a charge $Z_\sigma e$, mass m_σ and average number density $n_\sigma = N_\sigma/\Omega$.

In eq. (4.1), $a_\sigma = 1$ except for the self-motions, say $\sigma \equiv s$ and $N_s = 1$, in which case $a_s = N^{1/2}$, N being the total number of ions of the OCP.

The decay of the fluctuations are most conveniently described by considering the two-point correlation function:

$$S_{\sigma\sigma}(\mathbf{r} - \mathbf{r}', t - t'; \mathbf{pp}') = \langle \delta f_\sigma(\mathbf{r}pt)\delta f_\sigma(\mathbf{r}'pt') \rangle_\Omega \quad (4.2)$$

of the equilibrium fluctuation $\delta f_\sigma = f_\sigma - \langle f_\sigma \rangle_\Omega$. In eq. (4.2) $\langle \dots \rangle_\Omega = \int d\Gamma \dots \rho(\Gamma)$ denotes the canonical equilibrium average over the initial phase $\Gamma = \{\mathbf{r}_j(0), \mathbf{p}_j(0)\}$, the canonical distribution $\rho(\Gamma)$ being normalised to one, $\langle 1 \rangle_\Omega = 1$. Henceforth the implicit dependence of f_σ on the initial phase Γ will always be omitted so that elsewhere Γ will always denote the coupling parameter $\Gamma = \beta Z^2 e^2/a$. For many purposes, it will be convenient to consider the Fourier transform (see appendix 1) of eq. (4.2):

$$S_{\sigma\sigma}(\mathbf{k}, t - t'; \mathbf{pp}') = \Omega^{-1} \langle \delta f_\sigma(\mathbf{k}pt)\delta f_\sigma^*(\mathbf{k}pt') \rangle_\Omega \quad (4.3a)$$

$$= (\delta f_\sigma(\mathbf{k}pt)|\delta f_\sigma(\mathbf{k}pt')) \quad (4.3b)$$

which is seen from eq. (4.3a) to be the correlation function of the \mathbf{k} -space fluctuations:

$$\delta f_\sigma(\mathbf{k}pt) = a_\sigma \sum_{j=1}^{N_\sigma} \delta(\mathbf{p} - \mathbf{p}_j(t)) \exp\{-i\mathbf{k} \cdot \mathbf{r}_j(t)\} - a_\sigma N_\sigma \varphi_\sigma(\mathbf{p}) \quad (4.4)$$

$\varphi_\sigma(\mathbf{p}) = (\beta/2\pi m_\sigma)^{3/2} \exp(-\beta p^2/2m_\sigma)$ being the Maxwellian. In eq. (4.3b) we have also introduced a scalar product in phase space, a convenient notation to be used below. Finally, because of the invariance of the equations of motion for space-time reflections, the Fourier- and Laplace-transforms with respect to time (see appendix 1) of eq. (4.3) are related as:

$$S_{\sigma\sigma}(\mathbf{k}\omega; \mathbf{pp}') = S_{\sigma\sigma}(\mathbf{k}, Z = \omega + i0; \mathbf{pp}') + S_{\sigma\sigma}^*(\mathbf{k}, Z = \omega + i0; \mathbf{pp}') \quad (4.5)$$

where, here and in eq. (4.3a), A^* say denotes the complex conjugate of A . Using the standard Mori projection-operator algebra [4.3–5] one can obtain, starting from the Liouville equation $\partial_t f_\sigma = iL f_\sigma$, the following exact kinetic equation:

$$zS_{\sigma\sigma'}(\mathbf{k}z; \mathbf{pp}') - \sum_{\sigma_1} \int d\mathbf{p}_1 \Sigma_{\sigma\sigma_1}(\mathbf{k}z; \mathbf{pp}_1) S_{\sigma_1\sigma'}(\mathbf{k}z; \mathbf{pp}') = iS_{\sigma\sigma'}(\mathbf{k}t = 0; \mathbf{pp}'). \quad (4.6)$$

containing a memory function $\Sigma_{\sigma\sigma'}$ which we split into three distinct parts, say $\Sigma = \Sigma^0 + \Sigma^s + \Sigma^c$, namely a free streaming term:

$$\Sigma_{\sigma\sigma'}^0(\mathbf{k}\mathbf{p}\mathbf{p}') = \frac{\mathbf{k} \cdot \mathbf{p}}{m_\sigma} \delta(\mathbf{p} - \mathbf{p}') \delta_{\sigma\sigma'}, \quad (4.7a)$$

a static self-consistent field term:

$$\Sigma_{\sigma\sigma'}^s(\mathbf{k}\mathbf{p}\mathbf{p}') = - \frac{\mathbf{k} \cdot \mathbf{p}}{m_\sigma} \cdot \frac{n_\sigma}{n_{\sigma'}} \cdot \varphi_\sigma(\mathbf{p}) \cdot c_{\sigma\sigma'}(k), \quad (4.7b)$$

and a non-local collision term:

$$\Sigma_{\sigma\sigma'}^c(\mathbf{k}\mathbf{z}; \mathbf{p}\mathbf{p}') = (\delta f_\sigma(\mathbf{k}\mathbf{p}) | LQ(z - QLQ)^{-1} QL | \delta f_{\sigma'}(\mathbf{k}\mathbf{p}')) (n_{\sigma'} \varphi_{\sigma'}(\mathbf{p}'))^{-1}. \quad (4.7c)$$

In eq. (4.7c) the projection operator $Q = I - P$ is such that P projects any phase space function, say $a(\Gamma)$, onto the one-particle states $|\delta f_\sigma(\mathbf{k}\mathbf{p})\rangle$ according to:

$$P|a\rangle = \sum_{\sigma,\sigma'} \int d\mathbf{p} d\mathbf{p}' \sum_{\mathbf{k}} |\delta f_\sigma(\mathbf{k}\mathbf{p})\rangle \mathcal{P}_{\sigma\sigma'}(\mathbf{k}\mathbf{p}\mathbf{p}') (\delta f_{\sigma'}(\mathbf{k}\mathbf{p}')) |a\rangle \quad (4.8)$$

where:

$$\mathcal{P}_{\sigma\sigma'}(\mathbf{k}\mathbf{p}\mathbf{p}') = \delta_{\sigma\sigma'} \delta(\mathbf{p} - \mathbf{p}') (n_\sigma \varphi_\sigma(\mathbf{p}))^{-1} - c_{\sigma\sigma'}(k)/n_{\sigma'} \quad (4.9)$$

is the matrix inverse of:

$$S_{\sigma\sigma}(\mathbf{k}, t = 0; \mathbf{p}\mathbf{p}') = n_\sigma \varphi_\sigma(\mathbf{p}) [\delta_{\sigma\sigma'} \delta(\mathbf{p} - \mathbf{p}') + h_{\sigma\sigma'}(\mathbf{k}) \varphi_{\sigma'}(\mathbf{p}')] \quad (4.10)$$

as a result of the Ornstein-Zernike relation between the correlation functions $h_{\sigma\sigma'}(k)$ and the direct correlation functions $c_{\sigma\sigma'}(k)$:

$$\sum_{\sigma_1} (\delta_{\sigma\sigma_1} - c_{\sigma\sigma_1}(k)) (\delta_{\sigma_1\sigma'} + h_{\sigma_1\sigma'}(k)) = \delta_{\sigma\sigma'}. \quad (4.11)$$

Notice that in the literature one often encounters the alternative definitions:

$$n_\sigma h_{\sigma\sigma}(k) = (n_\sigma n_{\sigma'})^{1/2} \hat{h}_{\sigma\sigma'}(k) \quad (4.12a)$$

$$c_{\sigma\sigma'}(k) n_{\sigma'} = (n_\sigma n_{\sigma'})^{1/2} \hat{c}_{\sigma\sigma'}(k). \quad (4.12b)$$

Next we shift our attention to the momentum-independent, or purely space-time dependent, correlation functions which can be obtained by taking moments of eq. (4.6) with respect to the momentum variables. This is most easily performed with the aid of the following scalar product in momentum space:

$$\langle u | \bar{A} | v \rangle = \sum_{\sigma,\sigma'} \int d\mathbf{p} d\mathbf{p}' u_\sigma(\mathbf{p}) A_{\sigma\sigma'}(\mathbf{p}\mathbf{p}') v_{\sigma'}^*(\mathbf{p}') n_{\sigma'} \varphi_{\sigma'}(\mathbf{p}') \quad (4.13)$$

where $u_\sigma(\mathbf{p})$ are the σ - \mathbf{p} components of the abstract vector $|u\rangle$ whereas $A_{\sigma\sigma'}(\mathbf{p}\mathbf{p}')$ denote the matrix elements of the abstract \bar{A} . We will also denote by $|u_{\sigma_1}\rangle$ the vector whose σ - \mathbf{p} components are $\delta_{\sigma\sigma_1} u_\sigma(\mathbf{p})$ while $I_{\sigma\sigma'}(\mathbf{p}\mathbf{p}') = \delta_{\sigma\sigma'} \delta(\mathbf{p} - \mathbf{p}')$ represents the unit operator which is such that $\langle a | I | b \rangle \equiv \langle a | b \rangle$. Introducing finally a complete ortho-normalized set in momentum space, $\langle i_\sigma | i'_{\sigma'} \rangle = \delta_{\sigma\sigma'} \delta_{ii'}$, we define the space-time correlation functions $G_{ij}^{\sigma\sigma'}(\mathbf{k}\mathbf{z}) = \langle i_\sigma | \bar{S}(\mathbf{k}\mathbf{z}) | j_{\sigma'} \rangle$ where $\bar{S}(\mathbf{k}\mathbf{z})$ has $S_{\sigma\sigma'}(\mathbf{k}\mathbf{z}; \mathbf{p}\mathbf{p}') \times (n_{\sigma'} \varphi_{\sigma'}(\mathbf{p}'))^{-1}$ as components. We will henceforth only be interested in a restricted set of momentum states closely related to the multi-fluid hydrodynamic variables. These can be thought of as

the first members of the complete basis $|i_\sigma\rangle$ represented by $i_\sigma(\mathbf{p}) = u_\sigma^i(\mathbf{p})/a_\sigma^i$, a_σ^i being a normalisation constant. The states of interest to us are then: 1) the density state denoted by $|n_\sigma\rangle$ with $u_\sigma^n(\mathbf{p}) = 1$, $(a_\sigma^n)^2 = n_\sigma$; 2) the longitudinal momentum state $|l_\sigma\rangle$ with $u_\sigma^l(\mathbf{p}) = \hat{\mathbf{k}} \cdot \mathbf{p}$, $(a_\sigma^l)^2 = n_\sigma m_\sigma \beta^{-1}$; 3) the transverse momentum states $|t_i\rangle$ ($i = 1, 2$) with $u_\sigma^{t_i}(\mathbf{p}) = \mathbf{t}_i(\mathbf{k}) \cdot \mathbf{p}$, $a_\sigma^{t_i} = a_\sigma^l$ such that $\mathbf{t}_1(\mathbf{k}), \mathbf{t}_2(\mathbf{k}), \hat{\mathbf{k}} = \mathbf{k}/|\mathbf{k}|$ form an orthogonal system of unit vectors and, 4) the excess kinetic energy state $|\varepsilon_\sigma\rangle$ with $u_\sigma^\varepsilon(\mathbf{p}) = \mathbf{p}^2/2m_\sigma - \frac{3}{2}\beta^{-1}$ and $(a_\sigma^\varepsilon)^2 = \frac{3}{2}n_\sigma\beta^{-2}$. For each σ these states will be designed as $|i_\sigma\rangle$, $i = 1, \dots, 5$. Projecting now eq. (4.6) onto these momentum states with the aid of $\bar{P} = \sum_{i=1}^5 |i_\sigma\rangle \langle i_\sigma|$ we obtain, applying once more the Mori-algebra, a set of transport equations:

$$\sum_{\sigma_1} \sum_{j_1=1}^5 (z\delta_{jj_1}\delta_{\sigma\sigma_1} - \Omega_{jj_1}^{\sigma\sigma_1}(kz)) G_{j_1 j'}^{\sigma\sigma'}(kz) = iG_{jj'}^{\sigma\sigma'}(k, t=0) \quad (4.14)$$

for the multi-fluid hydrodynamic correlation functions $G_{ij}^{\sigma\sigma'}(kz)$ ($i, j = 1, \dots, 5$), involving a transport matrix:

$$\Omega_{ij}^{\sigma\sigma'}(kz) = \langle i_\sigma | \bar{\Sigma} | j_{\sigma'} \rangle + \langle i_\sigma | \bar{\Sigma} \bar{Q}(z - \bar{Q}\bar{\Sigma}\bar{Q})^{-1} \bar{Q} \bar{\Sigma} | j_{\sigma'} \rangle \quad (4.15)$$

where $\bar{Q} = \bar{I} - \bar{P}$ whereas the matrix elements, $\Sigma_{\sigma\sigma'}(\mathbf{k}z; \mathbf{pp}')$ of $\bar{\Sigma}$ have been defined in eq. (4.7). This is as far as we need to go here. More details can be found in the original works of Akcasu and Duderstadt [4.3], Forster and Martin [4.4], Mazenko [4.5], Gross [4.2] and Baus [4.6]. Before closing this subsection we introduce a more standard notation for the frequently used space-time correlation functions. The correlation function of number- and charge-density are defined, respectively, by:

$$S_{nn}(\mathbf{r}, t) = \sum_{\sigma, \sigma'} \int d\mathbf{p} d\mathbf{p}' S_{\sigma\sigma'}(\mathbf{r}, t; \mathbf{pp}') = \sum_{\sigma, \sigma'} (n_\sigma n_{\sigma'})^{1/2} G_{nn}^{\sigma\sigma'}(\mathbf{r}, t) \quad (4.16a)$$

and:

$$S_{\rho\rho}(\mathbf{r}, t) = \sum_{\sigma, \sigma'} Z_\sigma Z_{\sigma'} e^2 \int d\mathbf{p} d\mathbf{p}' S_{\sigma\sigma'}(\mathbf{r}, t; \mathbf{pp}') = \sum_{\sigma, \sigma'} Z_\sigma Z_{\sigma'} e^2 (n_\sigma n_{\sigma'})^{1/2} G_{nn}^{\sigma\sigma'}(\mathbf{r}, t). \quad (4.16b)$$

For the OCP the fluctuations in number, mass and charge densities are proportional to each other and hence it is sufficient to consider the unique quantity:

$$S(\mathbf{r}, t) = S_{nn}(\mathbf{r}, t) = S_{\rho\rho}(\mathbf{r}, t)/Z^2 e^2 \quad (\text{OCP}) \quad (4.17)$$

which is usually called the Van Hove or intermediate scattering function, $S(\mathbf{k}, t)$ being the dynamic generalisation of the static structure factor $S(\mathbf{k})$ of eq. (3.18) to which it reduces at $t = 0$:

$$S(\mathbf{k}, t=0) = nS(\mathbf{k}) \quad (\text{OCP}) \quad (4.18)$$

while $S(\mathbf{k}, \omega)$ is the so-called dynamic structure factor. Notice that in the case of the self-motions, $S_s(\mathbf{k}, t)$, we have $S_s(\mathbf{k}, t=0) = n$ instead of eq. (4.18). Similarly, the fluctuations in the mass- and electric-currents are proportional in the OCP and, because of rotational invariance, it will be sufficient to consider the longitudinal (i.e. along \mathbf{k}) and transverse (i.e. perpendicular to \mathbf{k}) mass current correlation functions defined by:

$$S_l(\mathbf{k}, t) = nm\beta^{-1} G_{ll}(\mathbf{k}, t) \quad (\text{OCP}) \quad (4.19a)$$

$$S_\perp(\mathbf{k}, t) = nm\beta^{-1} G_{t_i t_i}(\mathbf{k}, t) \quad (i = 1, 2) \quad (\text{OCP}). \quad (4.19b)$$

Moreover, because of mass conservation, we have $m^2 \partial_t^2 S(\mathbf{k}, t) = k^2 S_l(\mathbf{k}, t)$, hence a thorough knowledge of the collective- and single-particle motions of the OCP can be obtained from the three *independent* correlation functions: $S(\mathbf{k}, t)$, $S_{\perp}(\mathbf{k}, t)$ and $S_s(\mathbf{k}, t)$. A final quantity which will be used frequently is the dielectric constant $\epsilon(k, z)$ defined, in general, from eq. (4.16b) by:

$$\frac{1}{\epsilon(kz)} = 1 - \frac{4\pi\beta}{k^2} (izS_{\rho\rho}(kz) + S_{\rho\rho}(k, t=0)) \quad (4.20a)$$

and which for the OCP is usually written as:

$$\frac{1}{\epsilon(kz)} = 1 - \frac{k_D^2}{k^2} \chi(kz) \quad (\text{OCP}) \quad (4.20b)$$

where eq. (4.17) has been used, whereas $\chi(kz) = S(k) + izS(kz)/n$ is the susceptibility.

4.2. Short-time behaviour

Now that we have defined the objects of major interest to us, we come back to the OCP and just as we did for the static case in subsection 3.3, look for a number of limiting values against which the theoretical predictions can be easily checked. We start by relating the short-time behaviour of the time-dependent correlation functions to the system's static properties. That this is possible is already clear from eq. (4.18). To proceed in a somewhat more general setting, we can relate:

(1) the short-time Taylor expansion of $S(kt; \mathbf{pp}')$:

$$S(kt; \mathbf{pp}') = \sum_{n=0}^{\infty} \frac{t^n}{n!} a_n(\mathbf{k}; \mathbf{pp}') \quad (4.21)$$

(2) the high-frequency expansion of $S(kz; \mathbf{pp}')$:

$$S(kz; \mathbf{pp}') = \frac{i}{z} \sum_{n=0}^{\infty} \frac{i^n}{z^n} a_n(\mathbf{k}; \mathbf{pp}') \quad (4.22)$$

(3) the frequency moments of $S(k\omega; \mathbf{pp}')$:

$$\int_{-\infty}^{\infty} \frac{d\omega}{2\pi} (-i\omega)^n S(k\omega; \mathbf{pp}') = a_n(\mathbf{k}; \mathbf{pp}') \quad (4.23)$$

to:

$$a_n(\mathbf{k}; \mathbf{pp}') = \Omega^{-1} \langle \delta f(-\mathbf{k}\mathbf{p}'t = 0) (iL)^n \delta f(\mathbf{k}\mathbf{p}t = 0) \rangle_{\Omega} \quad (4.24)$$

which is an equilibrium quantity which in principle can be computed explicitly. Similar expressions also hold for $S_s(kt; \mathbf{pp}')$. The information contained in eqs. (4.21–24) has played an important role in the theory of liquids [1.2]. The reason why we have to repeat it here is that for the OCP the final expressions come out slightly different because of the presence of the background and of the fact that one cannot freely integrate by parts over the Coulomb potential because of its slow decay at large distances. As is well known, the explicit evaluation of $a_n(\mathbf{k}; \mathbf{pp}')$ becomes rapidly, as n increases, very cumbersome and involves inaccessible higher-order correlation functions. Only

the first few terms are therefore important. Some of them have been computed with their full momentum dependence [4.3–4] but here we shall restrict ourselves to the most useful ones:

$$a_n(k) = \int d\mathbf{p} d\mathbf{p}' a_n(\mathbf{k}; \mathbf{pp}') \quad (4.25a)$$

$$a_n^\perp(k) = \int d\mathbf{p} d\mathbf{p}' \mathbf{t}(\mathbf{k}) \cdot \mathbf{p} \mathbf{t}(\mathbf{k}) \cdot \mathbf{p}' a_n(\mathbf{k}; \mathbf{pp}') \quad (4.25b)$$

$$a_n^s(k) = \int d\mathbf{p} d\mathbf{p}' a_n^s(\mathbf{k}; \mathbf{pp}') \quad (4.25c)$$

corresponding respectively to $S(k, t)$, $S_\perp(k, t)$ and $S_s(k, t)$. The known results are summarized in table 2.

Table 2

The available sum rules for $S(k, t)$, $S_\perp(k, t)$ and $S_s(k, t)$. We have put $\omega_p^2 = 4\pi Z^2 e^2 n/m$ and $v_0^2 = (m\beta)^{-1}$ while the detailed expressions of $I_i(k)$ ($i = 1, \dots, 4$) are given in [1.5, 3.9, 4.7, 4.8]

p	$a_p(k)/n$	$a_p^\perp(k)/nm\beta^{-1}$	$a_p^s(k)/n$
0	$S(k) = 1 + h(k)$	1	1
2	$-(kv_0)^2$	$-(kv_0)^2 - \omega_p^2 I_1(k)$	$-(kv_0)^2$
4	$3(kv_0)^4 + (kv_0)^2 \omega_p^2 (1 - 2I_1(k))$	$3(kv_0)^4 + (kv_0)^2 \omega_p^2 I_2(k)$	$3(kv_0)^4 + (kv_0)^2 \omega_p^2 / 3$
6	$-15(kv_0)^6 - (kv_0)^2 \omega_p^4 I_3(k)$	unavailable	$-15(kv_0)^6 - (kv_0)^2 \omega_p^4 I_4(k)$

A few remarks are in order. As all the correlation functions considered in table 2 are even functions of time, no odd n -values have to be considered here. This would not have been the case if we had retained the momentum dependence. All the results of table 2 naturally split into kinetic and potential contributions. The potential contributions are of two distinct types: those involving simply $\omega_p^2 = 4\pi Z^2 e^2 n/m$ and those containing Γ -dependent information through the integrals $I_n(k)$ ($n = 1, \dots, 4$) over the two- and three-body correlation functions. For instance, $I_1(k)$ is given by:

$$I_1(k) = \int_0^\infty \frac{dr}{r} \left(\frac{\sin kr}{kr} + \frac{3 \cos kr}{(kr)^2} - \frac{3 \sin kr}{(kr)^3} \right) (g(r) - 1) \quad (4.26)$$

which involves only the pair correlations $g(r)$ while I_2 , I_3 and I_4 involve complicated contributions from the triple correlations which can be found in [1.5, 3.9, 4.7, 4.8]. Most of the potential terms differ from their neutral liquid analogue. As a typical example, we can consider a_4^s . For an ordinary fluid we would have ($v_0 = (m\beta)^{-1/2}$):

$$a_4^s(k) = n(kv_0)^2 \left[3(kv_0)^2 + \frac{n}{3m} \int dr g(r) \nabla^2 v(r) \right] \quad (4.27)$$

in which for the OCP we have to replace $g(r)$ by $h(r) = g(r) - 1$ as a result of the presence of the background. For an ordinary potential this difference would reduce to a surface term and would not affect a_4^s . For the Coulomb potential, however, we have Poisson's equation, $\nabla^2 v(r) = -4\pi e^2 \delta(r)$ and hence $\int dr h(r) \nabla^2 v(r)$ reduces to $g(0) - 1$. As moreover $g(0) = 0$ we obtain the result listed in table 2 which, contrary to what happens for an ordinary fluid, is independent of the statics.

4.3. The long-wavelength behaviour

As stated above, the short-time behaviour very rapidly involves inaccessible information about the statics. It is thus of interest to inquire for other constraints on the dynamic behaviour of the OCP. For ordinary fluids, it is well known [1.3] that at the other extreme of long times the dynamic behaviour of the fluid becomes, at least in the macroscopic region of long-wavelengths, severely restricted by the conservation laws in such a way that a contracted description in terms of a few (conserved) variables and a few parameters (the thermodynamic and transport coefficients) becomes possible. This behaviour, usually referred to as hydrodynamic behaviour because it agrees with the predictions of the linearised hydrodynamic equations, is also reflected in the equilibrium space-time correlation functions of interest to us. For an ordinary fluid, one obtains in the long-time long-wavelength limit (indicated here by the superscript H) [1.3]:

$$S_{\perp}^H(k, t) = nm\beta^{-1} \exp(-k^2\eta t/nm) \quad (4.28a)$$

$$S_s^H(k, t) = n \exp(-k^2 D t) \quad (4.28b)$$

$$S^H(k, t) = n \frac{\chi_T}{\chi_T^0} \left[\left(1 - \frac{C_v}{C_p} \right) \exp(-k^2 \kappa t/nm C_p) + \frac{C_v}{C_p} \cos \bar{c} k t \exp(-k^2 \Gamma_n t) \right] \quad (4.28c)$$

where nm is the mass density, C_v/C_p the specific heat ratio, χ_T/χ_T^0 the dimensionless isothermal compressibility, \bar{c} the isentropic sound speed, η the shear viscosity, D the self-diffusion coefficient, κ the thermal conductivity and

$$\Gamma_n = \left[\frac{4}{3}\eta + \xi + \kappa \left(\frac{1}{C_v} - \frac{1}{C_p} \right) \right] / nm$$

the sound absorption coefficient involving moreover the bulk viscosity ξ . Unfortunately eqs. (4.28) represent only an asymptotic result and hence are accessible only with difficulty in real and numerical experiments. Nevertheless eqs. (4.28) severely limit the possible forms of the correlation functions and are of interest as such because they reveal all of the system's macroscopic parameters.

These results, eqs. (4.28), which are usually obtained from the Landau–Placzek theory (based on hydrodynamic plus thermodynamic fluctuation theory [1.2, 4.9]) can be very easily obtained from the microscopic theory [4.4, 4.6] sketched in subsection 4.1. Indeed the interplay between the system's microscopic conservation laws and its rotational invariance leads us, for the OCP, immediately to the following form for the non-vanishing elements of the transport matrix $\Omega_{ij}(kz)$ of eq. (4.15):

$$\Omega_{nl}(kz) = kv_0 \quad (4.29a)$$

$$\Omega_{ln}(kz) = kv_0(1 - \hat{c}(k)); \quad \Omega_{ll}(kz) = -ik^2 D_l(kz); \quad \Omega_{le}(kz) = kD_{le}(kz) \quad (4.29b)$$

$$\Omega_{el}(kz) = kD_{el}(kz); \quad \Omega_{ee}(kz) = -ik^2 D_e(kz) + zB_e(z) \quad (4.29c)$$

$$\Omega_{t_1 t_1}(kz) = \Omega_{t_2 t_2}(kz) = -ik^2 D_\perp(kz) \quad (4.29d)$$

$$\Omega_{nn}^s(kz) = -ik^2 D(kz) \quad (4.29e)$$

where eq. (4.29e) refers to the self-motions. Solving now the algebraic system (4.14) we obtain:

$$S_\perp(kz) = \frac{inm\beta^{-1}}{z + ik^2 D_\perp(kz)}; \quad S_s(kz) = \frac{in}{z + ik^2 D(kz)} \quad (4.30)$$

because for the self-motions there is only one conserved variable whereas in an isotropic system the transverse momentum decouples from the remaining collective variables, and:

$$S(kz) = inS(k) \left[\frac{(z + ik^2 D_l(kz))(z + ik^2 \alpha_e(kz)) - k^2 \gamma_{le}(kz)}{(z^2 - \omega^2(k) + zik^2 D_l(kz))(z + ik^2 \alpha_e(kz)) - zk^2 \gamma_{le}(kz)} \right] \quad (4.31)$$

where we have used the following abbreviations:

$$\omega^2(k) = (kv_0)^2(1 - \hat{c}(k)); \quad \alpha_e(kz) = \frac{D_e(kz)}{1 - B_e(z)}; \quad \gamma_{le}(kz) = \frac{D_{le}(kz)D_{el}(kz)}{1 - B_e(z)} \quad (4.32)$$

with $v_0 = (m\beta)^{-1/2}$. The main point here is that the various $D_{ij}(kz)$ functions appearing in eqs. (4.29) are to be regular at $k = 0$ and $z = 0$ if a hydrodynamic transport regime is to exist. If this is the case, then we have succeeded, by using only first principles, in building up successive equations connecting the microscopic mechanical description to the macroscopic hydrodynamical description. Indeed in the macroscopic region of small k and z hydrodynamic poles are seen, from eqs. (4.30–31), to show up in $S_\perp(kz)$, $S_s(kz)$ and $S(kz)$ which, for an ordinary fluid, ultimately lead to eqs. (4.28). Hence in the macroscopic region the transport equations (4.14) become equivalent to the linearised hydrodynamic equations with an explicit microscopic identification of the various transport coefficients:

$$\eta = nmD_\perp(\mathbf{0}\mathbf{0}); \quad D = D_s(\mathbf{0}\mathbf{0}) \quad (4.33a)$$

$$\frac{4}{3}\eta + \xi' = nmD_l(\mathbf{0}\mathbf{0}); \quad \xi'' = nmi \left. \frac{d\gamma_{le}(0z)}{dz} \right|_{z=+i0} \quad (4.33b)$$

$$\kappa = nmC_v\alpha_e(\mathbf{0}\mathbf{0}) \quad (4.33c)$$

where $\xi = \xi' + \xi''$, together with the thermodynamic parameters:

$$\frac{\chi_T}{\chi_T^0} = (1 - c^R(0))^{-1}; \quad \frac{C_v}{C_p} \cdot \bar{c}^2 = v_0^2(1 - c^R(0)) \quad (4.34a)$$

$$\bar{c}^2 \left(1 - \frac{C_v}{C_p} \right) = \gamma_{le}(\mathbf{0}\mathbf{0}); \quad \frac{C_v}{C_v^0} = 1 - B_e(0) \quad (4.34b)$$

where the superscript zero refers to the ideal gas value, while $c^R(k)$ denotes the regular part of $\hat{c}(k)$ (see eq. (3.27)) so as to make eq. (4.34a) also applicable to the OCP. Whereas in general everything will go through both for an ordinary fluid and the OCP, this is not the case for the density fluctuations $S(k, t)$ of the OCP for which, instead of the celebrated formula (4.28c) one obtains as shown by Baus [3.5]:

$$S^H(k, t) = n \frac{k^2}{k_D^2} \left\{ \left(1 - \frac{C_v}{C_p} \right) \frac{k^2 \bar{c}^2}{\omega_p^2} \exp(-k^2 \kappa t / nm C_v) + \left(1 - \frac{k^2 \operatorname{Re} \gamma_{le}(\theta, \omega_p)}{\omega_p^2} \right) \cos \left[\omega_p \left(1 + \frac{k^2}{2} \gamma_p \right) t \right] \exp \left[-\frac{k^2}{2} \Gamma_p t \right] \right\} \quad (4.35)$$

which differs from eq. (4.28c) because: 1) the overall amplitude given by $S^H(k, t = 0)$ is very small ($\sim k^2/k_D^2$), 2) the central Rayleigh peak has a vanishingly small amplitude ($\sim k^2 \bar{c}^2/\omega_p^2$), 3) the width of this Rayleigh peak differs by a factor C_v/C_p from its ordinary fluid counterpart (see eq. (4.28c)), 4) the Brillouin peaks are no longer due to sound modes but to the high-frequency plasma oscillations which by themselves exhaust the (small k) sum-rule

$$S^H(k, t = 0) = \int \frac{d\omega}{2\pi} S^H(k\omega),$$

5) the small k dispersion (γ_p) and damping (Γ_p) of the plasma modes can be given the following exact microscopic expression [3.5]:

$$\gamma_p = \frac{C_v}{C_p} \cdot \frac{\bar{c}^2}{\omega_p^2} + \frac{\operatorname{Re} \gamma_{le}(\theta \omega_p)}{\omega_p^2} + \frac{\operatorname{Im} D_l(\theta \omega_p)}{\omega_p} \quad (4.36a)$$

$$\Gamma_p = \operatorname{Re} D_l(\theta \omega_p) - \frac{\operatorname{Im} \gamma_{le}(\theta \omega_p)}{\omega_p}, \quad (4.36b)$$

where eq. (4.34a) has been used, but these expressions cannot be further related to the thermodynamic or transport coefficients as is the case for the sound modes. This profound modification of $S^H(k, t)$ is the most important macroscopic manifestation of the Coulomb effects on the dynamics of the OCP.

4.4. The hydrodynamic limit

The emergence of hydrodynamic behaviour in the limit of long times and small wavevectors is one of the central themes of present day statistical physics. As stated above, this results directly from the conservation- and invariance laws under the very weak assumption of analyticity of the various $D_{ij}(kz)$ functions of eqs. (4.29) in the vicinity of $z = 0$ and $k = 0$. In this sense does the microscopic theory of subsections 4.1 and 4.3 constitute a proof of the relevance of the macroscopic equations of hydrodynamics together with the validity of the Green–Kubo formulae for the transport coefficients appearing in them. The statistical mechanical description has hereby reached its basic goal in connecting the microscopic to the macroscopic equations. This, however, is true only for the ordinary fluid. Indeed a straightforward application of the Landau–Placzek method to the macroscopic hydrodynamic equations of the OCP has led Vieillefosse and Hansen [3.9] to a result which differs from eqs. (4.35–36). We feel that this point is worth a more detailed discussion, and we will devote the present subsection to it. That a difficulty should arise here is already apparent from the fact that in the OCP the longitudinal waves are no longer low-frequency sound-waves but high-frequency (even at $k = 0$) plasma-waves and that such rapid variations are certainly not correctly described by the low-frequency hydrodynamical equations. In fact, one can wonder why hydrodynamics should describe plasma oscillations at all. The answer to this is to be found

in the fact that for the OCP one slightly modifies the usual macroscopic hydrodynamic equations by adding a posteriori a term to the momentum balance equation to account for the macroscopic electric field set up by a macroscopic charge imbalance or, equivalently, by adding the electric stresses to the usual mechanical stress tensor. Explicitly, one writes [3.9, 4.10] for the local stress tensor σ :

$$\sigma(\mathbf{r}, t) = p(\mathbf{r}, t)\mathbf{1} - \eta(\nabla\mathbf{u}(\mathbf{r}, t) + \tilde{\nabla}\mathbf{u}(\mathbf{r}, t)) - (\xi - \frac{2}{3}\eta)\mathbf{1}\nabla \cdot \mathbf{u}(\mathbf{r}, t) + Z\epsilon\varphi(\mathbf{r}, t)\mathbf{1} \quad (4.37)$$

where the terms involving the pressure p and the velocity field \mathbf{u} correspond to the standard mechanical stresses whereas the term involving the electric potential $\varphi(\mathbf{r}, t)$, related to the charge density by Poisson's equation, accounts for the electric stresses. Although this is quite reasonable from a macroscopic point of view, the microscopic justification of this procedure is not straightforward. Indeed, if we remind ourselves of the kinetic theoretical derivation of the hydrodynamic equations, then the electric stresses in eq. (4.37) are easily traced back to the presence of a self-consistent electric field term in any kinetic equation describing the OCP. If one is willing to proceed with the derivation of the hydrodynamic equations one has then to perform a Chapman–Enskog expansion [4.9] of this kinetic equation. This expansion is, however, based on the fact that in the small-gradient region of interest to hydrodynamics the kinetic equation is always dominated by the collision term so that the remaining terms can be treated as small perturbations. In the case of the OCP, the self-consistent field term can, however, not be considered as small since its straightforward small-gradient expansion diverges with the characteristic Coulomb divergence [4.11]. For the OCP the condition that the kinetic equation be collision dominated for small k becomes a *supplementary* condition which was roughly estimated by Baus [4.12] as:

$$\omega_c/\omega_p > k_D/k > 1 \quad (4.38)$$

where the magnitude of the collision term was estimated by the collision frequency ω_c . For a weakly coupled OCP we have, as is well known (see e.g. [4.12]), $\omega_c \sim \lambda\omega_p \ln \lambda^{-1}$ with $\lambda \sim \Gamma^{3/2}$ (see eq. (3.7)) and eq. (4.38) cannot be satisfied. Hence, no hydrodynamic description of a weakly coupled OCP is to be expected. As Γ increases we also expect ω_c to increase (although no formal proof of this statement is known to us) so that eq. (4.38) is eventually satisfied for a strongly coupled OCP. A nice illustration of this *approximate* character, even for small k , of the hydrodynamic description of the OCP is provided by comparing the results obtained for $S(k, t)$ from: 1) the microscopic theory of subsection 4.3 leading to eq. (4.35) and 2) the Landau–Placzek method applied to the linearised hydrodynamic equations modified for the OCP as indicated in eq. (4.37). As far as the (small) Rayleigh peak is concerned, the agreement between both methods is complete. This is clearly related to the fact that the thermal mode is a low-frequency mode. The results for the Brillouin doublet of plasma modes do differ however. If we distinguish the values obtained from the macroscopic theory [3.9] from those of [4.12] by a prime, both sets of results read:

$$A_p = 1 - \frac{k^2 \operatorname{Re} \gamma_{le}(0\omega_p)}{\omega_p^2}, \quad A'_p = 1 - \frac{k^2 \bar{c}^2}{\omega_p^2} \left(1 - \frac{C_v}{C_p} \right) \quad (4.39a)$$

$$\gamma_p = \frac{C_v}{C_p} \cdot \frac{\bar{c}^2}{\omega_p^2} + \frac{\operatorname{Re} \gamma_{le}(0\omega_p)}{\omega_p^2} + \frac{\operatorname{Im} D_l(0\omega_p)}{\omega_p}; \quad \gamma'_p = \frac{\bar{c}^2}{\omega_p^2} \quad (4.39b)$$

$$\Gamma_p = \operatorname{Re} D_l(0\omega_p) - \operatorname{Im} \gamma_{le}(0\omega_p)/\omega_p; \quad \Gamma'_p = (\frac{4}{3}\eta + \xi' + \xi'')/nm \quad (4.39c)$$

where the notation of eqs. (4.35–36) has been used while A_p denotes the amplitude of the plasmon doublet (compare eq. (4.39a) with eq. (4.35)). As expected, in the macroscopic theory, the amplitude (A'_p), dispersion (γ'_p) and damping (Γ'_p) of the plasma modes are expressed in terms of the thermodynamic (\bar{c} , C_v/C_p) and transport ($\eta, \xi = \xi' + \xi''$) properties whereas the microscopic theory yields closely related (compare eqs. (4.39) with eqs. (4.33–34)) but different expressions. In the weak-coupling ($\Gamma \rightarrow 0$) or nearly collisionless ($\omega_c/\omega_p \rightarrow 0$) regime we obtain for eqs. (4.39):

$$\lim_{\Gamma \rightarrow 0} A_p = 1 - \frac{2}{3} \frac{k^2 v_0^2}{\omega_p^2} = \lim_{\Gamma \rightarrow 0} A'_p \quad (4.40a)$$

$$\lim_{\Gamma \rightarrow 0} \gamma_p = \frac{v_0^2}{\omega_p^2} + \frac{2}{3} \frac{v_0^2}{\omega_p^2} + \frac{4}{3} \frac{v_0^2}{\omega_p^2} \equiv 3 \frac{v_0^2}{\omega_p^2} \neq \lim_{\Gamma \rightarrow 0} \gamma'_p = \frac{5}{3} \frac{v_0^2}{\omega_p^2} \quad (4.40b)$$

$$\lim_{\Gamma \rightarrow 0} \Gamma_p = O(\Gamma^{3/2}) \neq \lim_{\Gamma \rightarrow 0} \Gamma'_p = O(\Gamma^{-3/2}) \quad (4.40c)$$

and we indeed find that the hydrodynamic equations are not applicable to a weakly coupled OCP. In the opposite limit of strong coupling ($\Gamma \gg 1$) we expect the collisions to dominate ($\omega_p/\omega_c \rightarrow 0$) so that $\gamma_{le}(0\omega_p)$ and $D_l(0\omega_p)$ become eventually well approximated by their low-frequency values: $\gamma_{le}(00)$ and $D_l(00)$. If this is the case, we obtain, using eqs. (4.33–34), from eqs. (4.39):

$$\lim_{\omega_c \gg \omega_p} A_p = 1 - \frac{k^2 \bar{c}^2}{\omega_p^2} \left(1 - \frac{C_v}{C_p} \right) + O(\omega_p/\omega_c) \quad (4.41a)$$

$$\lim_{\omega_c \gg \omega_p} \gamma_p = \frac{C_v}{C_p} \cdot \frac{\bar{c}^2}{\omega_p^2} + \left(1 - \frac{C_v}{C_p} \right) \frac{\bar{c}^2}{\omega_p^2} + O(\omega_p/\omega_c) \quad (4.41b)$$

$$\lim_{\omega_c \gg \omega_p} \Gamma_p = (\frac{4}{3}\eta + \xi')/nm + O(\omega_p/\omega_c). \quad (4.41c)$$

Here the agreement with the macroscopic treatment is striking. Indeed comparing eqs. (4.41) with eqs. (4.39) we see that, taking into account that ξ'' is of higher order with respect to ω_p/ω_c than ξ' , the agreement is complete to dominant order in ω_p/ω_c . Notice, however, that A_p and γ_p differ from A'_p and γ'_p when terms of higher order in ω_p/ω_c are retained. As the macroscopic description becomes better with increasing ω_c/ω_p , i.e. presumably with increasing Γ , this immediately raises the question of just how strong the coupling Γ has to be for the hydrodynamic equations to become applicable. This is, in our opinion, one of the most challenging problems in this field and hopefully more attention will be given to it in the near future.

4.5. Computer “experiments”

It was shown in subsection 3.4 that computer “experiments”, taken over from the theory of liquids, have been instrumental in the recent progress of our knowledge of the static properties of the OCP. The same is true for the dynamic properties. While the Monte Carlo (MC) method is best suited for the study of the statics, the time-dependent properties can be simulated by the “Molecular Dynamics” (MD) method, which was first introduced by Alder and Wainwright in their study of the dynamics of the hard sphere fluid [3.15]. Briefly speaking, the method amounts to solving the $3N$ coupled classical equations of motion for a system of N particles of mass m enclosed in a fixed volume Ω with periodic boundary conditions. N is of the order 10^2 – 10^4 and the second order differential equations are replaced by finite difference equations with a fixed time

step Δt . The simplest integration procedure is based on the Taylor expansions of the positions of a particle at times $t + \Delta t$ and $t - \Delta t$ about its position at time t and leads to the very simple algorithm [4.13]:

$$\mathbf{r}_i(t + \Delta t) = 2\mathbf{r}_i(t) - \mathbf{r}_i(t - \Delta t) + \frac{(\Delta t)^2}{m} \sum_{\substack{j=1 \\ j \neq i}}^N \mathbf{F}_{ij}(t) \quad (4.42)$$

where $\mathbf{F}_{ij}(t)$ is the force exerted by particle j on particle i at time t . The error introduced by the algorithm is of order $(\Delta t)^4$. The velocity of particle i at time t can be calculated from:

$$\mathbf{v}_i(t) = \frac{1}{2\Delta t} [\mathbf{r}_i(t + \Delta t) - \mathbf{r}_i(t - \Delta t)] \quad (4.43)$$

with an error of $(\Delta t)^3$. The trajectories of the N particles are followed for a large number, v , of time steps ($10^3 \leq v \leq 10^5$) and the microscopic variables are averaged over time. Here the appropriate statistical ensemble is hence the microcanonical ensemble: the total energy of the system is constant while the temperature fluctuates around its mean value given by the average kinetic energy per particle:

$$T = \frac{m}{3k_B} \cdot \frac{1}{vN} \cdot \sum_{n=1}^v \sum_{j=1}^N |\mathbf{v}_j(n\Delta t)|^2. \quad (4.44)$$

Static properties can be computed by the MD method with an accuracy comparable to that obtained in MC “experiments”. The fundamental dynamical properties which are computed in MD simulations are the time correlation functions of two dynamical variables, say A and B :

$$\begin{aligned} C_{AB}(t - t') &= \langle A(t)B(t') \rangle = \lim_{\tau \rightarrow \infty} \frac{1}{\tau} \int_0^\tau ds A(t - t' + s)B(s) \\ &\simeq \frac{1}{v - \mu} \sum_{n=1}^{v-\mu} A((\mu + n)\Delta t)B(n\Delta t) \end{aligned} \quad (4.45)$$

where the last line is the MD estimate of the time average with $t - t' = \mu\Delta t$. In Coulomb fluids the long range of the forces between the particles must be correctly treated by appropriate Ewald summations similar to those used to calculate potential energies for periodic systems in MC simulations (see subsection 3.4). Extensive MD investigations of the OCP dynamics have been made in the intermediate ($\Gamma \sim 1$) and strong coupling ($\Gamma \gg 1$) regimes [4.14–16]. The system size was generally $N = 250$ while the chosen time-step was typically $\Delta t = 0.02\omega_p^{-1}$ in the intermediate coupling regime and $\Delta t = 0.1\omega_p^{-1}$ in the strong coupling (i.e. low temperature) regime. We now successively present a summary of the results for the single particle (“self”) motion, the collective modes and the transport coefficients.

4.5.1. Single particle motion

The single particle motion is generally analysed in terms of the self density correlation function $S_s(k, t)$, defined in subsection 4.1, and the normalised velocity autocorrelation function:

$$\psi(t) = \langle \mathbf{v}_i(t' + t) \cdot \mathbf{v}_i(t') \rangle / \langle \mathbf{v}_i(t') \cdot \mathbf{v}_i(t') \rangle \quad (4.46)$$

where $\mathbf{v}_i = \dot{\mathbf{r}}_i$ is the velocity of any one particle of the system. For a stationary system eq. (4.46) is of course independent of the time origin t' . Note that since all particles are equivalent, $\psi(t)$ can be averaged over the N particles of the MD ‘‘experiment’’, thus improving the statistics considerably. $\psi(t)$ is directly related to the long wavelength limit of $S_s(k, t)$:

$$\psi(t) = -\lim_{k \rightarrow 0} \frac{d^2}{dt^2} \left(\frac{S_s(k, t)}{nv_0^2 k^2} \right) \quad (4.47)$$

while the self-diffusion coefficient D is proportional to the time integral of $\psi(t)$ [1.2]:

$$D = v_0^2 \int_0^\infty dt \psi(t). \quad (4.48)$$

$\psi(t)$ has been computed for several values of Γ by Hansen et al. [4.14]. The most striking result is the appearance of oscillations in $\psi(t)$, at a frequency close to ω_p , for $\Gamma \gtrsim 10$. These oscillations become more and more pronounced as Γ increases and are a consequence of the strong coupling between the single particle motion and the collective plasma oscillation. This behaviour will be further analysed in subsection 4.6. The reduced self-diffusion coefficient $D^* = D/\omega_p a^2$ decreases rapidly with increasing Γ ; the MD data for $\Gamma \gtrsim 1$ are well represented by the simple interpolation formula:

$$D^* = \alpha \Gamma^{-\beta}$$

with $\alpha = 2.95$ and $\beta \simeq \frac{4}{3}$.

Bernu [4.16] has computed the self density correlation function $S_s(k, t)$ for $\Gamma \simeq 1, 10$ and 100 and a series of wave-numbers k , the possible values of the wave-vectors \mathbf{k} being determined by the periodic boundary conditions:

$$\mathbf{k} = \frac{2\pi}{L} (n_x, n_y, n_z)$$

where $L = \Omega^{1/3}$ is the edge of the cubic box containing the N particles, and n_x, n_y, n_z are integers. In particular, the smallest dimensionless wave-number $q = ka$ compatible with the periodic boundary conditions, is:

$$q_{\min} = (6\pi^2/N)^{1/3}.$$

Note that since the OCP is isotropic in the fluid phase, the statistics on $S_s(k, t)$ can be improved by averaging over all wave-vectors \mathbf{k} of identical length k . Bernu’s results indicate that the Gaussian approximation [1.2], explicitly given by eq. (4.63) below, is fairly accurate for the OCP at all wave-numbers and coupling constants.

4.5.2. Longitudinal collective modes

As indicated in eq. (4.17) the longitudinal collective modes can be studied by examining the number density correlation function $S(k, t)$ whose Fourier transform is directly related to the longitudinal mass current correlation function $S_l(k, t)$ of eq. (4.19a) by:

$$S(k\omega) = \frac{k^2}{m^2 \omega^2} S_l(k\omega). \quad (4.49)$$

The dynamical structure factor $S(k\omega)$ has been computed by MD simulations for $\Gamma \simeq 1, 2, 10, 110$ and 150 , the last value being close to the freezing point, by Hansen et al. [4.14, 4.17]. The most striking features of the computed spectra are the following:

- a) Plasma oscillations manifest themselves at small reduced wave-numbers q by a sharp peak centered near the plasma frequency. The peak broadens and shifts as q increases. For fixed q the “plasmon” peak is sharpest at high Γ .
- b) At $\Gamma = 1$ the plasmon peak shifts to higher frequencies as q increases, in qualitative agreement with mean-field (Vlasov) theory which describes correctly the collisionless or weak coupling limit ($\Gamma \rightarrow 0$). However, for $\Gamma = 10$ and higher the dispersion is *negative*, i.e. the frequency of the “plasmon” mode *decreases* with increasing q . This behaviour was quite unexpected but has since been confirmed and interpreted by a number of theories [3.9, 4.7, 4.12]. A number of dispersion curves corresponding to different values of Γ are shown in fig. 7.
- c) At small q there is no trace of a central (Rayleigh) peak linked to heat diffusion in agreement with the exact long-wavelength behaviour described in subsections 4.3 and 4.4. Even at intermediate q values ($q \simeq 2$) the “mechanical” plasmon mode dominates the spectrum and heat diffusion contributes virtually nothing to the density fluctuation spectrum.
- d) Beyond a critical wave-number, which in the strong coupling limit is of the order of $q = 2.5$, the plasmon peak vanishes and the spectrum reduces rapidly to its Gaussian non-interacting limit.

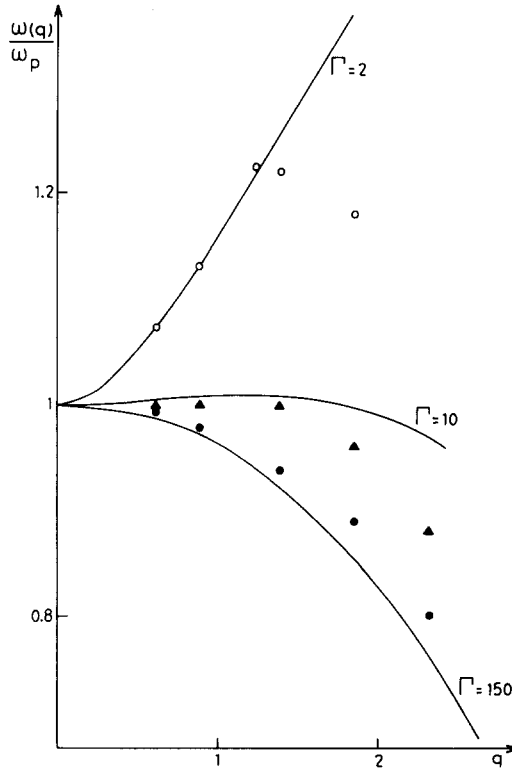


Fig. 7. OCP plasma dispersion $\omega(q)/\omega_p$ versus $q = ak$, for $\Gamma = 2$ (circles), $\Gamma = 10$ (triangles) and $\Gamma = 150$ (dots), based on the MD results [4.14, 4.17]. The full curves are the corresponding dispersion curves based on the approximation (4.58) [4.20]. The frequencies $\omega(q)$ are determined from the peak positions in $S(q, \omega)$.

A comment is in order concerning the MD results at $\Gamma = 1$. The theoretical analysis of several authors (see e.g. [4.14] and [4.34]) while yielding good overall agreement with the MD data at higher values of Γ , have failed to reproduce the MD values of $S(k\omega)$ at $\Gamma = 1$; in particular the theoretical and “experimental” peak positions, and hence the dispersion curves, do not agree as well for $\Gamma = 1$ as they do in the strong coupling regime. This can be traced back to the fact that the $\Gamma = 1$ MD run was done with the “nearest image” convention (see subsection 3.4), i.e. without the time-consuming Ewald summations over periodic images. Such a procedure is sufficient if one is interested in the *static* properties in the weak and intermediate coupling regime [3.17], but the dynamic properties are much more sensitive to a potential cut-off. Hence we believe that the MD results are not as reliable for $\Gamma = 1$ as they are for the higher Γ values, for which the long range of the Coulomb forces was correctly treated by Ewald summations.

The density fluctuation spectra were analysed in [4.14] with the help of a standard memory (or damping) function approach [4.18, 1.2] involving a Gaussian spectral function depending on a single adjustable q -dependent relaxation time; the agreement with the “experimental” spectra is outstanding except for $\Gamma = 1$ as noted above. The relaxation time can in fact be determined with the help of the sixth ($n = 6$) frequency moment (cf. eq. (4.23) and subsection 4.2), leading to a theory which is free of adjustable parameters; the agreement with the MD data remains excellent [4.8]. An even simpler sum rule analysis, based on Mori’s continued fraction expansion [4.18, 1.2] and a simple recipe to determine the relaxation time [4.19], has been used with similar success by Abramo and Parinello [4.20], the corresponding explicit expression for $S(kz)$ is given in eq. (4.58) in the next subsection. A comparison of this theory to the MD data at $\Gamma = 2$ is made in fig. 8. The imaginary part of the electric susceptibility $\chi(k\omega)$ of eq. (4.20b) is connected to $S(k\omega)$ by the fluctuation-dissipation theorem (see eq. (4.20b)); the real part of $\chi(k\omega)$ can then be determined via the Kramers–Kronig relations and the results used to determine the dielectric function $\epsilon(k\omega)$ defined by eq. (4.20). The real and imaginary parts of $\epsilon(k\omega)$ obtained in this way are shown in fig. 9 for $\Gamma = 1$ and $\Gamma = 155$.

As a final comment we consider the intriguing question raised by the MD results as to the precise value of Γ at which the dispersion changes from positive (weak and intermediate coupling) to negative (strong coupling). The phenomenological hydrodynamic calculation [3.9, 4.10] links the small- k dispersion relation:

$$\omega(k) = \omega_p(1 + \frac{1}{2}k^2\gamma_p^H + O(k^4)) \quad (4.50)$$

with:

$$\gamma_p^H = \frac{C_p}{C_v} \cdot \frac{\chi_T^0}{\chi_T} \cdot k_D^{-2} \quad (4.51)$$

to the isothermal compressibility which changes sign at $\Gamma = 3$. However, as discussed in subsection 4.4, the transition from the exact value of γ_p given in eq. (4.36a) to its hydrodynamic value γ_p^H of eq. (4.51) involves the strong coupling limit ($\omega_c \gg \omega_p$, see eq. (4.41b)) and is probably unreliable at coupling constants as low as $\Gamma = 3$. Alternatively an approximate dispersion relation in the long-wavelength limit can be derived from a sum-rule analysis. The high-frequency expansion of the dielectric function $\epsilon(k\omega)$ is related to the expansion (4.22) of the charge density response function through eq. (4.20). Truncation of this expansion after the ω^{-4} term and use of the condition:

$$\epsilon(k, \omega = \omega(k)) = 0$$

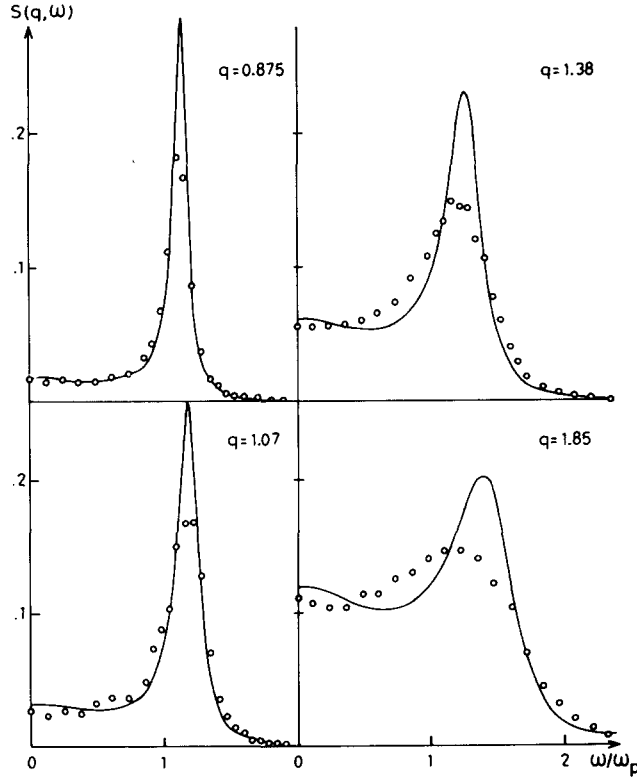


Fig. 8. OCP dynamical structure factor $S(q, \omega)$ versus ω/ω_p , at $\Gamma = 2$ and for indicated values of $q = ak$. The circles are the MD results [4.17] while the full curves are based on the simple “three-pole” approximation (4.58) [4.20].

to determine the frequency $\omega(k)$ of the plasma mode leads [4.21] to the dispersion relation of eq. (4.50) but with γ_p^H replaced by $\bar{\gamma}_p$:

$$\bar{\gamma}_p = (3 + \frac{4}{15}u)k_D^{-2}. \quad (4.52)$$

This leads to negative dispersion for $\Gamma \geq 14$. Ichimaru et al. [4.7] have extended this approach by including explicitly contributions of “collisional excitations” to the charge fluctuation spectrum. This leads to a modified expression for $\bar{\gamma}_p$ which now includes information from the long-wavelength limit of the sixth frequency moment.

The result (4.52) for the dispersion was derived independently by Abramo and Tosi [4.22] from a different viewpoint (see subsection 4.6). It follows also from the simple form of eq. (4.58) that the real part of the plasmon pole can be described by eq. (4.52) while the imaginary part of the pole, which governs the width of the plasmon peak, increases like k^3 , in qualitative agreement with the MD data.

By looking at fig. 7 we see however that the situation is actually more complicated than the long-wavelength dispersion relations would indicate. For $\Gamma \approx 10$, the higher order terms (k^4 and higher powers of k) tend to bend the dispersion curve downward in the region of intermediate wave numbers ($q \gtrsim 1$), so that the dispersion becomes in fact negative for wavelengths corresponding to a few interionic spacings. For $q \gtrsim 2$ the plasmon mode is less and less well defined

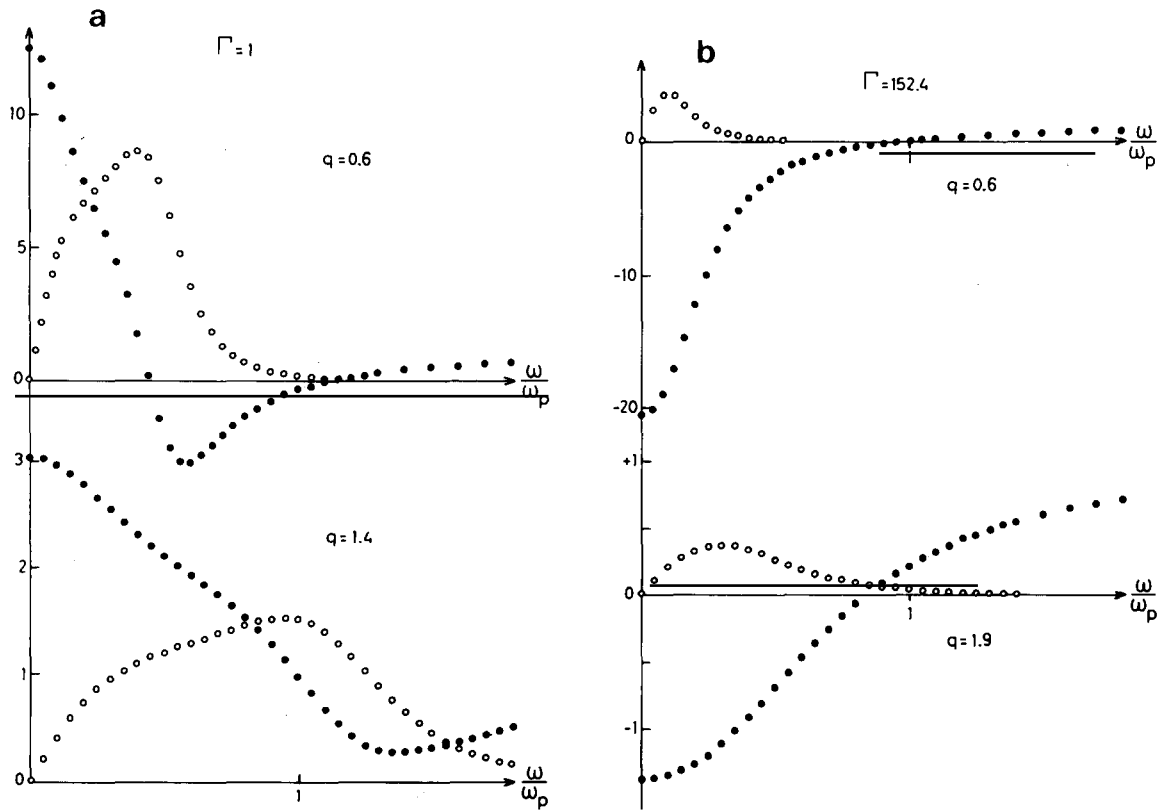


Fig. 9. (a) Real (dots) and imaginary (open circles) parts of the OCP frequency-dependent dielectric function $\epsilon(q, \omega)$, versus ω/ω_p , at $\Gamma = 1$ and for indicated values of $q = ak$. The points are based on the approximation (4.58) for $S(q, \omega)$, but lie very close to those calculated with the MD data for $S(q, \omega)$. (b) Same as (a), but for $\Gamma = 152.4$.

and there is some ambiguity in defining the frequency of the mode since the position of the maximum of $S(k\omega)$ does not coincide any more with the real part of the plasmon pole.

4.5.3. Transverse collective modes

The transverse current correlation function and its spectrum $S_{\perp}(k\omega)$ of eq. (4.19b) have also been computed in the MD simulations of Hansen et al. [4.14] for $\Gamma = 152.4$. A priori the shear modes are not expected to differ, at least qualitatively, from those observed in neutral liquids [1.2], since the Coulomb divergence affects only the longitudinal currents. Indeed, for $q \lesssim 2$, the MD computations near freezing show clear evidence for propagating shear modes reminiscent of the transverse phonon modes in the crystal. However at larger q ($q \gtrsim 2$), the same computations show a very unexpected feature of $S_{\perp}(k\omega)$: in this intermediate wavelength domain the peak in the spectrum splits into two clearly separated components; the peak at higher frequency is located close to (but slightly below) the plasma frequency. This very unusual behaviour has recently been interpreted in terms of a mode-coupling theory (see subsection 4.6).

4.5.4. Transport coefficients

The thermal conductivity κ and the shear and bulk viscosities η and ξ can be computed from the Green–Kubo relations [1.2]. The entropy and momentum current autocorrelation functions have been computed by MD simulations [4.15] and their time integrals lead to κ , η and ξ . Results for $\Gamma = 1, 10$ and 100 have thus been obtained. Although the standard Green–Kubo formulae are also valid for the OCP, some care must be taken in defining the microscopic currents in order to avoid divergences due to the long range of the Coulomb interactions [4.15]. The computed longitudinal entropy current autocorrelation function exhibits pronounced oscillations at a frequency roughly equal to ω_p for $\Gamma = 10$ and 100 . The bulk viscosity correlation function exhibits even more pronounced oscillations at roughly twice the plasma frequency for $\Gamma = 1, 10$ and 100 . The autocorrelation function associated with the shear viscosity, on the other hand, behaves very differently. At $\Gamma = 1$ and 100 it decays monotonically and very slowly, whereas at $\Gamma = 10$ it appears to oscillate weakly after an initial rapid decay.

The resulting dimensionless transport coefficients vary rather differently with Γ . The reduced bulk viscosity $\xi^* = \xi/nm\omega_p a^2$ decreases monotonically as Γ increases from 1 to 100 . The reduced shear viscosity $\eta^* = \eta/nm\omega_p a^2$ and the reduced thermal conductivity $\kappa^* = \kappa/k_B n \omega_p a^2$ are lower at $\Gamma = 10$ than at $\Gamma = 1$ and 100 . This minimum of η^* as a function of Γ had been predicted theoretically [3.9, 4.35] (see subsection 4.6) but no similar theoretical estimates of κ^* have yet been published.

4.6. Approximate theoretical results

Various theories have intended to explain the “experimental” results discussed in the previous section on the basis of more or less microscopic considerations. The existing theoretical approaches have been divided, somewhat arbitrarily, into three groups to which we now turn our attention.

4.6.1. The extended mean field theories

Under this label we can re-group all the theoretical attempts [4.22–28] based on the introduction of a static and/or dynamic local field correction into the ordinary mean field (RPA) approximation to the dielectric constant $\epsilon(kz)$ of eq. (4.20). The local field correction, $t(kz)$, can then be introduced by writing the electric susceptibility $\chi(kz)$ of eq. (4.20b) as:

$$\chi(kz) = \frac{\chi_0(kz)}{1 + (k_D^2/k^2 - t(kz))\chi_0(kz)} \quad (4.53)$$

which leads to:

$$\epsilon(kz) = 1 + \frac{k_D^2}{k^2} \cdot \frac{\chi_0(kz)}{(1 - t(kz)\chi_0(kz))} \quad (4.54)$$

where $\chi_0(kz)$ is the RPA value of $\chi(kz)$:

$$\chi_0(kz) = \int d\mathbf{p} \frac{\mathbf{k} \cdot \mathbf{v}}{\mathbf{k} \cdot \mathbf{v} - z} \varphi(\mathbf{p}); \quad \text{Im } z > 0 \quad (4.55)$$

$\varphi(\mathbf{p})$ being the Maxwellian normalized to one. In the form of eq. (4.54) it is easily recognized that $t(kz)$ is the dynamic generalization of $t(k)$ of eq. (3.55) to which it reduces in the static limit,

$t(k, z = 0) \equiv t(k)$, whereas the ordinary mean field theory is obtained by setting $t(kz) \equiv 0$. To go beyond the RPA one has to relate $t(kz)$ back to $\epsilon(kz)$ or to a related quantity. It does however not appear to be easy to do this in a meaningful *and* manageable manner. In the early versions [4.22–23, 4.25–26] of these theories $t(kz)$ was approximated by its static value $t(k)$ which was then further related to $S(k)$ by one of the static theories discussed in subsection 3.6. More recently genuine dynamic versions have been proposed [4.24–27] which result in self-consistent equations for $t(kz)$ and $\epsilon(kz)$. For instance, in [4.24] Ichimaru has proposed a scheme in which $\epsilon(kz)$ is rewritten in terms of a renormalized propagator $G(\mathbf{kp}; \omega)$ as:

$$\epsilon(k\omega) = 1 + \frac{k_D^2}{k^2} \int d\mathbf{p} G(\mathbf{kp}; \omega) \mathbf{k} \cdot \mathbf{v} \varphi(\mathbf{p}) \quad (4.56)$$

which is to be compared with eqs. (4.54–55). This propagator $G(\mathbf{kp}; \omega)$ obeys a nonlinear integral equation involving the dielectric constant $\epsilon(k\omega)$ and the dynamic structure factor $S(k\omega)$. The system of equations is then closed by another nonlinear integral relation between $S(k\omega)$ and $\epsilon(k\omega)$. In [4.26–27] Golden et al. have rewritten $\epsilon(k\omega) = 1 + \alpha(k\omega)$ in the form:

$$\frac{\alpha(k\omega)}{\epsilon(k\omega)} = \frac{\alpha_0(k\omega)}{\epsilon_0(k\omega)} (1 + w(k\omega)) \quad (4.57)$$

where the subscript zero denotes again the RPA values while $w(k\omega)$ is expressed in terms of the three-point generalization of $S(k\omega)$. Using the nonlinear version of the fluctuation-dissipation theorem, $w(k\omega)$ can be re-expressed in terms of the nonlinear dielectric constant. Approximating this nonlinear dielectric constant by its RPA value or reexpressing it in terms of the linear dielectric constant $\epsilon(k\omega)$ will again close the system of equations. Unfortunately many of these equations turn out to be rather complicated while no numerical analysis of them has yet been reported. A slightly different approach was followed by Abramo and Tosi [4.22]. As in the (liquid argon) theory of Pathak and Singwi [4.28], these authors start from eq. (4.54) but moreover replace $\text{Im } \chi_0(k, z = \omega + i0)$, which according to eq. (4.55) is a Gaussian, by a broadened Gaussian ($\sim \exp -\omega^2/(2v_0^2 k^2 + \gamma(k))$) and determine then $t(k) \equiv t(k, z = 0)$ and $\gamma(k)$ by requiring that the zeroth and fourth frequency sum-rule of $S(k\omega)$ (see eq. (4.23)) be satisfied exactly. The results of this theory with respect to the plasmon peaks of $S(k\omega)$ have been compared with the MD data by Abramo and Parrinello [4.20]. The latter authors have also compared the MD data with an approximation to $S(kz)$ first proposed by Lovesey [4.19] for ordinary liquids. Both these simple forms yield $S(k\omega)$ functions which are in quite reasonable overall agreement with the MD results. This is especially true for Lovesey's approximation which reads in our notation:

$$S(kz) = \frac{nS(k)\omega_p^2(z - ic(k))}{z^3 - iz^2c(k) - za(k) + ic(k)b(k)} \quad (4.58)$$

with $a(k) = a_4(k)/a_2(k)$, $b(k) = a_2(k)/a_0(k)$, $c(k) = [(4/\pi)(a(k) - b(k))]^{1/2}$ where the various moments $a_n(k)$ are given in table 2. Lovesey's approximation is in fact a particularly simple member of the group of theoretical approaches discussed in the next subsection (4.6.2) and we will briefly discuss its derivation there. From the analysis by Abramo and Parrinello [4.20] we learn that very simple theories can yield the correct structure of $S(k\omega)$. The more difficult problem, which largely remains unsolved, being the more accurate description of the changes which occur in the position and width of the plasmon peaks of $S(k\omega)$ as Γ varies throughout the whole fluid phase. The widths,

for instance, are slightly underestimated by eq. (4.58), the “best candidate” in this category. The collision processes, overlooked by eq. (4.58), might well be essential for certain values of Γ .

4.6.2. The mode-coupling theories

Under this heading we consider those theories which do start from a straightforward microscopic basis but without carrying along any momentum-dependent information, the latter being typical of the so-called “kinetic” theories to be discussed subsequently. In the mode-coupling theories one usually performs a Mori-type projection analysis but directly on the microscopic variables of interest (e.g. the number, momentum and energy densities). This leads to a memory kernel, for ex. in eq. (4.30) $D_{\perp}(kz)$ is the kernel of $S_{\perp}(kz)$, whose microscopic expression is now no longer expressed in terms of a collision operator like in eq. (4.15) but in terms of the Liouville operator projected onto the variables orthogonal to those of interest (e.g. the transverse momentum density in the case of $S_{\perp}(kz)$). Such expansions can be pursued further (continued fraction expansion) but will eventually have to be stopped somewhere by re-expressing the ultimate kernel into the (momentum-independent) correlation functions of interest. The resulting equations acquire then the form of self-consistent equations for the various correlation functions ($S(k\omega)$, $S_{\perp}(k\omega)$, $S_s(k\omega)$) such as the equations encountered in the mode-mode coupling theories of ordinary liquids already reviewed by Pomeau and Résibois [3.29]. Lovesey’s approximation, eq. (4.56), corresponds to the particularly simple case where the third kernel in the continued fraction expansion (“three-pole” approximation) for $S(kz)$ is approximated by a frequency independent constant fitted so as to yield the correct large- k behaviour of $S(k, \omega = 0)$. A genuine mode-coupling theory, proposed originally by Bosse, Götze and Lücke [4.29] for liquids, has recently been applied to the OCP by Bosse and Kubo [4.30]. In this theory the continued fraction expansion, for ex. for $S_{\perp}(kz)$, is written as:

$$S_{\perp}(kz) = \frac{ia_0^{\perp}(k)}{z + M_0^{\perp}(kz)}; \quad M_0^{\perp}(kz) = \frac{a_2^{\perp}(k)}{z + M_2^{\perp}(kz)} \quad (4.59)$$

where the $a_n^{\perp}(k)$ have been listed in table 2 whereas $M_0^{\perp}(kz)$ corresponds to $ik^2 D_{\perp}(kz)$ of eq. (4.30). This expansion, eq. (4.59) is then truncated by re-expressing $M_2^{\perp}(kz)$ in terms of $S_{\perp}(kz)$ and $S(kz)$. This is achieved by retaining only that part of the orthogonal space which can be constructed with the aid of products of only two of the relevant variables in the same way as in the standard mode-mode coupling theories [3.29]. The result is an approximation for $M_2^{\perp}(kz)$ which can be written as the sum of a free-particle contribution and a two-mode coupling term of the form:

$$M_2^{\perp}(kt) = \sum_{\alpha, \beta} \int \frac{d\mathbf{k}'}{8\pi^3} V_{\alpha\beta}(\mathbf{k}, \mathbf{k}') S_{\alpha}(\mathbf{k}', t) S_{\beta}(\mathbf{k} - \mathbf{k}', t) \quad (4.60)$$

where $S_{\alpha}(k, t)$ denotes $S(k, t)$, $S_l(k, t)$ or $S_{\perp}(k, t)$, while $V_{\alpha\beta}(\mathbf{k}, \mathbf{k}')$ is a “vertex” function which contains static information some of which, e.g. the triple correlations, is not readily accessible. The resulting set of equations was solved in [4.30] for $\Gamma = 140$ and compared with the MD data at $\Gamma = 152.4$. The variation of $S(k\omega)$ and $S_{\perp}(k\omega)$ with k and ω is in fair agreement with the MD data (see fig. 10). For instance, this is the first theory to reproduce the double-peak structure of $S_{\perp}(k\omega)$ at the intermediate k -values. The main uncertainties of this theory can be summarised as follows: 1) there is the traditional Kirkwood superposition approximation for the triple correlations which the authors show explicitly to be bad at large interparticle separations; a first cut-off is introduced somewhat arbitrarily here; 2) a second cut-off is introduced in order to cut down the vertex function

for small k , 3) for $S(k\omega)$ the coupling between the density and the energy was neglected. This latter point corresponds to putting $\gamma_{le}(kz) \simeq 0$ in eq. (4.31). It should be noticed however that the argument invoked, namely $\gamma_{le}(00) \sim (1 - C_v/C_p) \simeq 0$ the latter equality being correct for the OCP at large Γ , would be applicable to an ordinary liquid where the quantity of interest is $\gamma_{le}(0, 0)$, but is not applicable when, as for the OCP, $\gamma_{le}(0, \omega_p)$ is involved (see eq. (4.36)), except if, as pointed out in subsection 4.4, $\gamma_{le}(0, \omega_p)$ can again be approximated by $\gamma_{le}(0, 0)$ for large Γ . Finally, it would be of interest to study the Γ -dependence of the various cut-offs and to test whether this theory also reproduces the variations in the shapes of $S(k\omega)$ and $S_\perp(k\omega)$ when Γ varies over the fluid phase.

In the case of the self-motions the quantity of current interest has been the velocity auto-correlation function $\psi(t)$ of eq. (4.46) and its associated memory function $M(t)$:

$$\psi(z) = i(z - M(z))^{-1}.$$

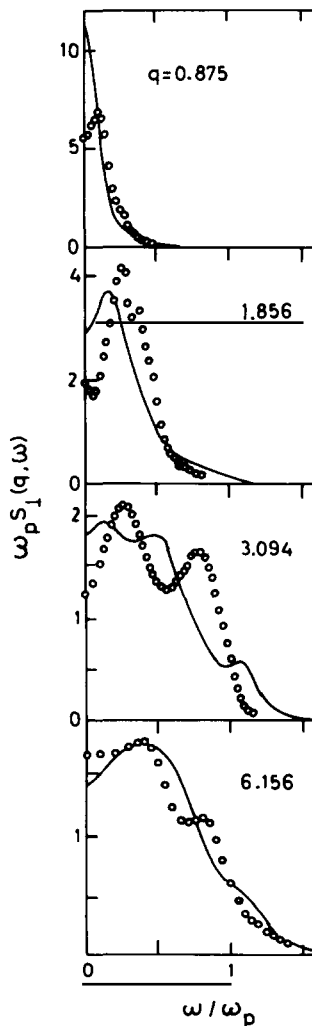


Fig. 10. The transverse momentum fluctuation spectrum $S_\perp(q\omega)$ as a function of ω for various $q = ak$ values at $\Gamma = 140$. The circles correspond to the MD data [4.14] while the full lines are the results of the mode-coupling theory of Bosse and Kubo [4.30].

Various authors [4.31–34] have obtained a mode-coupling formula for $M(t)$. A $k - t$ derivation in the spirit of this section was proposed by Gaskell and Chiakwelu [4.32–33]. These authors did not use the Mori-procedure discussed above but instead a somewhat ad hoc equation of motion technique both for the self-motions [4.32] and for the transverse motions [4.33]. Their result for $M(t)$ is similar to eq. (4.60). It reads explicitly:

$$M(t) = \int \frac{d\mathbf{k}}{8\pi^3} V_{ns}(\mathbf{k}, \theta) S(kt) S_s(kt) \quad (4.61)$$

and agrees with the earlier finding of Gould and Mazenko [4.31] up to a “renormalization” of the vertex function $V_{ns}(\mathbf{k}, \theta)$. In [4.31] the latter authors found:

$$V_{ns}(\mathbf{k}, \theta) = \frac{nk^2}{3m^2 v_0^2} \left(\frac{\hat{c}(k)}{n\beta} \right)^2$$

whereas in [4.32] Gaskell and Chiakwelu obtained:

$$V_{ns}(\mathbf{k}, \theta) = \frac{nk^2}{3m^2 v_0^2} (v(k))^2.$$

As observed in [4.32] the exact result $M(t = 0) = \omega_p^2/3$ (which follows from the discussion following eq. (4.27)) requires however:

$$V_{ns}(\mathbf{k}, \theta) = \frac{nk^2}{3m^2 v_0^2} \cdot \left(-\frac{\hat{c}(k)}{n\beta} \right) \cdot v(k).$$

This, a posteriori, justification of the proper choice of the vertex function V_{ns} is realized a priori in the kinetic theory of Wallenborn and Baus [4.39] which will be discussed in the next subsection 4.6.3. After this short remark about the proper vertex function to be used in eq. (4.61) we return to the work of Gaskell and Chiakwelu [4.32]. The latter authors have computed $M(t)$ and the self-diffusion coefficient D , eq. (4.48), by choosing a Gaussian form for $S_s(k, t) = n \exp(-k^2 a(t))$. Together with the following two-peak hydrodynamic-like approximation:

$$S(k\omega) = nS(k) \frac{\omega^2(k) \cdot \alpha(k)}{(\omega^2 - \omega^2(k))^2 + \omega^2 \alpha^2(k)} \quad (4.62)$$

with $\omega(k)$ given by eq. (4.32) and $\alpha(k) = (\frac{4}{3}\eta + \xi)/nm(1 + k\lambda(k))$. The functions $a(t)$, $\alpha(k)$ and $\lambda(k)$ were chosen in such a way as to reproduce the MD data at $\Gamma = 110$. As moreover these authors also modify the Coulomb potential by cutting its short-distance part it is not very surprising that they can reproduce the MD data for $M(t)$ and D at $\Gamma = 110$ rather well. In our opinion more work is necessary here. A satisfactory theory should explain the dynamics of the OCP for at least a range of Γ values while using only the statics as input.

4.6.3. The kinetic theories

We finally consider the more sophisticated “kinetic” theories proposed by Gould and Mazenko [4.31], Wallenborn and Baus [4.35] and Sjödin and Mitra [4.34]. In all these theories one eventually starts from the exact kinetic equation (4.6) involving still the complete momentum dependence. The central quantity becomes then the collision operator or memory function of eq. (4.7c). For the case of, for instance, the collective motions of the OCP, we have the alternative forms:

$$i\Sigma^c(12; t) = \langle \delta f(1) | LQ e^{iQLQt} QL | \delta f(2) \rangle (n\varphi(\mathbf{p}_2))^{-1} \quad (4.63a)$$

$$= \int d\mathbf{l}' d\mathbf{l}'' L_l(11') L_l(22') C(11', 22'; t) (n\varphi(\mathbf{p}_2))^{-1} \quad (4.63b)$$

$$= \partial_1 \cdot \mathbf{L}(12; t) \cdot (\mathbf{v}_2 + \beta^{-1} \partial_2) \quad (4.63c)$$

where the first form, eq. (4.63a), which is nothing but the $\mathbf{r} - t$ formulation of eq. (4.7c) with $1 \equiv (\mathbf{r}_1, \mathbf{p}_1)$ etc., is useful mainly for the study of the general properties outlined in subsections 4.2 and 4.3. The second form, eq. (4.63b), is the proper kinetic theoretic form first introduced by Mazenko [4.36] and subsequently used by Gould and Mazenko [4.31] and Wallenborn and Baus [4.11, 4.35]. It contains the two-body interaction operator $L_l(12) = -\nabla_1 v(\mathbf{r}_1 - \mathbf{r}_2) \cdot (\partial_1 - \partial_2)$, $\nabla_1 = \partial/\partial\mathbf{r}_1$, $\partial_1 = \partial/\partial\mathbf{p}_1$ and a (contracted) four-point correlation function $C(12, 34; t)$. The equivalence between these two forms was demonstrated, for example, by Lindenfeld [4.37]. The last form, eq. (4.63c), was used by Sjögren and Sjölander [4.38] for ordinary liquids and applied to the OCP by Sjödin and Mitra [4.34]. It can be obtained from eq. (4.63b) and eq. (4.6) by integrating the latter equation by parts over \mathbf{p}_2 and commuting ∂_2 with $\varphi(\mathbf{p}_2)$. In the differential form of eq. (4.63c) Σ^c is usually referred to as the (linearized) collision operator whereas in the equivalent form eq. (4.63b) Σ^c is usually denoted as the (collisional or dynamic) memory function. Although the starting point of the three theories under discussion are equivalent the manner in which the further approximations are introduced makes them very different.

In the work of Sjödin and Mitra [4.34], the kinetic theory treatment is not pursued but approximation to $\mathbf{L}(12; t)$ of eq. (4.63c) are introduced on intuitive grounds, first developed in [4.38], which allow $S(kz)$ to be put in the following extended mean field form:

$$S(kz) = nS(k) \cdot \left[\frac{S_s(kz) - (\beta/k^2)L(kz)(izS_s(kz) + n)}{1 + (\tilde{c}(k) - (\beta z/k^2)L(kz))(izS_s(kz) + n)} \right] \quad (4.64)$$

to be compared with eq. (4.53). We see that the free-particle expression of the RPA theory, $n\chi_0(kz) \equiv izS_0(kz) + n$, has been replaced in eq. (4.64) by the self-correlations $S_s(kz)$ whereas $L(kz)$ plays the role of a dynamic local field correction. The latter quantity being defined here as:

$$L(kz) = \langle n | \hat{\mathbf{k}} \cdot (\mathbf{L}(kz) - \mathbf{L}_s(kz)) \cdot \hat{\mathbf{k}} | n \rangle$$

\mathbf{L}_s being the quantity corresponding to \mathbf{L} , eq. (4.63c), but for the self-motions. In the present approximation $L(kz)$ is given a mode-coupling form in terms of $S(kz)$ and $S_s(kz)$. This theory appears thus as a compromise between a kinetic theory, a mode-coupling theory and an extended mean field theory. This compromise has however been obtained through a very cavalier treatment of the momentum dependence. Indeed by neglecting all non-hydrodynamic momentum states these authors have prevented their theory from reducing to the proper weak-coupling limit where the transport coefficients have a typical dependence on the inverse of the collision operator acting on the non-conserved momentum states as displayed for instance in the second term of eq. (4.15) (see also eq. (4.67) below). This theory should therefore run into trouble when $\Gamma \ll 1$. The neglect of the coupling between the conserved states corresponding to the number density and the energy is moreover subject to the same criticism as for the mode-coupling theory (see the discussion following eq. (4.59)). It is therefore not clear a priori for what region of Γ values this theory is expected to work well. Numerical results have been reported for $\Gamma = 1$ and $\Gamma = 10$.

They have been obtained by solving iteratively eq. (4.64) together with the Gaussian approximation for $S_s(kt)$:

$$S_s(kt) = n \exp \left\{ -k^2 m \beta \int_0^t dt' (t - t') \psi(t') \right\} \quad (4.65)$$

where $\psi(z) = i(z - M(z))^{-1}$ while $M(t)$ is given by eq. (4.61) with $V_{ns}(\mathbf{k}, \theta)$ chosen so as to yield the correct $M(t = 0)$ value. As a starting point for their iterations these authors have used Lovesey's approximation eq. (4.58) for $S(kt)$ and:

$$S_s(kt) = n \exp \{ -k^2 D [t + m \beta D (\exp(-t/m \beta D) - 1)] \} \quad (4.66)$$

for $S_s(kt)$. Notice that eq. (4.66) requires the MD data for D as input. The overall agreement for $S(k\omega)$, $\psi(t)$ and D is satisfactory.

The theories proposed by Gould and Mazenko [4.31] and Wallenborn and Baus [4.35] are closely related kinetic theories for, respectively, the self- and the collective-motions. These are genuine kinetic theories in the sense that they start from the exact microscopic expressions for the correlation functions and the transport coefficients which are then evaluated with the aid of an approximate collision operator constructed in such a way that it reduces to the well-known weak-coupling results for small Γ . At present these theories have not yet been applied to the more difficult problem of calculating the correlation functions themselves but only to the determination of the transport coefficients D [4.31] and η [4.35] as a function of Γ throughout the fluid phase ($0 < \Gamma < 160$). For a proper understanding of the interplay between the approximations and the particular features of each transport coefficient it might be worthwhile to recall here a few technicalities. The exact expression of the shear-viscosity η in terms of the collision operator Σ^c , eq. (4.63), and the free-flow term Σ^0 , eq. (4.7a) reads from eqs. (4.30) and (4.33a):

$$\begin{aligned} \eta = nm \lim_{k \rightarrow 0} \frac{1}{k^2} & [\langle \perp | i\Sigma^c(\mathbf{k}, z = 0) | \perp \rangle \\ & + \langle \perp | (\Sigma^0 + \Sigma^c(\mathbf{k}0)) Q(Q i\Sigma^c(00) Q)^{-1} Q(\Sigma^0 + \Sigma^c(\mathbf{k}0)) | \perp \rangle] \end{aligned} \quad (4.67)$$

where $|\perp\rangle$ denotes the transverse momentum state. The corresponding expression for D reads however from eqs. (4.30) and (4.33a):

$$D = \lim_{k \rightarrow 0} \frac{1}{k^2} [\langle n | \Sigma^0 Q_s (Q_s i\Sigma_s^c(00) Q_s)^{-1} Q_s \Sigma^0 | n \rangle] \quad (4.68)$$

where $|n\rangle$ denotes the density state whereas Σ_s^c is the collision operator of the kinetic equation for the self-motions. In the case of the self-motions there is only one conserved state, namely $|n\rangle$, so that $Q_s = 1 - |n\rangle \langle n|$ in eq. (4.68) whereas the Q of eq. (4.67) projects onto the momentum space orthogonal to the five conserved states. As moreover the density is conserved by the collisions for all k (and z) values we have $\langle n | \Sigma_s^c(kz) \equiv 0$ whereas the transverse momentum is conserved only at $k = 0$; i.e. $\langle \perp | \Sigma^c(kz) = O(k)$. As a consequence all contributions involving the nonlocal (i.e. finite k) collision operator in eq. (4.67) do not contribute to D and only the purely kinetic term survives in eq. (4.68). Hence D requires only the knowledge of the Markovian collision operator $\Sigma_s^c(00)$. As a corollary we notice that if, as is often done in kinetic theory, the collision operator is approximated by a local or spatially Markovian operator, then eq. (4.67) will reduce to the kinetic shear-viscosity η_K :

$$\eta_K = nm \lim_{k=0} \frac{1}{k^2} [\langle \perp | \Sigma^0 Q(Q i\Sigma^c(\mathbf{0}\mathbf{0})Q)^{-1} Q \Sigma^0 | \perp \rangle] \quad (4.69)$$

quite similar to eq. (4.68). From eqs. (4.67–68) it is clearly seen that the computation of D and η requires the inverse of the collision operator. This cannot be done exactly and here a first approximation is introduced. Both D and η have been computed in the so-called one-Sonine-polynomial approximation [4.9]. For D this amounts to approximate Q_s in eq. (4.68) by $|\ell\rangle\langle\ell|$, $|\ell\rangle$ being the longitudinal momentum state, with the result:

$$D = v_0^2 / \langle \ell | i\Sigma_s^c(\mathbf{0}\mathbf{0}) | \ell \rangle \quad (4.70)$$

$v_0 = (m\beta)^{-1/2}$ being the thermal velocity. For η this amounts to approximate Q in eq. (4.67) by $|\perp\ell\rangle\langle\perp\ell|$, $|\perp\ell\rangle$ denoting the normalized product of a longitudinal and transverse momentum component, resulting in

$$\eta = nm \lim_{k=0} \frac{1}{k^2} \left[\langle \perp | i\Sigma^c(k\mathbf{0}) | \perp \rangle + \frac{\langle \perp | (\Sigma^0 + \Sigma^c(k\mathbf{0})) | \perp \rangle^2}{\langle \perp | i\Sigma^c(\mathbf{0}\mathbf{0}) | \perp \rangle} \right]. \quad (4.71)$$

At this stage it might be of interest to make the following remarks. As we expect the collisional effects to increase with Γ we deduce from eq. (4.70) that D will be a decreasing function of Γ in contrast to η which according to eq. (4.71) is the sum of a decreasing and an increasing term and hence can exhibit a minimum. These qualitative observations are in fact corroborated by the experimental findings discussed in subsection 4.5. A second remark which may clarify our criticism (just after eq. (4.64)) of the work reported in [4.38] and used in [4.34] concerns the neglect of all non-conserved momentum states. If this is done, i.e. if we neglect states like $|\perp\ell\rangle$, then the second term of eq. (4.71) will drop out and we are left with only the first term which can be reduced to the expression reported in [4.38]. As stated above this however amounts to neglect the term, η_K of eq. (4.69), which becomes dominant for weak-coupling:

$$\eta \simeq \eta_K \simeq \frac{nmv_0^2}{\langle \perp | i\Sigma^c(\mathbf{0}\mathbf{0}) | \perp \rangle}; \quad \Gamma \ll 1. \quad (4.72)$$

Indeed, a straightforward computation of eq. (4.72) with the Balescu–Guernsey–Lenard (BGL) approximation [1.4] to $\Sigma^c(\mathbf{0}\mathbf{0})$ leads to the well-known Spitzer-type formula:

$$\eta_{BGL} = \frac{5\sqrt{\pi}}{2} \cdot \frac{nm\omega_p k_D}{\varepsilon (\ln \varepsilon^{-1} + 0.346)}; \quad \varepsilon \ll 1 \quad (4.73)$$

where ε is related to Γ by eq. (3.7).

In the one-Sonine-polynomial approximation the computation of the transport coefficients reduces to the computation of a few matrix elements of the collision operator for which an explicit expression is needed. It is at this stage that the theories of [4.31] and [4.35] start to differ (besides the fact that one is concerned with the self-motions while the other considers the collective motions). Indeed, the common idea of pulling out of the dynamics (i.e. of Σ^c) as much static information as possible has been realized in two distinct ways, the details of which are discussed in [4.35]. Here it may suffice to say that the approximation of Wallenborn and Baus [4.35] guarantees that $\Sigma^c(k, t = 0)$ takes on its exact value while that of [4.31] does not, which leads to observable discrepancies between the short-time behaviour of $M(t)$ as calculated in [4.31] and the MD values

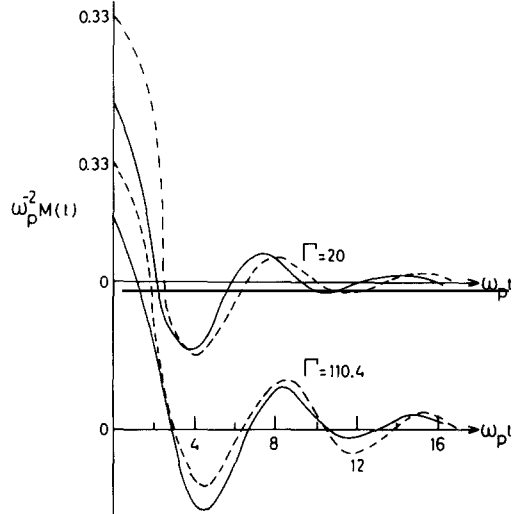


Fig. 11. The memory function $M(t)$ as a function of t for two values of Γ . The dashed curves represent the MD data [4.14] while the full curves are the results of the kinetic theory of Gould and Mazenko [4.31]. Notice the discrepancies in the initial values.

(see fig. 11). These kinetic theories are then “closed” by re-expressing $C(t)$ of eq. (4.63b) in terms of $S(t)$ as:

$$C(12, 34; t) \simeq S(13; t)S(24; t) + S(14; t)S(23; t) \quad (4.74)$$

for the collective motions, and as:

$$C_s(12, 34; t) = S_s(13; t)S(24; t) \quad (4.75)$$

for the self-motions. Notice that eq. (4.74) leads to a closed kinetic equation for $S(12; t)$ while eq. (4.75) couples the kinetic equation for $S_s(12; t)$ to that of $S(12; t)$. Although realized in a slightly different manner (see [4.35]) eqs. (4.74–75) constitute the second approximation of these kinetic theories. This approximation is usually called the “disconnected approximation” to the dynamics. It contains as a particular case the BGL approximation of which it constitutes a generalization to finite k, z and Γ values. With the aid of this approximation the various matrix elements entering eqs. (4.70–71) can be computed. They then acquire the form of ($k = 0$) mode-coupling expressions of the general form given in eq. (4.60). These mode-coupling integrals are then computed using the collisionless or mean field approximation for the various functions, $S(k, t)$, $S_\perp(k, t)$ and $S_s(k, t)$, appearing in them. This requires a knowledge of the $S(k)$ data which are taken as input. This then constitutes the last approximation in these theories. The most difficult point here concerns the rapid oscillations of these mode-coupling integrands. Here one has to distinguish the cases where the oscillations occur around a finite value (for ex., $\langle \perp | \Sigma^c | \perp \rangle$) from those where they occur around zero (for ex., $\langle \ell | \Sigma_s^c | \ell \rangle$, $\langle \perp \ell | \Sigma^c | \perp \ell \rangle$). In the latter case the result will be very sensitive to small changes in the integrand. An idea about the form of these oscillations can be obtained from the study of the asymptotic time-behaviour (“long-time tails”) of these mode-coupling integrals [3.29, 4.39–41]. Typically one has for the integrand of $\langle \perp | \Sigma^c | \perp \rangle$; i.e. the direct [4.39] contribution η_{dir} to η :

$$\lim_{t \rightarrow \infty} \eta_{\text{dir}}(t) = \frac{(\pi \Gamma_p t)^{-3/2}}{120\beta} \left[1 + \left(1 + \left(\frac{\omega_p \gamma_p}{\Gamma_p} \right)^2 \right)^{-3/4} \cos \left(2\omega_p t + \frac{3}{2} \arctg \frac{\omega_p \gamma_p}{\Gamma_p} \right) \right] \quad (4.76)$$

whereas for the self-diffusion ($\langle \ell | \Sigma_s^c | \ell \rangle$) one has:

$$M(t) = \frac{(Ze)^2}{6\sqrt{\pi m}} \left(\left(D + \frac{\Gamma_p}{2} \right) t \right)^{-3/2} \left(1 + \left(\frac{\omega_p \gamma_p}{\Gamma_p} \right)^2 \right)^{-3/4} \cos \left(\omega_p t + \frac{3}{2} \arctg \frac{\omega_p \gamma_p}{\Gamma_p + 2D} \right) \quad (4.77)$$

which corrects an earlier finding of [4.31]. This oscillation problem becomes worse for large Γ where the oscillations last longer (see subsection 4.5 for a related discussion). Very fortunately, in the case of the shear viscosity the difficult term ($\langle \perp \ell | \Sigma^c | \perp \ell \rangle$) contributes little to η for large Γ as seen from eq. (4.71). For η one can thus neglect the oscillations and compute the mode-coupling integrals with a free-particle dynamics leaving all correlational aspects for the statics. This, in our opinion, explains the remarkable agreement (see fig. 12) between the MD values of η and the results of Wallenborn and Baus [4.35]. For the self-diffusion the situation is not so favorable since there is only one term present, $D^{-1} \sim \langle \ell | \Sigma_s^c | \ell \rangle$, which has to be described correctly both for weak and strong coupling. The theoretical computation of D for all Γ to within fifty percent remains therefore still an unsolved problem.

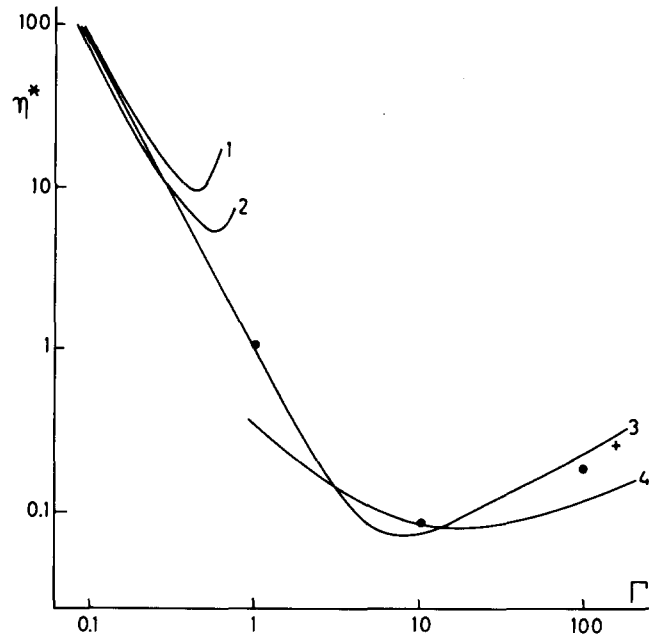


Fig. 12. The dimensionless shear viscosity $\eta^* = \eta / nm\omega_p a^2$ versus Γ as obtained from the kinetic equation of Landau (1), Balescu-Guernsey-Lenard (2) and Wallenborn-Baus (3) (see [4.35]). Curve 4 corresponds to the sum-rule analysis of Vieillefosse and Hansen [3.9], the dots represent the MD results [4.15] while the cross corresponds to the estimate of [4.14].

5. An outlook on further Coulomb systems

Until now we have been focusing our attention on the classical OCP as a prototype of systems governed by Coulomb interactions. In this section we shall first consider a number of corrections

to, and variations of the OCP model which indicate how this model can be made more realistic. In the last subsection of this section we shall briefly consider some examples of classical two-component plasmas in which charge neutrality is guaranteed by the presence of two oppositely charged mobile species, rather than by a uniform neutralizing background. Within the limited size of this review it is of course impossible to treat two-component systems, which include electrolytes, molten salts and ion-electron plasmas, in any exhaustive way. Our aim is rather to show, from selected examples, how the concepts and techniques introduced for the OCP, can easily be generalized to more complex Coulomb systems.

5.1. Corrections to the classical OCP model: contact with the real world

It was shown in the introduction that the OCP is a reasonable approximation of matter under extreme conditions of temperature and density. More precisely a plasma of point ions and electrons reduces to the OCP in the limit $r_s \rightarrow 0$ and $\Lambda/a \rightarrow 0$, where r_s is defined by eq. (1.4) and the ionic de Broglie thermal wavelength Λ by eq. (1.5).

For finite but not too large values of Λ/a and r_s , it seems reasonable to calculate the static properties of an ion-electron plasma by perturbation theories, in which the OCP appears as the zeroth order approximation. We shall successively consider the quantum corrections, due to the finiteness of Λ/a , and the electron polarization corrections, due to the finiteness of r_s .

5.1.1. Quantum corrections

Contrarily to the case of neutral systems, where the pair potentials contain strongly repulsive hard cores, we must consider two distinct problems in the case of the OCP: the corrections to the thermodynamic properties, which are essentially determined by the behaviour of the pair distribution function $g(r)$ at interionic distances of the order of the ion sphere radius a , and the corrections to $g(r)$ itself in the range $r \lesssim \Lambda$. While the former problem can be handled by perturbation theory as long as $\Lambda/a < 1$, the latter problem cannot since the quantum-mechanical $g(r)$ does not vanish as $r \rightarrow 0$ due to tunnelling through the “soft” Coulomb barrier. $g(0)$ will generally remain quite small, so that the thermodynamic properties like the excess internal energy, will not be affected by tunnelling. The effect is however crucial in determining the enhancement factor of pycnonuclear reaction rates [2.11, 3.10–3.13, 5.1, 5.2].

The deviation of the Helmholtz free energy from its classical value can be expanded in powers of Λ^2 (i.e. of h^2), as first shown by Wigner [5.3]. The first order correction involves the classical ensemble average of the Laplacian of the pair potential. In the case of the OCP, use of Poisson’s equation leads immediately to the simple result [3.20]:

$$\frac{\beta F^{(1)}}{N} = \frac{\pi \hbar^2 n Z^2 e^2 \beta^2}{6m} = \frac{\Gamma^2}{8r_s} \times \frac{m_e}{m} \times \frac{1}{Z^{7/3}}. \quad (5.1)$$

This correction is structure-independent, so that to lowest order in h^2 , the fluid-solid transition is not shifted from its classical location by quantum corrections. The second order term ($O(h^4)$) is more complicated, since it involves integrals over the pair and triplet distribution functions [5.4].

It is important to realize that a high temperature is *not* a sufficient criterion for convergence of the Wigner expansion. Indeed, as stressed in the Introduction, the classical distance of closest approach (or Landau length) $l = Z^2 e^2 / k_B T$ becomes always shorter than Λ at sufficiently high temperatures, so that quantum effects must be treated in a non-perturbative way in the weak

coupling limit, e.g. by the introduction of an effective pair potential which takes quantum effects at short distances into account [5.42].

For similar reasons the Wigner expansion may also be used to compute quantum corrections to $g(r)$ for $r \gg \Lambda$, but it must break down for sufficiently short distances, since quantum effects always dominate the pair correlations for $r < \Lambda$. In fully ionized dense stellar matter, the rate of nuclear reactions per nucleus and per unit time is proportional to $ng(r)$, where r is of the order of the nuclear diameter ($\sim 10^{-13}$ cm), which is much shorter than both a and Λ under typical white dwarf conditions (see table 1). If $g_0(r)$ is the quantum-mechanical pair distribution function in the zero density limit (which is easily calculated by solving a two-body problem), the enhancement factor is defined as the ratio:

$$E = \lim_{r \rightarrow 0} \frac{g(r)}{g_0(r)}. \quad (5.2)$$

This factor is much larger than 1 and increases rapidly with density; it is due to screening which effectively reduces the Coulomb barrier and hence increases the rate of tunnelling.

A systematic approach to the calculation of E has recently been formulated by Jancovici and Alastuey [3.11, 5.2]. These authors reduce the quantum many-body problem to a one-body problem involving a complicated potential which depends on the coordinates of $N - 2$ particles; this one-body problem is then treated by semi-classical path integral techniques which lead to an expression of $\ln E$ in terms of known classical quantities. To lowest order they recover the purely classical result $\ln E = C$, where C is defined in eq. (3.36a); the leading corrections are proportional to $h^{4/3}$ and h^2 . Under the ^{12}C white dwarf conditions of table 1, $\ln E$ is calculated to be 18, corresponding to an enhancement factor of 7×10^7 !

Very recently these same authors have investigated the effects of a strong magnetic field on the static properties of the OCP [5.13]. They have generalized the Wigner expansion to compute the induced magnetization to order h^4 ; the leading term ($O(h^2)$) turns out to be independent of the interactions between particles, while the h^4 term is structure-independent for the OCP.

5.1.2. Electron screening corrections

The potential energy (2.5) for a periodic OCP of N ions in a volume Ω can be reexpressed in terms of the Fourier components $n(\mathbf{k})$, defined in eq. (3.19), of the microscopic number density, in the form:

$$V_N(\mathbf{r}^N, \Omega) = \frac{1}{2\Omega} \sum'_{\mathbf{k}} v(k) [n(\mathbf{k})n(-\mathbf{k}) - N] \quad (5.3)$$

where the prime means that the singular term $\mathbf{k} = 0$ is to be left out to take proper account of the uniform background, and $v(k) = 4\pi Z^2 e^2 / k^2$. It was pointed out earlier that the degenerate electron gas, which constitutes the physical neutralizing background, is polarized by the ionic charge distribution, having Fourier components $Z\epsilon_e(\mathbf{k})$, for finite values of r_s . The formation of non-uniform electron “clouds” around each ion will modify the ion-ion interaction. A standard linear response calculation shows that the resulting effective ion-ion potential is simply [1.7, 5.5, 3.25]

$$v_{\text{eff}}(k) = v(k)/\epsilon_e(k) \quad (5.4)$$

and the total potential energy of the system is still given by (5.3), with $v(k)$ replaced by $v_{\text{eff}}(k)$. Non-linear terms, leading to effective interactions between three and more ions, have been derived [5.6], but are expected to remain small as long as $r_s < 1$. The static dielectric constant $\varepsilon_e(k)$ of the fully degenerate electron gas has been calculated by various authors (see e.g. [4.25]); in the high density limit, $\varepsilon_e(k)$ reduces to the well-known form obtained by Lindhard [1.7] in the framework of the RPA.

The range of the effective potential $v_{\text{eff}}(r)$ in \mathbf{r} -space is of the order of the electron screening length which is roughly equal to the Thomas–Fermi length (1.7). Clearly, for $r_s \ll 1$, we are in the “weak screening” regime, while for $r_s \gtrsim 1$, λ_{TF} is of the order of the inter-ionic spacing, and we are in a “strong screening” regime.

Hubbard and Slattery [5.5] have carried out some Monte Carlo computations for a hydrogen plasma (H^+ ions and electrons) both in the weak ($r_s = 0.1$) and strong ($r_s = 1$) screening regimes; they used the Lindhard dielectric function and their computations cover the range $10 \leq \Gamma \leq 75$ which includes Jovian conditions (see table 1). Considering the small number of particles (27 or 32), the number of configurations (12000) generated in each run, and the very approximate treatment of the Ewald sums, the results quoted by these authors are probably affected by relatively large errors. Their computations have however the merit of showing that the thermodynamic properties are little changed compared to the OCP results ($r_s = 0$). On the other hand the effect of electron screening in reducing the degree of correlation among ions is clearly exhibited by the computed pair distribution functions.

The potential energy for a system of ions in a responding background can be rewritten in the form:

$$V_N(\mathbf{r}^N, \Omega) = \frac{1}{2\Omega} \sum_{\mathbf{k}} \frac{4\pi Z^2 e^2}{k^2} [n(\mathbf{k})n(-\mathbf{k}) - N] + \frac{1}{2\Omega} \sum_{\mathbf{k}} \frac{4\pi Z^2 e^2}{-\mathbf{k}^2} \left[\frac{1}{\varepsilon_e(k)} - 1 \right] n(\mathbf{k})n(-\mathbf{k}). \quad (5.5)$$

The first term in (5.5) accounts for the direct ion–ion interaction; it is identical with the potential energy of the unscreened OCP. The second term corresponds to the indirect, or electron-induced, ion–ion interaction, which vanishes in the limit $r_s \rightarrow 0$. For sufficiently weak screening it is hence natural to treat this second term by thermodynamic perturbation theory [5.8, 3.25] using the OCP as a “reference” system. The first order correction to the free energy is simply the canonical average of the second term in eq. (5.5) over the reference system ensemble. Using (3.19) this yields in the thermodynamic limit:

$$\frac{\beta F_1}{N} = f_1(\Gamma; r_s) = \frac{1}{2} \int \frac{d\mathbf{k}}{(2\pi)^3} w(k) S_0(k) \quad (5.6)$$

where $S_0(k)$ is the structure factor of the OCP and $w(k)$ is the perturbation potential:

$$w(k) = v_{\text{eff}}(k) - v(k) = \frac{4\pi Z^2 e^2}{-\mathbf{k}^2} \left[\frac{1}{\varepsilon_e(k)} - 1 \right]. \quad (5.7)$$

Higher order terms have been considered in reference [3.25] and the perturbation series appears to converge well for $q_{\text{TF}} = a/\lambda_{\text{TF}} < 1$. The dominant contribution to $\beta F_1/N$ is of order q_{TF}^2 , i.e. *linear* in r_s , and independent of the precise approximation made for $\varepsilon_e(k)$, provided the dielectric function reduces correctly to the Lindhard form as $r_s \rightarrow 0$. For a hydrogen plasma the linear variation in r_s dominates up to $r_s \sim 1$, as shown by the MC results of De Witt and Hubbard [5.7].

On the other hand in the strong screening regime ($q_{\text{TF}} > 1$), the perturbation theory breaks

down and variational theories have been used to calculate the thermodynamics of a screened ionic plasma. These theories are based on the well-known Gibbs–Bogoliubov inequality [1.2] which states that the Helmholtz free energy of any system is bounded from above by the sum of the Helmholtz free energy of any reference system plus the first order correction (5.6) of thermodynamic perturbation theory:

$$\beta F/N \leq \beta F_0/N + \beta F_1/N. \quad (5.8)$$

In a variational calculation the right-hand side of the inequality is minimized with respect to one or several parameters characterizing the reference potential. Two very different choices for the reference system have been made: Ross and Seale [5.9] chose the hard sphere fluid as a reference, with the diameter d (or equivalently the packing fraction $\eta = \pi n d^3 / 6$) as variational parameter, whereas Galam and Hansen [3.25] chose the unscreened OCP as reference system, the charge Z_e (or equivalently the coupling parameter Γ) being the parameter. Both calculations yield upper bounds to the free energy which are quite close under strong screening conditions. The former choice of reference system has the advantage of leading to expressions which can be evaluated analytically, while the latter choice yields somewhat lower free energies; moreover the screened system reduces correctly to the OCP reference system in the weak screening limit.

The most striking feature of the MC and variational results is that even under relatively strong screening conditions ($q_{TF} \simeq 1$), the screening corrections to the thermodynamic properties are much smaller than their OCP values. Typically for a hydrogen plasma at $r_s = 1$, the pressure differs by less than 1% from its OCP value, while the free energy correction is of the order of a few percent in the range $\Gamma > 100$. It should however be noted that the screening corrections are rather sensitive to the exact form of $\varepsilon_e(k)$ when $r_s \gtrsim 1$.

The variational calculations of Ross and Seale [5.9] have been extended by Stroud and Ashcroft [5.10] to the case of zero electron screening (i.e. $\varepsilon_e(k) = 1$); in other words these authors have derived an upper bound to the Helmholtz free energy of the OCP by using a hard sphere reference system! Despite the fact that the two systems differ so widely the calculated upper bound turns out to be surprisingly close to the “exact” free energy of the OCP in the strong coupling limit: for $\Gamma \gtrsim 100$, the upper bound lies only about 1% above the free energy of the OCP obtained from the MC computations. This excellent agreement is reminiscent of the observation that the structure factors of the hard sphere fluid and of the OCP are strikingly similar near the fluid-solid transition [5.11].

Before closing this section it is worth mentioning two other calculations which illustrate the relation between the OCP and the “real world”. Minoo et al. have used the OCP structure factors to compute the electronic transport coefficients of the hydrogen plasma and of liquid alkali metals [5.12] using Ziman’s theory of electronic transport in liquid metals [5.14]. The work on the liquid alkali shows the striking resemblance between the structure factors of liquid Na and K and the structure factor of the OCP under identical conditions of temperature and density, i.e. without any adjustable parameter. This is an indication that the OCP might be a good starting point for the description of simple liquid metals.

5.2. The classical electron layer: a 2-D OCP

One of the favourite games of present-day statistical physics is the study of the influence of spatial dimensionality on various physical phenomena. In the case of Coulomb systems there is no

unique way to do this. Indeed one can assume the particles to interact via the pair potential $v(r) = Z^2 e^2 / r$, where r is the d -dimensional distance between two particles. In this case the Fourier transform $v(k)$ of the potential becomes a sensitive function of d . One can however also define the interaction potential via the d -dimensional Poisson equation. In the latter case it is $v(r)$ which becomes a sensitive function of dimensionality while $v(k) \sim k^{-2}$ remains unchanged. In the former case ($v(r) \sim r^{-1}$, all d), one thinks of a system of particles whose motion is, to a good approximation, restricted to a d -dimensional subspace of ordinary space, whereas in the latter case ($v(k) \sim k^{-2}$, all d), the motion is supposed to be strictly d -dimensional. Although the latter case has been studied by a number of authors (see, e.g. [5.15–5.18, 2.6]), especially for $d = 2$, where it is related to a number of field-theoretical models, we shall restrict ourselves to the former case here, because of its direct experimental interest. Indeed, as discussed in detail in the review by Cole [1.8], one can fix extra electrons on the surface of dielectric liquids by means of an external electric field and the image-potential of the electrons. In this way the extra electrons can be trapped in the lowest quantum state of their motion away from the surface. The motion of these electrons in a plane parallel to the surface can be described *classically* under the current experimental conditions [1.8]. Although no genuine background is present here, the charges on the metallic plates producing the external electric field render the system electrically neutral. Moreover these electrons interact via the usual 3-D Coulomb law $v(r) = e^2 / r$, where e represents an effective charge (close to the bare electron charge) to account for the presence of the adjacent dielectric media. What has been realized in this way is nothing but a classical 2-D OCP.

This system has been studied through laboratory [5.19, 5.20] and numerical [5.21–5.23] experiments. The early theoretical investigations [5.24, 5.25] were restricted to the weak-coupling (RPA) region, while more recent studies [5.26–5.30] deal with the static properties outside the RPA domain, up to the crystallization region [5.31–5.33] and with the magnetic properties [5.13]. Two investigations of the dynamic properties have also been reported [5.34–5.35]. Because of the close analogy with the results for the 3-D OCP, we shall be brief and point out only those features which are modified by the change in dimensionality.

Keeping the notations of the 3-D case, we first define the characteristic constants appropriate for the 2-D OCP. The modifications result from the fact that the 2-D Fourier transform of the Coulomb potential $v(r) = e^2 / r$ reads $v(k) = 2\pi e^2 / k$. As a result the Debye wave number becomes $k_D = 2\pi n \beta e^2$, where n is the average number of electrons per unit area. The 2-D plasma frequency $\omega_p \equiv v_0 k_D = 2\pi n e^2 (\beta/m)^{1/2}$ is here temperature dependent. The dimensionless coupling constants are chosen to be $\Gamma = \beta e^2 / a$ and $\lambda = k_D^2 / n$, where a is the ion-circle radius $\pi a^2 = n^{-1}$. Note that $\Gamma = (\lambda / 4\pi)^{1/2}$ and $a k_D = 2\Gamma$.

5.2.1. Static properties

Just as in the 3-D case, the Coulomb interactions manifest themselves in the typical long wavelength behaviour of the static structure factor $S(k)$:

$$\lim_{k \rightarrow 0} S(k) = \left(\frac{k_D}{k} + \frac{\chi_T^0}{\chi_T} \right)^{-1} \simeq \frac{k}{k_D}. \quad (5.9)$$

Comparing this with eq. (3.34) and the discussion of subsection 3.3 we see that the Coulomb divergence of $\hat{c}(k)$ has been weakened in 2-D. Eq. (5.9) however still leads to Stillinger–Lovett spatial sum-rules analogous to eqs. (3.31). The Debye–Hückel approximation is similarly obtained from

$\hat{c}_{\text{DH}}(k) = -k_{\text{D}}/k$ [5.24, 5.26, 5.28]. The major point here is that in the DH approximation the pair distribution function:

$$g_{\text{DH}}(r) = 1 - \frac{\beta e^2}{r} \int_0^\infty dx \frac{x J_0(x)}{x + k_{\text{D}} r} \quad (5.10)$$

decays algebraically ($\sim r^{-3}$) at large r , rather than exponentially as in the 3-D case (see eq. (3.45a)); the integral yielding the equation of state:

$$\frac{U - U^0}{2U^0} = \frac{P - P^0}{P^0} = -\frac{\lambda}{8\pi} \int_0^\infty \frac{dy}{y} \int_0^\infty dx \frac{x J_0(x)}{x + y} \quad (5.11)$$

diverges logarithmically (for small $y = k_{\text{D}}r$) pointing to the non-applicability of the DH approximation in 2-D. In eqs. (5.10–5.11) $J_0(x)$ is the zeroth-order Bessel function of the first kind.

The weak coupling ($\lambda \ll 1$) thermodynamic properties have been computed by Chalupa [5.26] and Totsuji [5.27, 5.28] using the Mayer cluster expansion. The correct small λ equation of state reads [5.27]:

$$\frac{P - P^0}{P^0} = \frac{\varepsilon}{4} [\ln 2\varepsilon - 1 + 2\gamma + O(\varepsilon)] \quad (5.12)$$

where $\varepsilon = \lambda/2\pi$. This result is to be compared with eqs. (3.7) and (3.47a) for the 3-D case.

The inadequacy of $g_{\text{DH}}(r)$, eq. (5.10), for computing the thermodynamic properties reflects the increased importance of the short range correlations in 2-D. These are treated more correctly by the HNC equation (3.67) which has been solved numerically for the 2-D OCP by Lado [5.30]. His results are in good agreement with the MC data of Totsuji [5.22] and of Gann et al. [5.23]. In the weak coupling limit the HNC data agree with the first two terms of the Salpeter Debye-chain expansion of $g(r)$ [5.36] obtained by Totsuji [5.28], which in turn are consistent with the plasma parameter expansion (5.12). For larger values of λ , short range order develops above a critical value $\Gamma_c \simeq 2.5$ [5.22, 5.30]. For $\Gamma \gtrsim 1$ the HNC and MC data for the excess internal energy per particle, $u(\Gamma) = (U - U^0)/U^0$, are well represented by the simple form (3.40), already familiar from the 3-D case. The optimum parameters are the following:

$$\text{HNC: } a = -1.105564; \quad b = 0.52248; \quad c = -0.1979; \quad s = 0.3 \quad (5.13)$$

$$\text{MC: } a = -1.107763; \quad b = 0.76373; \quad c = -0.4419; \quad s = 0.2. \quad (5.14)$$

Note that the coefficients of the linear term are close to the triangular lattice result, $a_{\text{triang.}} = -1.106103$.

At $\Gamma = 95 \pm 2$ a fluid-solid transition has been observed by Hockney and Brown [5.21], who used a variant of the MD method on a system of 10^4 particles. This phase transition occurs between a fluid and a poly-crystalline phase and appears to be of second order since it is characterized by a specific heat anomaly $c_v \sim |\varepsilon|^{-\alpha}$, where $\varepsilon = (T - T_f)/T_f$ with $\alpha = 0.14 \pm 0.04$ for $\varepsilon > 0$, and $\alpha' = 0.08 \pm 0.02$ for $\varepsilon < 0$ ("lambda-type" transition). Very recently Gann et al. [5.23] have performed MC simulations of the fluid and solid phases on smaller systems ($N \leq 100$), and reached somewhat different conclusions; they locate the melting point at $\Gamma = 125 \pm 15$ (compared to 155 ± 10 in 3-D [3.23]), and the transition appears to be weakly first order. The long standing

theoretical arguments against 2-D crystalline order [5.37] have recently been shown not to apply to this 2-D OCP [5.38].

The perfect crystal phase was studied by Crandall [5.31]. Theoretical estimates of the melting temperature of the 2-D OCP based on the Kosterlitz–Thouless theory of dislocations [5.39] have recently been reported [5.32, 5.33]; Thouless [5.32] predicts melting at $\Gamma = 78$, in fair agreement with the computer simulation results.

5.2.2. Dynamic properties

The dynamic properties of the 2-D OCP are dominated by the fact that in this system the plasma mode is a *low* frequency mode. This is already apparent from the RPA [5.24, 5.25, 5.27] which amounts to replacing $c(k)$ of eq. (4.32) by its DH value $c_{\text{DH}}(k) = -k_{\text{D}}/k$, leading for small k to the characteristic frequency:

$$\lim_{k \rightarrow 0} \omega(k) = \omega_p \left(\frac{k}{k_{\text{D}}} \right)^{1/2} + \mathcal{O}(k^{3/2}). \quad (5.15)$$

This peculiar dispersion of the 2-D plasma mode has been verified in the laboratory experiment of Grimes and Adams [5.19]. Unfortunately the damping of this plasma mode, as observed experimentally, is dominated by non-Coulombic phenomena, essentially the scattering of the electrons on the surface waves (riplons) of the under-lying dielectric liquid. The further discussion of the dynamics of the 2-D OCP in the context of its laboratory realization is quite fascinating, but somewhat outside the scope of this review. For instance, it has been reported recently by Voldin et al. [5.40] that under certain conditions the planar surface can become hydrodynamically unstable leading to the production of electron bubbles. The lifetime of surface state electrons has also been considered by Nagano et al. [5.41].

The theoretical study of the 2-D OCP by itself, i.e. as a model for future MD experiments and a first approximation to the laboratory electron layer, can however be pursued along the lines developed in subsection 4.3. The results obtained by Baus [5.35] can be summarized in the following expression for the Van Hove function $S(k, t)$ valid in the limit of small wave numbers and long times:

$$S^{\text{H}}(k, t) = n \frac{k}{k_{\text{D}}} \left\{ \frac{k}{k_{\text{D}}} \frac{\bar{c}^2}{v_0^2} \left(1 - \frac{C_v}{C_p} \right) \exp \left[-k^2 \frac{\kappa(k)}{nmC_v} t \right] \right. \\ \left. + \left[1 - \frac{k}{k_{\text{D}}} \frac{\bar{c}^2}{v_0^2} \left(1 - \frac{C_v}{C_p} \right) \right] \cos \left[\sqrt{\frac{k}{k_{\text{D}}}} \omega_p \left(1 + \frac{1}{2} \frac{k}{k_{\text{D}}} \frac{\bar{c}^2}{v_0^2} \right) t \right] \exp \left[-\frac{k^2}{2} \frac{v(k)}{nm} t \right] \right\} \quad (5.16)$$

where we have used the notations of eqs. (4.33–4.34), while $v = \eta + \xi$ denotes the 2-D longitudinal viscosity. This form is quite similar to the 3-D result, eq. (4.35), except for two points: 1) the various strengths which are of order k^2 in 3-D are of order k in 2-D as a result of the weakening of the Coulomb divergence; 2) all quantities can be expressed in terms of thermodynamic and transport parameters as a consequence of the fact that in 2-D both the thermal and the plasma mode are low frequency modes for small k . The situation is somewhat complicated by the fact that the ordinary transport coefficients κ and v do not exist in 2-D as a result of the non-integrability of the long time tails of the Kubo integrands (see eqs. (4.76–4.77) for the 3-D case). This weak singularity ($\sim |\ln k|^{1/2}$) is taken care of in eq. (5.16) by the k -dependence of the thermal conductivity $\kappa(k)$ and of the longitudinal viscosity $v(k)$. For a more detailed discussion and references to the extensive

literature on this subject one can consult [4.11], [3.29] and [5.35]. Qualitatively similar results for the thermal and plasma modes have been obtained independently by Onuki [5.34] with the aid of a Boltzmann model collision operator and the hydrodynamic equations, both of which are, strictly speaking, not applicable to the 2-D OCP.

Finally it is worthwhile to point out that the exact result of eq. (5.16) is, as far as the plasma frequency is concerned, in conflict with the RPA result. Indeed the small k dispersive correction to eq. (5.15) as calculated in the RPA [5.24, 5.25, 5.27] reads $\omega(k) = \sqrt{k/k_D} \omega_p(1 + \frac{3}{2}k/k_D)$, whereas eq. (5.16) yields for weak coupling ($\bar{c}^2/v_0^2 \approx 2$ in 2-D) $\omega(k) = \sqrt{k/k_D} \omega_p(1 + k/k_D)$. Hence we reach the rather surprising conclusion that one cannot use neither the DH theory nor the RPA to describe the static or dynamic properties of a weakly coupled 2-D OCP.

5.3. Binary ionic mixtures

The 3-D OCP model can be generalized in another direction by mixing two (or more) distinct ionic species having different charges and masses. If the two charges are of the same sign, charge neutrality must again be guaranteed by a neutralizing uniform background. We then deal with binary ionic mixtures which are of interest for two reasons. Firstly it has become clear in recent years that such mixtures phase separate under conditions of pressure and temperature which are of astrophysical interest. Secondly the additional macroscopic variable, i.e. concentration, renders the dynamical collective modes in a sense richer than in the one component plasma. The exact nature of these modes has recently been elucidated by theoretical analysis and computer “experiments”. The thermodynamics, structure and phase diagram of ionic mixtures will be examined in subsections 5.3.1 and 5.3.2, while the dynamics are studied in subsection 5.3.3.

5.3.1. Static properties

We restrict ourselves to binary mixtures (the generalizations to more components being obvious), made up of N_1 point ions of charge $Z_1 e$ and mass m_1 , and N_2 ions of charge $Z_2 e$ ($Z_2 > Z_1$) and mass m_2 in a volume Ω . The partial number densities are $n_\sigma = N_\sigma/\Omega$ ($\sigma = 1, 2$) and the number concentrations are $x_\sigma = N_\sigma/N$; the total number density is $n = n_1 + n_2 = N/\Omega$ and the charge density is $\rho = \sum_\sigma Z_\sigma e n_\sigma = \bar{Z} e n$, where $\bar{Z} = \sum_\sigma x_\sigma Z_\sigma$ is the mean valence. If the neutralizing background is rigid, the potential energy for the periodic system is most compactly expressed as a generalization of eq. (5.3):

$$V_N(\mathbf{r}^N, \Omega) = \frac{1}{2\Omega} \sum_{\mathbf{k}}' \frac{4\pi}{k^2} [\rho(\mathbf{k})\rho(-\mathbf{k}) - N\bar{Z}^2 e^2] \quad (5.17)$$

where $\rho(\mathbf{k})$ is a Fourier component of the charge density:

$$\rho(\mathbf{k}) = \sum_\sigma Z_\sigma e n_\sigma(\mathbf{k}) \quad (5.18a)$$

$$n_\sigma(\mathbf{k}) = \sum_{i=1}^{N_\sigma} \exp \{ik \cdot \mathbf{r}_i\} \quad (5.18b)$$

$$\bar{Z}^2 = \sum_\sigma x_\sigma Z_\sigma^2. \quad (5.19)$$

As in the case of the OCP, we define the “ion-sphere” radius a from the total number density (see eq. (1.1)), whereas from the charge density ρ we define the radius:

$$a' = (3e/4\pi\rho)^{1/3} = a/\bar{Z}^{1/3}. \quad (5.20)$$

Apart from the ideal gas contributions, the thermodynamic state of the binary ionic mixture is completely determined by one concentration, say x_1 , and by either of the dimensionless coupling parameters:

$$\Gamma = \frac{e^2}{ak_B T} \quad (5.21)$$

or

$$\Gamma' = \frac{e^2}{a'k_B T} \quad (5.22)$$

or

$$\epsilon = \frac{\bar{Z}^2 e^2}{\lambda_D k_B T} \quad (5.23)$$

where λ_D is the Debye length for the mixture, defined by:

$$\lambda_D^{-2} = k_D^2 = \sum_{\sigma} 4\pi n_{\sigma} Z_{\sigma}^2 e^2 \beta = 4\pi n \bar{Z}^2 e^2 \beta. \quad (5.24)$$

The pair structure of a binary ionic mixture is characterized by three pair distribution functions $g_{11}(r)$, $g_{12}(r) \equiv g_{21}(r)$ and $g_{22}(r)$. The three direct correlation functions $c_{\sigma\sigma'}(r)$ are defined in terms of the pair correlation functions $h_{\sigma\sigma'}(r) = g_{\sigma\sigma'}(r) - 1(\sigma, \sigma' = 1, 2)$ through three Ornstein-Zernike relations which generalize the one component relation (3.17). Introducing the dimensionless Fourier transforms $\hat{c}_{\sigma\sigma'}(k) = nc_{\sigma\sigma'}(k)$ and $\hat{h}_{\sigma\sigma'}(k)$, these relations read:

$$\hat{h}_{\sigma\sigma'}(k) = \hat{c}_{\sigma\sigma'}(k) + \sum_{\sigma_1=1}^2 x_{\sigma_1} \hat{h}_{\sigma\sigma_1}(k) \hat{c}_{\sigma_1\sigma'}(k). \quad (5.25)$$

The three partial structure factors are defined as:

$$\begin{aligned} S_{\sigma\sigma'}(k) &= \frac{1}{(N_{\sigma} N_{\sigma'})^{1/2}} \langle n_{\sigma}(k) n_{\sigma'}(-k) \rangle_{\Omega} \\ &= \delta_{\sigma\sigma'} + (x_{\sigma} x_{\sigma'})^{1/2} \hat{h}_{\sigma\sigma'}(k). \end{aligned} \quad (5.26)$$

A quantity of central importance is the charge density structure factor $S_{\rho\rho}(k) \equiv n \bar{Z}^2 S'(k)$, where:

$$\begin{aligned} S'(k) &= \frac{1}{N \bar{Z}^2 e^2} \langle \rho(k) \rho(-k) \rangle_{\Omega} \\ &= \frac{1}{N \bar{Z}^2} \sum_{\sigma} \sum_{\sigma'} (x_{\sigma} x_{\sigma'})^{1/2} Z_{\sigma} Z_{\sigma'} S_{\sigma\sigma'}(k). \end{aligned} \quad (5.27)$$

The usual charge neutrality and perfect screening conditions imply for $S'(k)$ a similar long wavelength limit as for the OCP structure factor:

$$S'(k) = \frac{k^2}{k_D^2} + O(k^4) = \frac{(ak)^2}{3\Gamma \bar{Z}^2} + O(k^4).$$

The excess internal energy is most compactly expressed as an integral over the charge density structure factor, as is immediately clear from eqs. (5.17) and (5.27):

$$\frac{\beta U^{\text{ex}}}{N} = u(\Gamma, x_1) = \frac{\beta}{2} \int \frac{d\mathbf{k}}{(2\pi)^3} \frac{4\pi \bar{Z}^2 e^2}{k^2} [S(k) - 1]. \quad (5.28)$$

The equation of state then follows from eq. (3.11). A suitable generalization of the compressibility equation (3.33) for the OCP expresses the isothermal compressibility of the mixture in terms of the regular part of the three direct correlation functions:

$$\begin{aligned} \frac{\chi_T}{\chi_T^0} &= [1 - \sum_{\sigma} \sum_{\sigma'} x_{\sigma} x_{\sigma'} c_{\sigma\sigma'}^R(k=0)]^{-1} \\ c_{\sigma\sigma'}^R(k) &= \hat{c}_{\sigma\sigma'}(k) + \frac{4\pi n \beta Z_{\sigma} Z_{\sigma'} e^2}{k^2}. \end{aligned} \quad (5.29)$$

In the weak coupling limit ($\Gamma \ll 1$) the various static properties reduce to their Debye–Hückel expressions which are obvious generalizations of eqs. (3.47) and (3.48); in particular:

$$u^{\text{DH}}(\Gamma, x_1) = -\frac{1}{2}\epsilon = -\frac{1}{2}\sqrt{3}(\Gamma \bar{Z}^2)^{3/2}. \quad (5.30)$$

The Mermin inequality [2.9] states that (5.30) is a lower bound to u for all Γ and x_1 . In the strong coupling limit ($\Gamma \gg 1$) we expect the Lieb–Narnhofer bound [2.4], suitably generalized to the case of mixtures, to be more useful:

$$u \geq -0.9\Gamma \bar{Z}^{1/3} \bar{Z}^{5/3} = -0.9\Gamma' \bar{Z}^{5/3}. \quad (5.31)$$

It is interesting to note that the crude “ion-sphere model” for ionic mixtures [2.11] yields an internal energy which is precisely equal to the lower bound (5.31).

The various weak, intermediate and strong coupling theories which have been developed for the OCP (see subsections 3.5–3.7) could in principle be generalized to treat the two component fluid. In fact only the most successful among these theories, i.e. HNC theory, has been investigated in some detail. In the case of a binary mixture three equations, one for each partial correlation function $h_{\sigma\sigma}(r)$, replace the single eq. (3.58). Together with the three OZ relations (5.25), these equations form a closed set which must be solved iteratively. Numerical solutions have been obtained, for ionic charge ratios $Z_2/Z_1 = 2$ and 3, over an extensive range of Γ values and compositions [5.45, 5.46]. Some “exact” Monte Carlo computations were carried out in parallel to check the HNC results [5.46] which turn out to be very accurate; as in the one component case, the HNC thermodynamic properties differ by less than 1% from the MC results at any Γ or composition.

Both sets of data show that for strong coupling ($\Gamma \gtrsim 1$), the excess thermodynamic properties of mixing at constant temperature and *charge* density are practically negligible compared to the corresponding properties of the pure phases. In other words the excess Helmholtz free energy (or any other thermodynamic function) of the mixture can be written, to a very good accuracy, as a linear combination of the free energies of the corresponding pure phases taken at constant Γ' :

$$\beta F^{\text{ex}}/N = f(\Gamma', x_1) \simeq x_1 f_0(\Gamma' Z_1^{5/3}) + (1 - x_1) f_0(\Gamma' Z_2^{5/3}) \quad (5.32)$$

where $f_0(\Gamma)$ is the excess free energy of the OCP. It is interesting to note that the Lieb–Narnhofer lower bound (5.31) satisfies this linear relation exactly. On the other hand this relation must break

down at sufficiently weak coupling ($\Gamma \ll 1$), since it does not satisfy the correct Debye–Hückel limit (5.30).

The deviations from the linear relation (5.32) increase with increasing charge ratio Z_2/Z_1 . Brami et al. [5.47] have developed a systematic procedure which improves upon eq. (5.32) by expressing the thermodynamics of mixtures for arbitrary charge ratio in terms of the corresponding properties of the pure phases and of infinitely dilute solutions of each species in a pure fluid of the other species. This procedure has been checked by explicit HNC computations and proves to be very accurate for charge ratios as high as 24 to 1!

In the spirit of the Van der Waals “one fluid theory” [1.2], it is tempting to express the thermodynamic properties of an ionic mixture in terms of the properties of an underlying pure “reference” fluid (i.e. an OCP) of ions carrying an *effective* charge Z_{eff} . In such a “one fluid approximation”, the excess free energy of the mixtures is simply given in terms of the free energy of the OCP by:

$$f(\Gamma', x_1) = f_0(\Gamma_{\text{eff}})$$

with

$$\Gamma_{\text{eff}} = \Gamma Z_{\text{eff}}^2 = \Gamma' Z_{\text{eff}}^2 / \bar{Z}^{1/3}. \quad (5.33)$$

The DH limit suggests $Z_{\text{eff}}^2 = \bar{Z}^2$, while for strong coupling, the Lieb–Narnhofer bound (5.31) suggests $Z_{\text{eff}}^2 = \bar{Z}^{1/3} \bar{Z}^{5/3}$ [5.48, 5.49]. The latter choice predicts reasonable thermodynamic properties of strongly coupled mixtures as long as the charge ratio is not too high ($Z_2/Z_1 \lesssim 2$), but in any case a comparison with HNC and MC results shows that the approximation (5.32) is always superior to the “one-fluid approximation” (5.33) with $Z_{\text{eff}}^2 = \bar{Z}^{1/3} \bar{Z}^{5/3}$ [5.46].

5.3.2. Phase separation

One of the most fascinating aspects of ionic mixtures is that they demix below a pressure-dependent critical temperature. The miscibility problem was first investigated in the solid phase by Dyson [5.43] who showed that certain cubic binary compound lattices have lower static Coulomb energies than the pure lattices at the same density and that under pressure and temperature conditions typical of neutron star crusts, the stability of these compound lattices is not altered by electron screening effects. In the fluid phase the miscibility problem has been studied by a number of authors over the last few years starting with Stevenson’s pioneering work [5.50] on $\text{H}^+ - \text{He}^{++}$ mixtures inside the heavy planets. The available calculations can be schematically sub-divided into two categories, according to whether electron-screening is systematically included from the onset or treated as a correction to the model of an ionic mixture in a rigid uniform background which we have introduced in subsection 5.3.1. The distinction is similar to that made for a pure ionic fluid in subsection 5.1.2. The latter point of view was adopted by Hansen and collaborators [5.45–5.47]. Hansen and Vieillefosse [5.45] used the results of numerical solutions of the HNC equations for binary mixtures to establish the phase diagram of $\text{H}^+ - \text{He}^{++}$ and $\text{H}^+ - \text{Li}^{+++}$ mixtures in a rigid background of fully degenerate electrons. The critical parameters of a $\text{H}^+ - \text{He}^{++}$ mixture under a pressure of 60 Mbar (which is typical of the deep interior of Jupiter) are compared in table 3 to the results of other authors. Under those conditions, $r_s \approx 0.85$, so that electron screening corrections are not, *a priori*, negligible. Their inclusion via thermodynamic perturbation theory as well as ionic quantum corrections do not lead to sizeable changes [5.46]. The critical temperature drops with increasing pressure, but varies slowly with P in the high pressure limit.

Pollock and Alder [5.49] determined the $\text{H}^+ - \text{He}^{++}$ phase diagram in the rigid background

Table 3
Critical temperature and helium number concentration under a pressure of 60 Mbar, as determined by various theories

Reference	T_c (K)	x_c (He)
[5.45–47]	6300	0.28
[5.49]	12700	0.30
[5.50]	8500	0.37
[5.51]	4900	0.34

approximation by using a “one-fluid” approximation with $Z_{\text{eff}}^2 = \bar{Z}^{5/3} \bar{Z}^{1/3}$. Their critical temperatures are about a factor two too high; this deficiency can be traced back to the inadequacy of the “one-fluid” approximation. On the basis of a simple lattice model these authors showed that demixing is essentially a consequence of the more efficient local charge neutralization in the pure phases as compared to the mixture. They also showed that singly ionized or neutral helium should always be miscible in metallic hydrogen.

The rigid background calculations have been extended by Brami et al. [5.47] to several other ionic mixtures corresponding to charge ratios $2 \leq Z_2/Z_1 \leq 8$. As expected demixing is enhanced (i.e. T_c increases) for the more dissymmetric mixtures.

The alternative point of view stresses electron screening from the start; in the corresponding calculations the ions interact via an effective screened potential (cf. eq. (5.6)) which is short-ranged. As in the one-component case, discussed in subsection 5.1.1, a hard sphere reference system is used in conjunction with the variational principle based on the Gibbs–Bogoliubov inequality (5.11). Since there are two ionic species, the reference system is taken to be a binary mixture of hard spheres of different diameters, which are the variational parameters in the calculation. Stevenson used this procedure to describe $\text{H}^+–\text{He}^{++}$ mixtures and chose the Hubbard dielectric function to describe the polarization of the electron gas; he also included corrections due to the non-linear response of the electron gas to the ionic charge distribution and higher order terms in the thermodynamic perturbation series around the hard sphere reference system. His critical temperatures lie systematically above the rigid background results, indicating that electron screening effects might *enhance* the miscibility gap. Stevenson’s calculations were repeated by Firey and Ashcroft [5.51] who used the simple Thomas–Fermi dielectric function; although the latter is known to be much less reliable than the Lindhard or Hubbard dielectric functions, it has the advantage of leading to simple analytic expressions in conjunction with a hard sphere reference system. As can be seen from table 3, their critical temperatures are a factor two lower than Stevenson’s results; this is probably a consequence of the drastic reduction of the range of the effective ion–ion interaction (a Yukawa potential) by Thomas–Fermi screening.

De Witt and Hubbard [5.7] have performed some MC computations for $\text{H}^+–\text{H}^{++}$ mixtures; electron screening is described by the Lindhard dielectric function. Unfortunately their calculations extend only over a limited range of helium number concentrations ($x_{\text{He}} \leq 0.2$) so that they could not construct the phase diagram. Where they can be compared, their thermodynamic data agree rather well with Stevenson’s results, despite the use of somewhat different dielectric functions.

Stevenson has extended a simplified version of his hard sphere model to several other ionic

mixtures [5.52]. For sufficiently small ratios Z_1/Z_2 , he finds simple analytic expressions for the critical concentration and temperature; the latter reads:

$$T_c = 3426Z_2(Z_2^{2/3} - Z_1^{2/3})^2 [1 + \frac{1}{2}Z_1/Z_2 + O(Z_1^2/Z_2^2)] \quad \text{K} \quad (5.34)$$

and is pressure-independent. Since Stevenson neglects electron screening in these calculations, the results can be compared to the high pressure limit of the results of Brami et al. [5.47]. The agreement is surprisingly good, considering the crudeness of Stevenson's model which has the merit of leading to simple analytic expressions.

$H^+ - He^{++}$ mixtures in the solid phase have been considered by Straus et al. [5.53]. A band structure calculations leads to a critical temperature which is much higher than in the fluid phase. The relevance of immiscibility in $H^+ - He^{++}$ mixtures to the interior of Jupiter is discussed by Stevenson and Salpeter [5.54].

Another interesting astrophysical problem is the possible limited solubility of iron in the sun's interior which may lead to an explanation of the neutrino dilemma. Preliminary calculations [5.55] indicate that the critical temperatures of mixtures of protons and fully or partially ionized iron is of the order of magnitude of the temperature in the interior of the sun ($T \simeq 10^7 \text{ K}$). More complete calculations are under way.

5.3.3. The dynamic properties

We shall briefly discuss the collective modes in binary ionic mixtures [5.44, 5.56–5.59]. As already discussed in subsection 4.3, the long wavelength modes are associated with the conserved variables, of which there are six for a mixture: the number density n , the charge density ρ , the total momentum and the total energy. The important point here is that the electric current is a variable which is *not* conserved, but nevertheless of macroscopic interest. This is a characteristic feature which distinguishes the binary ionic mixture (or any other multi-component charged fluid) from the OCP and the ordinary liquid mixtures. Indeed in the OCP fluctuations in the electric and mass currents are proportional to each other, so that the latter variable suffices to characterise the system (note that only the fluctuations are to be considered here, since the OCP can carry no macroscopic electric current at equilibrium). In an ordinary uncharged mixture there is no electric current variable, while the charge density is usually replaced by the concentration variable. As noted by Baus [5.56] a good, first principles reason to introduce the electric current variable from the start in any microscopic theory of the collective modes of multi-component charged fluids stems from the fact that the self-consistent field term, which because of its small k singularity is a central quantity here, acts directly on this variable. The somewhat redundant (with respect to the energy) but quite symmetric (with respect to the species) proposal by Baus [5.56] consists in using the multi-fluid hydrodynamic variables, i.e. the variables of density, momentum and energy defined for each species separately, as basic set of macroscopic variables. A microscopic theory of the collective modes of binary ionic mixtures can then be set up in close analogy with the one discussed in subsection 4.3 for the OCP. Eqs. (4.29) now become in the notations of subsection 4.1:

$$\Omega_{nl}^{\sigma\sigma'}(kz) = \delta_{\sigma\sigma'} k v_\sigma$$

$$\Omega_{ln}^{\sigma\sigma'}(kz) = k v_\sigma \left(\frac{n_\sigma}{n_{\sigma'}} \right)^{1/2} [\delta_{\sigma\sigma'} - \hat{c}_{\sigma\sigma'}(k)] \quad (5.35a)$$

$$\Omega_{ll}^{\sigma\sigma'}(kz) = -i[\gamma_l^{\sigma\sigma'}(z) + k^2 D_l^{\sigma\sigma'}(kz)] \quad (5.35b)$$

$$\begin{aligned}\Omega_{le}^{\sigma\sigma'}(kz) &= kD_{le}^{\sigma\sigma'}(kz) \\ \Omega_{el}^{\sigma\sigma'}(kz) &= kD_{el}^{\sigma\sigma'}(kz)\end{aligned}\quad (5.35c)$$

$$\begin{aligned}\Omega_{ee}^{\sigma\sigma'}(kz) &= -i[\gamma_e^{\sigma\sigma'}(z) + k^2 D_e^{\sigma\sigma'}(kz)] \\ \Omega_{t_j t_j}^{\sigma\sigma'}(kz) &= -i[\gamma_\perp^{\sigma\sigma'}(z) + k^2 D_\perp^{\sigma\sigma'}(kz)] \quad j = 1, 2\end{aligned}\quad (5.35d)$$

while the other $\Omega_{ij}^{\sigma\sigma'}(kz)$ matrix elements are identically zero. The appearance in eq. (5.35) of the microscopic relaxation frequency $\gamma_i^{\sigma\sigma'}(z)$ ($i = l, e, \perp$) is a direct consequence of the fact that only the sums over the species of the multi-fluid hydrodynamic variables are conserved. As a further consequence the dispersion relation

$$\det |z\delta_{ij}\delta_{\sigma\sigma'} - \Omega_{ij}^{\sigma\sigma'}(kz)| = 0$$

describes now both genuine hydrodynamical modes, i.e. solutions of the above dispersion relation which vanish with $k(z(k=0)=0)$, and inter-species relaxation modes characterized by $z(k=0)\neq 0$, which describe how the momentum and energy are equilibrated between the different species.

Although originally developed for a genuine two component plasma [5.56], this scheme, when applied to a binary ionic mixture, predicts four hydrodynamical modes and six relaxation modes. The former include a twice degenerate shear mode $zt_j(k) = -ik^2 D_\perp$ and two diffusion modes $z_\pm(k) = -ik^2 D_\pm$ mixing, as in ordinary liquid mixtures, the heat conduction and mutual diffusion processes. The relaxation modes consist of three momentum and one energy inter-species relaxation modes together with two charge relaxation or plasma modes which are the finite coupling generalizations of the usual mean-field plasma oscillations. As far as the strength of these modes is concerned, we have to distinguish the two-component generalization of the Van Hove function $S_{nn}(k, t) = \sum_{\sigma, \sigma'} S_{\sigma\sigma'}(k, t)$ from the charge density correlation function $S_{\rho\rho}(k, t) = \sum_{\sigma, \sigma'} Z_\sigma Z_{\sigma'} \times e^2 S_{\sigma\sigma'}(k, t)$. Just as for the OCP, the plasma modes exhaust the small k , large t behaviour of $S_{\rho\rho}(k, t)$, whereas both the plasma modes and the hydrodynamical diffusion modes contribute to $S_{nn}(k, t)$. This result is in qualitative agreement with recent MD “experiments” [5.57, 5.60] on strongly coupled H^- -He $^{++}$ mixtures. The most challenging problem however appears to be the precise value of the frequency of the plasma mode in the $k = 0$ limit. Extensions to the case of mixtures of the simple-minded estimations of the OCP plasma frequency, $\omega_p = [4\pi ne^2/m]^{1/2}$, all lead to the mean-field or Vlassov result:

$$\Omega_p^2 = \sum_{\sigma} \omega_{p,\sigma}^2 = \sum_{\sigma} \frac{4\pi Z_{\sigma}^2 e^2 n}{m_{\sigma}} = \sum_{\sigma} \frac{4\pi \rho_{\sigma}^2}{\rho_{m,\sigma}} \quad (5.36)$$

where $\rho_{\sigma} = Z_{\sigma} e n_{\sigma}$ and $\rho_{m,\sigma} = m_{\sigma} n_{\sigma}$ are respectively the charge and mass density of species σ . The extrapolation to $k = 0$ of the MD results [5.57, 5.60] is however in conflict with eq. (5.36); this discrepancy was explained by Baus [5.58] on the basis of the above microscopic theory [5.56]. If we write the plasma modes as $z_p(k=0) = \pm \Omega - \frac{1}{2}i\Gamma$, then the frequency Ω and the damping Γ vary between the following limiting values [5.58]:

$$\Omega = \Omega_p \left[1 + \frac{v_l(\Omega_p)}{2\Omega_p} \cdot \frac{\Omega_0^2}{\Omega_p^2} \right]; \quad \Gamma = v_R(\Omega_p) \frac{\Omega_0^2}{\Omega_p^2} \quad (5.37)$$

for weak coupling, $|v_l(\Omega_p)/\Omega_p| \ll 1$, and

$$\Omega = \Omega'_p \left[1 - \frac{v_l(\Omega'_p)}{2\Omega'_p} \frac{\Omega_0^2}{|v_l(\Omega'_p)|^2} \right]; \quad \Gamma = v_R(\Omega'_p) \frac{\Omega_0^2}{|v_l(\Omega'_p)|^2} \quad (5.38)$$

for strong coupling, $|v_l(\Omega'_p)/\Omega'_p| \gg 1$. In eqs. (5.37) and (5.38) we have introduced the real and imaginary parts of the longitudinal relaxation frequency:

$$v_l(\omega) = \sum_{\sigma} i\Omega_{ll}^{\sigma\sigma}(k=0, z=\omega + i0) \equiv v_R(\omega) + iv_I(\omega)$$

together with:

$$\Omega'_p = \Omega_p^2 - \Omega_0^2 = 4\pi\rho^2/\rho_m \quad (5.39)$$

$$\Omega_0^2 = 4\pi \frac{\rho_{m,1}\rho_{m,2}}{\rho_m} \left[\frac{\rho_1}{\rho_{m,1}} - \frac{\rho_2}{\rho_{m,2}} \right]^2 \quad (5.40)$$

where $\rho = \sum_{\sigma} \rho_{\sigma}$ and $\rho_m = \sum_{\sigma} \rho_{m,\sigma}$ are the total charge and mass densities associated with the mobile species. Hence, as the coupling increases, Ω is expected to decrease from the Vlasov value Ω_p of eq. (5.36) to the value Ω'_p of eq. (5.39) which, in the present context, corresponds to the hydrodynamic value (see [5.57]). A purely phenomenological analysis based on the hydrodynamic equations is however once more in difficulty, since the result of the microscopic theory, eqs. (5.37) and (5.38), depends on the imaginary part of the relaxation “frequency” $v_l(\omega)$ evaluated at finite frequency ($\omega \neq 0$). Such effects are not properly described by phenomenological hydrodynamics which only involve the low frequency value $v_l(\omega = 0) \equiv v_R(0)$ which is real and leads to a collisional damping term Γ which is quantitatively different from the results of eqs. (5.38) and (5.39). This strong non-Markovian dependence of the plasma modes in binary ionic mixtures induces, even at $k = 0$, a strong plasma parameter dependence which is one of the most interesting features of the dynamics of this system. Recent MD simulations [5.60] indicate however that the hydrodynamic limit is not reached at a coupling as high as $\Gamma = 60$ for $H^+ - He^{++}$ mixtures.

5.4. An OCP with hard cores

The mobile ions of an OCP in a rigid or polarizable background have hitherto been considered to be point particles. In this subsection we generalize the OCP model by giving the ions a finite size, while keeping a rigid background to ensure charge neutrality. The corresponding simplest model is that of a system of N hard spheres of diameter d , each carrying a point charge Ze at its center. The non polarizable background can either penetrate the hard spheres or be excluded from the volume occupied by the hard cores. We shall first consider the case of the uniform penetrating background which occupies the total volume Ω of the system. The interaction potential between two ions splits into two parts:

$$v(r) = v_0(r) + w(r) \quad (5.41)$$

where v_0 is the hard sphere (HS) potential:

$$v_0(r) = \begin{cases} \infty, & r \leq d \\ 0, & r > d \end{cases} \quad (5.42a)$$

and

$$w(r) = Z^2 e^2 / r, \quad r > d \quad (5.42b)$$

but $w(r)$ can be left undefined for $r < d$.

The hard core diameter d introduces an additional length scale, so that the equilibrium properties now depend on two independent parameters: the usual coupling constant $\Gamma = Z^2 e^2 / (a k_B T)$ of the OCP and the packing fraction $\eta = \pi n d^3 / 6$ of the hard spheres. An alternative choice for the inverse temperature parameter is

$$\gamma = \frac{Z^2 e^2}{d k_B T} = \frac{\Gamma}{2\eta^{1/3}}. \quad (5.43)$$

Note that the excess properties of a fluid of neutral ($Z = 0$) hard spheres depend only on η , while those of an OCP of point ions ($d = 0$) depend only on Γ . The static properties of these two limiting cases are well known (see section 3 and ref. [1.2]). In particular we recall that the fluid phase of the HS fluid extends up to $\eta \simeq 0.5$ which corresponds roughly to two thirds of the density at close packing.

It seems natural to seek a description of the static properties of the charged HS fluid in the framework of thermodynamic perturbation theory [1.2], the role of the “reference system” being played by the neutral HS fluid with the same packing fraction. The theoretical interest of the present model lies in the fact that the Coulomb interaction $w(r)$ furnishes a strong and long-range perturbation, which puts the perturbation theories to a severe test. Some Monte Carlo results are available for thermodynamic states corresponding to high values of the packing fraction ($\eta = 0.343$ and $\eta = 0.4$) and of Γ (≥ 20) [5.61] and the various theories described below have been tested against these “exact” results.

A fundamental and generic approximation in the treatment of systems of particles interacting through a potential of general form (5.41), where $v_0(r)$ is the HS potential and $w(r)$ any smooth “perturbation”, is the so-called mean-spherical approximation (MSA) [5.62] which amounts to supplement the OZ relation (3.17) between $h(r) = g(r) - 1$ and $c(r)$ by the following closure relations:

$$g(r) = 0, \quad r < d \quad (5.44a)$$

$$c(r) = -\beta w(r), \quad r > d. \quad (5.44b)$$

Eq. (5.44a) is obviously exact and the approximation lies in eq. (5.44b), i.e. in the replacement of $c(r)$ by its asymptotic form $-\beta w(r)$ outside the core. If $w(r) = 0$ (i.e. $\Gamma = 0$ in our case), the MSA reduces to the well-known Percus–Yevick (PY) approximation for a HS fluid [5.63] while in the limit $d \rightarrow 0$, a system of charged hard spheres reduces to the OCP and the MSA goes over to the DH limit (see eq. (3.46a)). The main advantage of the MSA is that it can be solved analytically for several forms of the perturbation $w(r)$. In the special case of a fluid of charged hard spheres in a penetrating background, the analytic solution has been obtained by Palmer and Weeks [5.64]. The mathematical procedure is based on the classic work by Wertheim [5.65] and Thiele [5.66] who solved the PY equation for the HS fluid, i.e. the MSA in the case where $w(r) \equiv 0$. The solution yields a fifth degree polynomial for $c(r)$ inside the core. We quote here only the closed form obtained for the excess internal energy:

$$\begin{aligned} \frac{\beta U^{\text{ex}}}{N} &= u(\Gamma, \eta) = A(\eta)\Gamma + B(\eta)\Gamma^{1/2} \{1 - [1 + C(\eta)\Gamma^{1/2}]^{1/2}\} \\ A(\eta) &= -\frac{(1 + \eta - \eta^2/5)}{2\eta^{1/3}}; \quad B(\eta) = -\frac{\sqrt{3}(1 + 2\eta)}{12\eta^{2/3}}; \\ C(\eta) &= \frac{2\sqrt{12}(1 - \eta)^3\eta^{1/3}}{(1 + 2\eta)^2}. \end{aligned} \quad (5.45)$$

In the limit $d \rightarrow 0$, $u(\Gamma, \eta = 0)$ reduces to DH result (3.47) as expected. The agreement of the MSA energies, calculated from (5.45), with the MC results is excellent, for sufficiently high packing fractions. The MSA pair distribution functions differ however rather markedly from the “exact” results, especially near the core ($r \gtrsim d$) where $g(r)$ takes on negative values at low packing fractions, a typical deficiency of the MSA. Being an approximate theory, the MSA suffers from internal inconsistency, i.e. the thermodynamic properties derived from the energy equation (5.45) differ from the thermodynamics derived from the compressibility equation (3.33) or from the virial equation which is not, here, equivalent to the energy equation because of the presence of the hard cores; only the latter equation yields thermodynamics in good agreement with the MC results, provided η is sufficiently large.

Several schemes have been proposed in order to improve upon the MSA [5.63]. None is very successful in reproducing the MC results for charged hard spheres when the Coulomb perturbation (i.e. Γ) is large. We only briefly describe the most promising of these theories, due to Lado [5.67]. In Lado’s approach the pair correlation functions $h_0(r)$ and $c_0(r)$ of the reference system, which is characterized by a pair potential $v_0(r)$ (which need not be the HS potential (5.42)) are supposed to be known, either from “exact” simulation results or from the solution of an accurate integral equation (the PY equation in the case of a HS reference fluid). If $h(r)$ and $c(r)$ are the corresponding functions for a system of particles interacting through the full pair potential $v = v_0 + w$, the differences Δh and Δc are introduced through:

$$\begin{aligned} h(r) &= h_0(r) + \Delta h(r) \\ c(r) &= c_0(r) + \Delta c(r). \end{aligned} \quad (5.46)$$

From the Ornstein–Zernike relations (3.20) written for the reference potential and the full potential a similar relation between $\Delta \hat{c}(h)$ and $\Delta \hat{h}(k)$ is immediately derived in the form:

$$\Delta \hat{h}(k) = \frac{[1 + \hat{h}_0(k)]^2 \Delta \hat{c}(k)}{1 - [1 + \hat{h}_0(k)]\Delta \hat{c}(k)}. \quad (5.47)$$

The exact relations (3.65) and (3.66) can be rewritten by solving explicitly for $c(r)$:

$$c(r) = -\beta v(r) + h(r) - \ln g(r) + B(r) \quad (5.48)$$

subtracting from (5.48) the similar relation for $c_0(r)$, we arrive immediately at:

$$\Delta c(r) = -\beta w(r) + \Delta h(r) - \ln \left[\frac{g(r)}{g_0(r)} \right] + \Delta B(r) \quad (5.49)$$

where $\Delta B(r) = B(r) - B_0(r)$ is the difference between the bridge diagram contributions to $g(r)$ and $g_0(r)$. There is no simple functional relationship between ΔB , Δh and Δc . The simplest approxima-

tion is to set $\Delta B = 0$ [5.67]; under these conditions eqs. (5.47) and (5.49) constitute a closed set from which a self-consistent solution for Δh and Δc can be obtained by iteration. Eq. (5.49) with $\Delta B \equiv 0$ is frequently referred to as the “reference-HNC” (RHNC) equation, since it closely resembles the HNC equation (3.67), except that the bridge diagrams are not entirely neglected here, but rather the effect of the perturbing potential $w(r)$ on the bridge diagram contribution is ignored; in other words it is assumed that $B(r)$ for a fluid of particles interacting through the full potential $v(r)$ is identical to the reference system bridge function $B_0(r)$. Lado has solved the RHNC equation for a fluid of charged hard spheres in a penetrating background [5.68]; the resulting $g(r)$ are closer to the MC results than their MSA counterparts, without being totally satisfactory [5.61]. The iterative procedure for solving (5.47) and the RHNC version of (5.49) can be started by the initial guess $\Delta h(r) = 0$, i.e.:

$$\Delta c(r) = -\beta w(r) \quad (5.50a)$$

$$\Delta h(k) = \frac{[1 + h_0(k)]^2 \beta \hat{w}(k)}{1 + [1 + h_0(k)] \beta \hat{w}(k)} \quad (5.50b)$$

which leads immediately to the so-called “exponential” approximation [5.69]:

$$g(r) = g_0(r) \exp \{ \Delta h(r) \}. \quad (5.50c)$$

This simple non-iterative approximation can be “optimized” when the reference potential $v_0(r)$ is the HS potential (5.42a), by varying the form of the perturbation $w(r)$ inside the hard core where it is undefined [5.70]. In the case of strongly coupled charged hard spheres, the optimized “exponential” approximation yields however very poor results, both for the thermodynamics and the pair distribution functions [5.61]. It thus appears that there exists no theory yet which yields fully satisfactory results for charged hard spheres when the Coulomb “perturbation” is large.

Apart from its intrinsic theoretical interest the model of charged hard spheres in a uniform, penetrating background has been successfully used to describe the OCP ($d = 0$) statics [3.52]. Indeed we have seen that in the strong coupling regime ($\Gamma \gg 1$) the pair distribution function of the OCP is virtually zero over an extensive interval ($0 \leq x = r/a \lesssim 1$); in other words the strongly coupled OCP behaves as if the ions had an effective hard core of diameter $d/a \simeq 1$. Gillan made use of this observation to postulate eq. (5.44) (with $w(r)$ given by (5.42)) which corresponds precisely to the MSA for charged hard spheres. The effective core diameter d is determined by requiring that the MSA solution for $g(r)$ be continuous at $r = d$, i.e. the pair distribution function goes smoothly to zero as it should for the OCP (its derivatives remain however discontinuous at $r = d$). The effective packing fraction $\eta = \pi n d^3 / 6$ being thus determined the internal energy is given by eq. (5.45); the results are very well represented by the simple form [5.71]

$$u(\Gamma) = a\Gamma + b\Gamma^{1/2} + c \quad (5.51)$$

with $a = -0.9005$, $b = 0.2997$, $c = 0.0007$, which is reminiscent of the HNC result (3.75). In fact Gillan’s results lie closer to the “exact” energies, represented by eqs. (3.40) and (3.42), than their HNC counterparts, at least for $\Gamma \gtrsim 10$. The method is of course expected to break down at small Γ , since the effective hard core concept is not valid in that limit. The idea of using the MSA results for charged hard spheres to describe the OCP statics has recently been reexamined by Rosenfeld and Ashcroft [5.72] who investigated the lack of thermodynamic consistency of the model and pointed out that the choice of effective diameter, which guarantees that $g(r)$ be continuous at

$r = d$, also cancels the *linear* term in the MSA solution for $c(r)$ inside the core, in agreement with the exact behavior of $c(r)$ for the OCP. It has very recently been pointed out that for large Γ , $u(\Gamma)$ of eq. (5.45) tends exactly to the ion-sphere result -0.9Γ [5.103].

The case where the neutralizing background is not allowed to permeate the hard spheres has been considered by Waisman and Lebowitz [5.73], as a limit of the “primitive model” introduced in the next subsection, for which they solved the MSA analytically. The resulting internal energy is still given by eq. (5.45), but with:

$$A(\eta) = -\frac{1}{2\eta^{1/3}}; \quad B(\eta) = -\frac{\sqrt{3}}{12\eta^{2/3}} \frac{(1+2\eta)}{(1-\eta)} \quad (5.52)$$

$C(\eta)$ remaining unchanged.

5.5. More complex ionic systems

Before closing this review, devoted essentially to the Statistical Mechanics of the OCP and its extensions, it seems appropriate to make contact with more complex and “realistic” ionic systems, by summarizing the essential features of some simple models for genuine two component charged fluids. In all systems which we have considered until now, charge neutrality was guaranteed by the presence of a rigid or polarizable continuum carrying a charge density opposite to that of the mobile ions. Genuine two-component ionic fluids are made up of two mobile species of opposite charge. Since we limit ourselves to classical systems, these ions must have hard cores in order to prevent the system from collapsing. The physical systems which we have more particularly in mind are ionic solutions (electrolytes) and molten salts. The main goal of this section will be to demonstrate that many of the concepts and theoretical techniques, introduced previously in the study of the OCP and its extensions, apply also to these more complex ionic systems.

5.5.1. The “primitive model” of electrolytes

Electrolytes are made up of positive and negative ions dissolved in a polar solvent. The crudest picture of such complex systems is given by the so-called “primitive model” of electrolytes: the two ionic species are simply taken to be oppositely charged hard spheres with additive diameters, while the discrete solvent is replaced by a structureless continuum characterized by its macroscopic dielectric constant ϵ . If d_σ and $Z_\sigma e$ are the diameter and charge of species σ ($\sigma = +, -$), the interionic potentials are simply:

$$v_{\sigma\sigma'}(r) = \begin{cases} \infty & , \quad r < d_{\sigma\sigma'} = \frac{1}{2}(d_\sigma + d_{\sigma'}) \\ \frac{Z_\sigma Z_{\sigma'}}{\epsilon r} & , \quad r \geq d_{\sigma\sigma'}. \end{cases} \quad (5.53)$$

The partial densities $n_\sigma = N_\sigma/\Omega$ of the two species are linked by the charge neutrality condition:

$$Z_+ n_+ + Z_- n_- = 0. \quad (5.54)$$

Most of the theoretical work on the primitive model has dealt with its simplest version, where the two ionic species have equal diameters ($d_+ = d_- \equiv d$) and opposite charges ($Z_- = -Z_+$); this is the so-called “restricted primitive model” (RPM), in which $n_1 = n_2 = n/2$, due to eq. (5.54). Since the RPM is entirely symmetrical in the two species, it leads to only two independent pair

distribution functions: $g_{++}(r) = g_{--}(r)$ and $g_{+-}(r)$. Two linear combinations of the latter play a particularly important role; these are the sum (S) and difference (D) functions:

$$\begin{aligned} g_S(r) &= \frac{1}{2}[g_{++}(r) + g_{+-}(r)] \\ g_D(r) &= \frac{1}{2}[g_{++}(r) - g_{+-}(r)] \end{aligned} \quad (5.55)$$

which obviously describe the number density and charge density distributions around a given ion. Similar linear combinations can be defined for the direct correlation functions and it is easily verified that the two coupled Ornstein-Zernike relations between h_{++} , h_{+-} and c_{++} , c_{+-} in fact *decouple* for the linear combinations (5.55). We define the number density and charge density structure factors $S_S(k)$ and $S_D(k)$ from the Fourier transforms of $h_S(r) = g_S(r) - 1$ and $h_D(r) = g_D(r)$ (see eq. (3.20)). Since the number density and charge density fluctuations are entirely decoupled, it is clear that the long wave-length limits of $S_S(k)$ and $S_D(k)$ must be the same as those valid for neutral and charged one-component systems respectively, i.e.:

$$\lim_{k \rightarrow 0} S_S(k) = \frac{\chi_T}{\chi_T^0} \quad (5.56a)$$

$$\lim_{k \rightarrow 0} \frac{k_D^2}{k^2} S_D(k) = 1 \quad (5.56b)$$

where χ_T is the isothermal compressibility, and $k_D = \lambda_D^{-1}$ the inverse Debye screening length:

$$\begin{aligned} \lambda_D^{-2} &= 4\pi \frac{\beta e^2}{\epsilon} [n_+ Z_+^2 + n_- Z_-^2] = 4\pi \frac{\beta e^2}{\epsilon} n Z^2 \\ d^2 \lambda_D^{-2} &= 24\eta\gamma \end{aligned} \quad (5.57)$$

$\eta = \pi n d^3 / 6$ and $\gamma = \beta Z^2 e^2 / \epsilon d$ are the two dimensionless parameters which entirely characterize a thermodynamic state of the RPM.

The internal energy of the RPM is still given by eq. (3.21), with $g_D(r)$ replacing $g(r)$, while the presence of the discontinuous hard core potential adds an additional “contact” term to the virial expression of the osmotic coefficient:

$$\phi = \frac{\beta P}{n} = 1 + \frac{1}{3} \frac{\beta U^{\text{ex}}}{N} + 4\eta \lim_{r \rightarrow d^+} g_S(r). \quad (5.58)$$

Extensive Monte Carlo results for the static properties of the RPM are available both in the concentrated electrolyte regime ($\eta \lesssim 0.1$; $\gamma \lesssim 2$) [5.74, 5.75] and for stronger couplings ($0.1 \lesssim \eta \lesssim 0.4$; $\gamma \lesssim 100$), corresponding roughly to a molten salt regime [5.76]. The various theories introduced in the preceding section for a one-component fluid of charged hard spheres are easily generalized to the case of the RPM. The mean spherical approximation (MSA) closure relations become:

$$g_S(r) = 0, \quad r < d; \quad c_S(r) = 0, \quad r > d \quad (5.59a)$$

$$g_D(r) = 0, \quad r < d; \quad c_D(r) = -\frac{\beta Z^2 e^2}{\epsilon r}, \quad r > d. \quad (5.59b)$$

Note that (5.59) is just the PY equation for neutral hard spheres, the solution of which is well known [5.65, 5.66]. The closure relation (5.59b) is identical to that for charged hard spheres in a

penetrating background in subsection 5.4, except that here $h_D(r) = g_D(r)$ whereas $h(r) = g(r) - 1$ in the previous case, leading to an entirely different solution for $c_D(r)$ inside the core ($r < d$), which was first obtained by Waisman and Lebowitz [5.73]. Their result for the excess internal energy reads:

$$\frac{\beta U^{\text{ex}}}{N} = u(\eta, \gamma) = A\gamma + B(\eta)\gamma^{1/2} [1 - (1 + C(\eta)\gamma^{1/2})^{1/2}]$$

$$A = -1; \quad B(\eta) = -\frac{1}{2\sqrt{6}\eta^{1/2}}; \quad C(\eta) = 4\sqrt{6}\eta^{1/2}. \quad (5.60)$$

As in the one-component case of the preceding subsection, the MSA predicts energies in fair agreement with the “exact” results, but very poor pair distribution functions for large values of γ . The solution of the MSA has been generalized by Blum [5.77] to the case of the asymmetric primitive model (ions of different sizes and charges).

In order to overcome the thermodynamic inconsistency of the MSA, Hoye et al. [5.78] proposed a modification of the closure relation (5.59a) inspired by a similar procedure which had been successfully applied by Waisman [5.79] to the PY equation for the neutral hard sphere fluid. This generalized mean spherical approximation (GMSA) amounts to replacing $c_S(r)$ outside the core by a Yukawa potential:

$$c_S(r) = \frac{A_S}{r} e^{-\alpha_S r}, \quad r > d.$$

The GMSA can still be solved analytically for given values of the parameters A_S and α_S , and these are determined by imposing that the thermodynamics calculated from the energy, virial and compressibility equations be consistent with a prescribed equation of state, e.g. that derived from eq. (5.60). Besides satisfying thermodynamic consistency, this procedure leads to much improved pair distribution functions, especially at contact ($r \rightarrow d+$) [5.80]. Further improvement over the MSA can be achieved by also changing the closure relation (5.59b) for $c_D(r)$ [5.81].

Among the standard integral equations the HNC theory yields the best results for the RPM, just as in the case of the OCP. The coupled HNC equations have been solved numerically in the electrolyte regime by Rasaiah and Friedman [5.82] and in the molten salt regime by Larsen [5.83]. The HNC results for the thermodynamics and the pair distribution functions are in excellent agreement with the MC data for values of η and γ typical of ionic solutions [5.84], and are still very reasonable in the strong coupling regime [5.83]. In particular the HNC pair distribution functions exhibit the characteristic “charge ordering” at high values of γ , which manifests itself in an exact opposition of the phases of the long-range oscillations of $g_{++}(r)$ and $g_{+-}(r)$. The HNC equations have also been solved in some cases of asymmetric electrolytes [5.85, 5.86].

Somewhat surprisingly the extension of the “reference hypernetted chain” (RHNC) theory (see eq. (5.49), with $\Delta B(r) = 0$) to the RPM does not significantly improve on the HNC results in the molten salt regime [5.83]. Hence we expect the “exponential” approximation (see eqs. (5.50)), which corresponds to just *one* iteration of the RHNC equations, to yield rather poor results for the strongly coupled RPM, although it does lead to satisfactory results in the electrolyte regime [5.87].

From a careful analysis of the available MC and theoretical thermodynamic data for the RPM it has recently become clear that this model exhibits a liquid-gas phase transition at very low

densities [5.88, 5.89]. The most accurate determination of the critical point parameters yields $\gamma_c \simeq 11.8$, $\eta_c \simeq 0.057$ and $\phi_c \simeq 0.33$ [5.89].

5.5.2. Molten salts

Much recent theoretical work has been devoted to molten salts, and more particularly to the simplest among this class of ionic liquids, i.e. the alkali halides. To allow a quantitative comparison of calculated static properties with experimental results, the RPM model is too crude [5.76], and more “realistic” inter-ionic potentials must be used. These are reviewed by Sangster and Dixon [5.90]; “rigid ion” potentials contain a “soft” core repulsion (of the exponential or inverse power type), the Coulomb attraction or repulsion, and attractive Van der Waals interactions, but do not take into account ion polarization effects, which are essentially dynamical in nature.

Since the pioneering work of Woodcock and Singer [5.91] a vast body of MC and MD simulation data has become available, both for static and dynamical properties of molten alkali halides, particularly NaCl, KCl, KI and RbBr. Much of this work is reviewed in ref. [5.90]. These simulation data show that “rigid ion” models yield thermodynamic and structural properties in fair agreement with calorimetric and neutron diffraction data, but that ion polarization effects (due to the strong microscopic internal electric fields) are not entirely negligible in most cases. The cohesive energy of crystalline and molten salts is very large (which explains the very high melting temperatures, of the order of 10^3 K) and turns out to be to 90 % of Coulombic origin.

There has been much recent progress in our understanding of the dynamical properties in molten salts. The first complete MD study of collective mass and charge density fluctuations has been carried out by Hansen and McDonald [5.92] for a simple *symmetrical* model of a molten salt, in which the positive and negative ions are identical (same sizes and masses) except for the sign of their charges; this model is equivalent to the RPM (with $\epsilon = 1$), except that the hard sphere cores of the ions are replaced by a “soft” core repulsion proportional to $1/r^9$. The symmetry of the model leads to a remarkable simplification, since it is easily verified that the mass (or number) and charge density fluctuations are decoupled at all times. The main finding of that work is the existence of a well-defined plasmon mode in the charge fluctuation spectrum $S_{\rho\rho}(k, \omega)$ for finite wave numbers, reminiscent of the “optic” mode of ionic crystals. A subsequent analysis of the electric current autocorrelation function computed in ref. [5.92] has shown that this plasmon mode persists at zero wavenumber where it can be detected by infra-red optical reflectivity experiments [5.93]. The mode frequency is shifted above the plasma frequency (defined in eq. (5.36)) due to interspecies friction. The existence of a well-defined plasma oscillation mode contradicts the results of a simple long wavelength phenomenological analysis based on the linearized hydrodynamic equations, similar to that discussed in subsection 4.4 for the OCP, which yields a charge relaxation mode (or electrical conductivity mode) centered at zero frequency (i.e. a diffusive rather than propagating mode) [5.94, 5.95]. The situation has been clarified by Baus [5.56]. The exact Kinetic Theory analysis of the collective modes in a binary ionic mixture, sketched in subsection 5.3.3, can be extended to the case of a two component plasma (TCP) made up of two oppositely charged species, of which a molten salt is a special case. The long wavelength collective modes of the TCP differ significantly both from those of binary ionic mixtures and from those of binary neutral mixtures. Using two-fluid variables, whose sums correspond to the hydrodynamical variables, while their differences correspond to non-conserved relaxation variables including the electrical current (see subsection 5.3.3), Baus has shown that the TCP exhibits 5 hydrodynamical modes (against 6 in a neutral mixture and 4 in a binary ionic mixture) and 5 relaxation modes. Apart from the transverse

(shear) modes, there are three longitudinal hydrodynamical modes in the TCP (the heat mode and two conjugate sound modes) and three longitudinal relaxation modes (an interspecies energy relaxation and two charge relaxation modes). The hydrodynamic mass diffusion mode of binary neutral mixtures has turned here into two charge relaxation modes, which are damped even at $k = 0$. In the weak coupling limit these two relaxation modes correspond to slightly damped plasma oscillations occurring at a frequency slightly above Ω_p of eq. (5.36). In the strong coupling limit the charge relaxation modes turn into one interspecies momentum relaxation mode and an electrical conductivity mode which is reminiscent of the mass diffusion mode of neutral mixtures; it is this latter mode which is predicted by the phenomenological hydrodynamic calculation [5.94, 5.95]. The MD data for the simple molten salt [5.92] indicate a behaviour which is somewhat intermediate between the weak and strong coupling limits, since they exhibit a relatively strongly damped propagating plasmon mode.

It is worth noting that the electrical conductivity σ of the TCP is linked to the charge diffusion (or interdiffusion) constant D_ρ by an Einstein relation [5.96, 5.56]:

$$4\pi\sigma/D_\rho = k_s^2 \quad (5.61)$$

where k_s is a screening vector occurring in the long wave-length limit of the static dielectric constant $\epsilon(k)$ (see eq. (3.29) and [4.6]). On the other hand σ is approximately related to the self-diffusion coefficients D_+ and D_- of the two ionic species by a Nernst–Einstein relation [5.92, 5.97]

$$\sigma \simeq \frac{1}{2} \frac{nZ^2 e^2}{k_B T} (D_+ + D_-). \quad (5.62)$$

It is finally worth noting that inclusion of ion polarization effects in the MD computations leads to a reduction of the plasmon frequency and a considerable increase of its damping; the self diffusion coefficients D_+ and D_- increase with respect to their “rigid ion” values, while the shear viscosity decreases and the electrical conductivity remains essentially unchanged [5.98].

Molten salt are reviewed much more thoroughly in a recent review by Parrinello and Tosi [1.10].

5.5.3. Some other two component ionic fluids

Other examples of “two component plasmas” (TCP) which can be treated essentially by classical Statistical Mechanics, and which have received much recent interest are superionic conductors and strongly coupled ion–electron plasmas.

Superionic conductors, also called solid electrolytes, are fascinating ionic compounds which are in some sense intermediate between crystalline and molten salts: while they exhibit a well-defined crystalline structure, they have electrical conductivities comparable to those of the liquid phase. The situation is interpreted by assuming that one of the ionic species (generally the bigger anions) forms a stable, thermally vibrating lattice, while the sublattice of the oppositely charged species has melted, allowing the ions of this structurally disordered species to diffuse as in a liquid. The prototype of solid electrolytes is silver iodide which exhibits a first-order phase transition from a nearly insulating β -phase to an ionic conducting α -phase at 420 K; the electrical conductivity increases by four orders of magnitude at the transition point, while it increases only slowly with temperature in the α phase, where it is of the order of a few $\Omega^{-1} \text{ cm}^{-1}$. In α -Ag I, the iodine anions form a BCC lattice, while the much smaller silver cations (their size is roughly one third of the anion size) diffuse rapidly, leading to the high electrical conductivity.

Recent MD simulations of Ca F₂ (which is an anion conductor) [5.99] and α -Ag I [5.100] give very strong support to the interpretation of ionic conduction by jump diffusion between energetically favoured “residence” sites of the conducting ion in the framework of the stable lattice formed by the other species.

Strongly coupled ion-electron plasmas are created in highly compressed (“imploded”) pellets in the course of laser-driven fusion experiments [5.101]. At sufficiently low temperatures and high compressions, the electrons form a degenerate Fermi gas; under these conditions the OCP is a reasonable starting point for the description of strongly coupled plasmas. However in the final stages of the implosion process the temperature is generally sufficiently high for the electrons to form a nearly classical gas ($T > T_F$) and the two-component description becomes necessary. For short ion-electron separations, quantum diffraction effects become crucial to prevent collapse, and to cope with this problem in the framework of classical Statistical Mechanics, some effective ion-electron potential, which stays finite at zero separation, must be used [5.102]. Very recently a first MD simulation of the single particle motion and the charge and mass density fluctuations in a fully ionized hydrogen (electron-proton) plasma has been carried out [4.17]. The data are being presently analysed and more simulation work is in progress. The preliminary results indicate however that a microscopic simulation of genuine two-component plasmas is feasible and potentially very powerful; despite the large discrepancy of time scales due to the large proton to electron mass ratio.

6. Conclusions and perspectives

As should be clear from the main text, the statistical mechanics of the simplest classical Coulomb system is by now in a fairly advanced stage, comparable for instance, to our knowledge of the hard sphere fluid. It is therefore to be expected that in the future the main emphasis will shift towards more complex charged systems, such as the strongly coupled two component plasma, superionic conductors and polyelectrolytes. Our understanding of the simplest charged fluids, such as the OCP, is, however, bound to play an important role in the description of these more complicated systems.

It might therefore be of interest to summarize here those aspects of the OCP-like systems which in our opinion deserve further study. With respect to the static properties, we should mention the fluid-solid transition of the 2-D OCP, the demixing transition in the binary ionic mixtures and the macroscopic characterization of the onset of short-range order in the simple OCP. As regards the dynamics, we feel that the precise status of the hydrodynamic description of charged fluids is not yet fully understood, while the transport phenomena and collective modes of the 2-D OCP also deserve additional study. Further progress in these directions is to be expected in the coming years.

Acknowledgments

We thank I.R. McDonald and P. Vieillefosse for providing us with unpublished material, H. De Witt for useful correspondence and B. Bernu, J. Bosse and H. Gould for allowing us to reproduce, respectively, figures 1, 10 and 11. We also thank B. Bernu, G.V. Chester, C. Deutsch, H. Gould, S. Ichimaru, B. Jancovici, G. Kalman, B. Larsen, Y. Rosenfeld, H.B. Singh and M.P. Tosi for sending us preprints of their work prior to publication.

Appendix 1: Fourier and Laplace transforms

In order to simplify the notation we will distinguish a function and its transform only by the nature of its argument. The Fourier transform of $f(t)$ with respect to the time variable t will be defined as:

$$f(\omega) = \int_{-\infty}^{\infty} dt f(t) \exp(i\omega t)$$

together with the inverse transform:

$$f(t) = \int_{-\infty}^{\infty} \frac{d\omega}{2\pi} f(\omega) \exp(-i\omega t)$$

ω being a real frequency variable. The Laplace transform of $f(t)$ with respect to the time variable will instead be written as:

$$f(z) = \int_0^{\infty} dt f(t) \exp(izt); \quad \text{Im } z > 0$$

with the inverse transform defined as:

$$f(t) = \int_{-\infty + ia}^{\infty + ia} \frac{dz}{2\pi} f(z) \exp(-izt); \quad a > 0$$

z being now a complex frequency which eventually approaches the real value ω from above: $z = \omega + i0$. For the Fourier transform of $f(\mathbf{r})$ with respect to the spatial variable \mathbf{r} we change the above convention into:

$$f(\mathbf{k}) = \int_{\Omega} d\mathbf{r} f(\mathbf{r}) \exp(-i\mathbf{k} \cdot \mathbf{r})$$

\mathbf{k} being a wavevector and Ω the system's volume. This change in convention allows us to expand the function $f(\mathbf{r}, t)$ into plane waves of the form $\exp\{-i(\omega t - \mathbf{k} \cdot \mathbf{r})\}$. The inverse transform of $f(\mathbf{k})$ reads then:

$$\begin{aligned} f(\mathbf{r}) &= \lim_{\Omega \rightarrow \infty} \frac{1}{\Omega} \sum_{\mathbf{k}} f(\mathbf{k}) \exp(i\mathbf{k} \cdot \mathbf{r}) \\ &= \int \frac{d\mathbf{k}}{8\pi^3} f(\mathbf{k}) \exp(i\mathbf{k} \cdot \mathbf{r}). \end{aligned}$$

In the main text we will often use the more convenient dimensionless spatial Fourier transform:

$$\hat{f}(\mathbf{k}) = n \int_{\Omega} d\mathbf{r} f(\mathbf{r}) \exp(-i\mathbf{k} \cdot \mathbf{r}),$$

i.e. $\hat{f}(\mathbf{k}) = nf(\mathbf{k})$ with $n = N/\Omega$, such that $\hat{f}(\mathbf{k})$ and $f(\mathbf{r})$ have the same dimensions.

Appendix 2: The Debye–Hückel theory and the non-linear Poisson–Boltzmann equation

As is well-known the Debye–Hückel theory is based on the following nonlinear equations:

$$\Delta\varphi(r) = 4\pi Z e n(g(r) - 1) \quad (\text{A.1})$$

$$g(r) = \exp \{-\beta Z e \varphi(r)\} \quad (\text{A.2})$$

where eq. (A.1) is Poisson's equation for the mean potential $\varphi(r)$ produced by a charge density which by eq. (A.2) is re-expressed in terms of $\varphi(r)$ through the Boltzmann factor. When linearized with respect to $\varphi(r)$ eqs. (A.1–2) lead to the standard Debye–Hückel results of subsection 3.5. By re-exponentiating this result one obtains eq. (3.52) which is usually called, improperly, the nonlinear Debye–Hückel result. This cavaliery procedure is clearly not the correct way to treat the original nonlinear equations (A.1–2). We consider it of some interest to summarize here some physical consequences of the genuine nonlinear Debye–Hückel theory based on eqs. (A.1–2). As we could not find such a discussion in the current literature we will use here some unpublished material of P. Vieillefosse. We rewrite eqs. (A.1) as:

$$\frac{d^2\psi(x)}{dx^2} = 3x \left(1 - \exp \left\{ -\frac{\Gamma}{x} \psi(x) \right\} \right) \quad (\text{A.3})$$

where $x = r/a$ and $\beta\varphi(r) = (\Gamma/x)\psi(x)$. Eq. (A.3) should be used together with the boundary conditions $\psi(x=0) = 1$ and $\psi(x=\infty) = 0$. Integrating twice eq. (A.3), under the quite reasonable assumption that the first derivative of $\psi(x)$ vanishes at $x = \infty$, we obtain

$$\psi'(x) = - \int_x^\infty dx' 3x' \left(1 - \exp \left\{ -\frac{\Gamma}{x'} \psi(x') \right\} \right) \quad (\text{A.4})$$

and:

$$\psi(x) = 1 + x\psi'(0) + \frac{x^3}{2} - \int_0^x dx' 3x'(x-x') \exp \left\{ -\frac{\Gamma}{x'} \psi(x') \right\}. \quad (\text{A.5})$$

From eqs. (A.2), (A.4), (3.11) and (3.21) we obtain for the excess internal energy:

$$\beta(U - U^0)/N = \frac{1}{2}\Gamma\psi'(0) \quad (\text{A.6})$$

and hence $\psi'(0)$ determines the whole thermodynamics! As is well known nonlinear equations such as eq. (A.3) or eq. (A.5) can have different branches of solutions. For instance eq. (A.3) has the trivial solution $\psi_0(x, \Gamma) = 0$ (which does not satisfy our boundary condition at $x = 0$) and a branch $\psi_{\text{DH}}(x, \Gamma)$ which for small Γ reduces to the Debye–Hückel solution $\lim_{\Gamma \rightarrow 0} \psi_{\text{DH}}(x, \Gamma) = \exp(-x\sqrt{3\Gamma})$ (which satisfies our boundary conditions). Although it is not excluded that for a finite Γ eq. (A.3) could have another branch of solutions we will consider here only the Debye–Hückel branch, or better its extension to finite Γ values. On this branch we have, by continuity with the DH result, $\psi(x) \geq 0$ and hence from eqs. (A.3) and (A.4) we obtain $\psi''(x) \geq 0$ and $\psi'(x) \leq 0$. This branch corresponds thus to a monotonically decreasing $\psi(x)$ and hence the corresponding $g(r)$ will show no short-range order in contradiction with the MC data. The corresponding results

for the thermodynamics are however in much better shape. Indeed from eq. (A.5) we obtain for the Debye–Hückel branch:

$$0 \leq \psi(x) \leq 1 + x\psi'(0) + \frac{1}{2}x^3. \quad (\text{A.7})$$

The minimum of $1 + x\psi'(0) + \frac{1}{2}x^3$ occurs at $x_0 = (-\frac{2}{3}\psi'(0))^{1/2}$ and equals $1 - x_0$ which according to eq. (A.5) is still positive. From $1 - x_0 \geq 0$ we obtain $-\frac{3}{2} \leq \psi'(0) \leq 0$ or using eq. (A.6):

$$-\frac{3}{4}\Gamma \leq \frac{\beta}{N}(U - U^0) \leq 0 \quad (\text{A.8})$$

which is not too far from the Lieb–Narnhofer lower bound of eq. (2.17). Similarly, solving eq. (A.5) numerically one obtains from eq. (A.6) results which compare with the MC data for $(\beta/N)(U - U^0)$ to within twenty percent up to $\Gamma = 100$.

Appendix 3: Chemical potential in the HNC approximation

In this appendix we prove eq. (3.73) which is valid in the framework of HNC theory. From a standard coupling constant integration, the excess chemical potential of an ion is given by [3.65]:

$$\beta\mu^{\text{ex}} = n \int_0^1 d\lambda \int dr \beta v(r) h(r; \lambda) \quad (\text{A.3.1})$$

where $h(r; \lambda)$ is the pair correlation function between a single “test particle” and the ions of the fluid; the test particle interacts with the ions via the potential $\lambda v(r) = \lambda Z^2 e^2 / r$, with $0 \leq \lambda \leq 1$. Note that $h(r)$ replaces here the usual $g(r)$ to account for the background interaction. If we define the function $\gamma(r)$ through:

$$h(r; \lambda) = \exp \{-\lambda\beta v(r) + \gamma(r; \lambda)\} - 1 \quad (\text{A.3.2})$$

we obtain upon differentiation with respect to λ :

$$\beta v(r) h(r; \lambda) = -\frac{\partial}{\partial \lambda} h(r; \lambda) + \frac{\partial}{\partial \lambda} \gamma(r; \lambda) - \beta v(r) + h(r; \lambda) \frac{\partial}{\partial \lambda} \gamma(r; \lambda). \quad (\text{A.3.3})$$

Upon replacing eq. (A3.3) in eq. (A3.1), we can immediately perform the integration over λ for the first three terms on the r.h.s. of eq. (A3.3), and we are left with the exact relation

$$\beta\mu^{\text{ex}} = n \int dr [\gamma(r) - h(r) - \beta v(r)] + n \int_0^1 d\lambda \int dr h(r; \lambda) \frac{\partial}{\partial \lambda} \gamma(r; \lambda) \quad (\text{A.3.4})$$

where $h(r) \equiv h(r; \lambda = 1)$ and $\gamma(r) \equiv \gamma(r; \lambda = 1)$.

The second term on the r.h.s. of eq. (A3.4) can also be integrated over λ if we make the HNC approximation (3.67), according to which

$$\gamma(r; \lambda) = h(r; \lambda) - c(r; \lambda) \equiv N(r; \lambda). \quad (\text{A.3.5})$$

From the OZ equation (3.17) adapted to the present case and from eq. (A3.5) we derive the following relation in Fourier space:

$$\gamma(k; \lambda) = n h(k; \lambda) [h(k) - \gamma(k)]. \quad (\text{A3.6})$$

The second term on the r.h.s. of eq. (A3.4) then becomes, upon using Parseval's theorem and eq. (A3.6):

$$\begin{aligned} & n \int_0^1 d\lambda \int \frac{d\mathbf{k}}{8\pi^3} h(k; \lambda) \frac{\partial}{\partial \lambda} \gamma(k, \lambda) \\ &= n^2 \int \frac{d\mathbf{k}}{8\pi^3} \int_0^1 d\lambda h(k; \lambda) \frac{\partial}{\partial \lambda} \{h(k; \lambda) [h(k) - \gamma(k)]\} \\ &= \frac{n^2}{2} \int \frac{d\mathbf{k}}{8\pi^3} \int_0^1 d\lambda \frac{\partial}{\partial \lambda} \{h^2(k; \lambda) [h(k) - \gamma(k)]\} \\ &= \frac{n}{2} \int \frac{d\mathbf{k}}{8\pi^3} h(k) \gamma(k) \\ &= \frac{n}{2} \int dr h(r) \gamma(r). \end{aligned} \quad (\text{A3.7})$$

Gathering results, remembering the definition (3.27) of $c^R(k)$ and returning to reduced units ($x = r/a$, $na^3 = 3/4\pi$) we recover eq. (3.73).

References

- [1.1] N.H. March and M.P. Tosi, *Atomic Dynamics in Liquids* (Macmillan, London, 1976).
- [1.2] J.P. Hansen and I.R. McDonald, *Theory of Simple Liquids* (Academic Press, London, 1976).
- [1.3] D. Forster, *Hydrodynamic Fluctuations, Broken Symmetry and Correlation Functions* (Benjamin, Reading, Massachusetts, 1975).
- [1.4] S. Ichimaru, *Basic Principles of Plasma Physics* (Benjamin, Reading, Massachusetts, 1973).
- [1.5] G. Kalman, ed., *Strongly Coupled Plasmas* (Plenum Press, New York, 1978).
- [1.6] H.M. Van Horn, in: *White Dwarfs*, ed. W. Luyten (Dordrecht, Reidel, 1971).
- [1.7] D. Pines and P. Nozieres, *The Theory of Quantum Liquids*, Vol. 1 (Benjamin, New York, 1966).
- [1.8] M.M. Cole, *Rev. Mod. Phys.* 46 (1974) 451.
- [1.9] C.W. Outhwaite, in: *Statistical Mechanics*, Vol. 2, ed. K. Singer (The Chemical Society, London, 1975).
- [1.10] M. Parrinello and M.P. Tosi, *Riv. Nuovo Cim.* 2 (1979) no. 6.
- [1.11] *Superionic Conductors*, eds. G.D. Mahan and W.L. Roth (Plenum Press, New York, 1976).
- [1.12] J.H. Malmberg and T.M. O'Neil, *Phys. Rev. Letters* 39 (1977) 1333.
- [2.1] D. Ruelle, *Statistical Mechanics* (Benjamin, New York, 1969).
- [2.2] A. Lenard and F.J. Dyson, *J. Math. Phys.* 9 (1968) 698.
- [2.3] E.H. Lieb, *Rev. Mod. Phys.* 48 (1976) 553.
- [2.4] E.H. Lieb and H. Narhofer, *J. Stat. Phys.* 12 (1975) 291; *J. Stat. Phys.* 14 (1976) 465.
- [2.5] L. Onsager, *J. Phys. Chem.* 43 (1939) 189.
- [2.6] R.R. Sari and D. Merlini, *J. Stat. Phys.* 14 (1976) 91.
- [2.7] J.L. Lebowitz and E.H. Lieb, *Phys. Rev. Lett.* 22 (1969) 631.
- [2.8] R.A. Coldwell-Horsfall and A.A. Maradudin, *J. Math. Phys.* 1 (1960) 395.

- [2.9] N.D. Mermin, Phys. Rev. 171 (1968) 272.
- [2.10] Ph. Choquard, in: [1.5].
- [2.11] E.E. Salpeter, Austr. J. Phys. 7 (1954) 353.
- [2.12] L.L. Foldy, Phys. Rev. B17 (1978) 4289.
- [3.1] See e.g. [1.2].
- [3.2] See e.g. W.G. Hoover, S.G. Gray and K.W. Johnson, J. Chem. Phys. 55 (1971) 1128.
- [3.3] See e.g. [1.7].
- [3.4] M.C. Abram and M.P. Tosi, Nuovo Cimento 10B (1972) 21.
- [3.5] M. Baus, Physica 79A (1975) 377.
- [3.6] G. Stell, in: Statistical Mechanics, Part A, ed. B.J. Berne (Plenum Press, New York, 1977).
- [3.7] M. Baus, J. Phys. A11 (1978) 2451.
- [3.8] F.H. Stillinger and R. Lovett, J. Chem. Phys. 49 (1968) 1991.
- [3.9] P. Vieillefosse and J.P. Hansen, Phys. Rev. A12 (1975) 1106.
- [3.10] H.E. De Witt, H.C. Grabske and M.C. Cooper, Astrophys. J. 181 (1973) 439.
- [3.11] B. Jancovici, J. Stat. Phys. 17 (1977) 537.
- [3.12] N. Itoh, H. Totsuji and S. Ichimaru, Astrophys. J. 218 (1977) 477.
- [3.13] N. Itoh and S. Ichimaru, Phys. Rev. A16 (1977) 2178.
- [3.14] N. Metropolis, A.W. Rosenbluth, M.N. Rosenbluth, A.H. Teller and E. Teller, J. Chem. Phys. 21 (1953) 1087.
- [3.15] B.J. Alder and T.E. Wainwright, J. Chem. Phys. 31 (1959) 459.
- [3.16] W.W. Wood, in: Physics of Simple Liquids, eds. H.N.V. Temperley, J.S. Rowlinson and G.S. Rushbrooke (North-Holland, Amsterdam, 1968);
J.P. Valleau and S.G. Whittington, in: Statistical Mechanics, Part A, ed. B.J. Berne (Plenum Press, New York, 1977);
K. Binder, in: Monte Carlo Methods, ed. K. Binder (Springer, Berlin, 1978);
See also chapter 3 of [1.2].
- [3.17] S.G. Brush, H.L. Sahlin and E. Teller, J. Chem. Phys. 45 (1966) 2102.
- [3.18] A.A. Barker, Australian J. Phys. 18 (1965) 119.
- [3.19] P.P. Ewald, Ann. Physik 64 (1921) 253;
B.R.A. Nijboer and F.W. De Wette, Physica 23 (1957) 309.
- [3.20] J.P. Hansen, Phys. Rev. A8 (1973) 3096.
- [3.21] D.M. Ceperley and G.V. Chester, Phys. Rev. A15 (1977) 755.
- [3.22] F. Lado, Phys. Rev. A8 (1973) 2548.
- [3.23] E.L. Pollock and J.P. Hansen, Phys. Rev. A8 (1973) 3110.
- [3.24] H.E. De Witt, Phys. Rev. A14 (1976) 1290.
- [3.25] S. Galam and J.P. Hansen, Phys. Rev. A14 (1976) 816.
- [3.26] J.P. Hansen and D. Schiff, Mol. Phys. 25 (1973) 1281.
- [3.27] P. Debye and E. Hückel, Physik. Z. 24 (1923) 185 and 305.
- [3.28] L.D. Landau and E.M. Lifshitz, Statistical Physics (Pergamon Press, London, 1958).
- [3.29] See e.g. Y. Pomeau and P. Résibois, Physics Report 19 (1975) 63.
- [3.30] R. Abe, Progr. Theor. Phys. 22 (1959) 213.
- [3.31] C. Deutsch, Y. Furutani and M.M. Gombert, to be published.
- [3.32] E.G.D. Cohen and T.J. Murphy, Phys. Fluids 12 (1969) 1404.
- [3.33] For a review see T.J. Lie and Y.H. Ichikawa, Rev. Mod. Phys. 38 (1966) 680.
- [3.34] F. Del Rio and H.E. De Witt, Phys. Fluids 12 (1969) 791.
- [3.35] C. Deutsch, Y. Furutani and M.M. Gombert, Phys. Rev. A13 (1976) 2244.
- [3.36] P. Choquard and R.R. Sari, Phys. Lett. 40A (1972) 109.
- [3.37] J. Hubbard, Proc. Roy. Soc. A243 (1957) 336.
- [3.38] J. Hubbard, Phys. Lett. 25A (1967) 709.
- [3.39] K.S. Singwi, M.P. Tosi, R.H. Land and A. Sjölander, Phys. Rev. 176 (1968) 589.
- [3.40] K.S. Singwi, A. Sjölander, M.P. Tosi and R.H. Land, Phys. Rev. B1 (1970) 1044.
- [3.41] K.F. Berggren, Phys. Rev. A1 (1970) 1783.
- [3.42] T. Schneider, Physica 52 (1971) 481.
- [3.43] P. Vashista and K.S. Singwi, Phys. Rev. B6 (1972) 875.
- [3.44] S. Ichimaru, Phys. Rev. A2 (1970) 494.
- [3.45] H. Totsuji and S. Ichimaru, Progr. Theor. Phys. 50 (1973) 753; 52 (1974) 42.
- [3.46] M.C. Abram and M.P. Tosi, Nuovo Cimento 10B (1972) 21; 21B (1974) 363.
- [3.47] K.I. Golden, G. Kalman and M.B. Silevitch, Phys. Rev. Lett. 33 (1974) 1544.
- [3.48] K.I. Golden and M.B. Silevitch, Nuovo Cimento 4B (1971) 27.
- [3.49] G. Kalman, in: [1.5].

- [3.50] C.W. Hirt, *Phys. Fluids* 10 (1967) 565.
- [3.51] D.D. Carley, *Phys. Rev.* 131 (1963) 1406; *J. Chem. Phys.* 43 (1965) 3489.
- [3.52] J.F. Springer, M.A. Pokrant and F.A. Stevens Jr., *J. Chem. Phys.* 58 (1973) 4863.
- [3.53] K.C. Ng, *J. Chem. Phys.* 61 (1974) 2680.
- [3.54] M.S. Cooper, *Phys. Rev.* A7 (1973) 1.
- [3.55] M. Baus and J.P. Hansen, *J. Phys.* C12 (1979) L55.
- [3.56] P. Choquard, in: [1.5].
- [3.57] T. Morita and K. Hiroike, *Progr. Theor. Phys.* 23 (1960) 1003; L. Verlet and D. Levesque, *Physica* 28 (1962) 1124.
- [3.58] Y. Rosenfeld and N.W. Ashcroft, *Phys. Rev.* A20 (1979) 1208.
- [3.59] M.J. Gillan, *J. Phys.* C7 (1974) L1.
- [3.60] A. Maradudin, E.W. Montroll, G.H. Weiss and I.P. Ipatova, *Theory of Lattice Dynamics* (Academic Press, New York, 1971).
- [3.61] W.J. Carr, *Phys. Rev.* 122 (1961) 1437.
- [3.62] W.J. Carr, R.A. Coldwell-Horsfall and A.E. Fein, *Phys. Rev.* 124 (1961) 747.
- [3.63] A.E. Kugler, *Ann. Phys.* 53 (1969) 133.
- [3.64] J.P. Hansen, B. Jancovici and D. Schiff, *Phys. Rev. Lett.* 29 (1972) 991.
- [3.65] See e.g. T.L. Hill, *Statistical Mechanics* (McGraw-Hill, New York, 1956).
- [4.1] M.S. Jhon and D. Forster, *Phys. Rev.* A12 (1975) 254.
- [4.2] E.P. Gross, *J. Stat. Phys.* 11 (1974) 503; see also K.D. Bergeron and E.P. Gross, *J. Stat. Phys.* 13 (1975) 85.
- [4.3] A.Z. Akcasu and J.J. Duderstadt, *Phys. Rev.* 188 (1969) 479; see also E.J. Linnebur and J.J. Duderstadt, *Phys. Fluids* 16 (1973) 665.
- [4.4] D. Forster and P.C. Martin, *Phys. Rev.* A2 (1970) 1575; see also D. Forster, *Phys. Rev.* A9 (1974) 943.
- [4.5] G.F. Mazenko, *Phys. Rev.* A7 (1973) 209, 222 and 360; see also J.I. Castresana, G.F. Mazenko and S. Yip, *Ann. Physics* 103 (1977) 1.
- [4.6] M. Baus, *Physica* 79A (1975) 377, *Physica* 88A (1977) 319, 336 and 591.
- [4.7] S. Ichimaru, H. Totuji, T. Tange and D. Pines, *Progr. Theoret. Phys.* 54 (1975) 1077; see also [4.21].
- [4.8] H.B. Singh, A. Sharma and K.N. Pathak, *Phys. Rev.* A19 (1979) 899.
- [4.9] P. Résibois and M. De Leener, *Classical Kinetic Theory of Fluids* (Wiley-Interscience, New York, 1977) chap. 4.
- [4.10] R. Balescu, *Equilibrium and Non-equilibrium Statistical Mechanics* (Wiley-Interscience, New York, 1975) chap. 12.
- [4.11] M. Baus and J. Wallenborn, *J. Stat. Phys.* 16 (1977) 91.
- [4.12] M. Baus, *Phys. Rev.* A15 (1977) 790.
- [4.13] L. Verlet, *Phys. Rev.* 159 (1967) 98.
- [4.14] J.P. Hansen, I.R. McDonald and E.L. Pollock, *Phys. Rev.* A11 (1975) 1025; *Phys. Rev. Lett.* 32 (1974) 277.
- [4.15] B. Bernu and P. Vieillefosse, *Phys. Rev.* A18 (1978) 2345; B. Bernu, P. Vieillefosse and J.P. Hansen, *Phys. Lett.* 63A (1977) 301.
- [4.16] B. Bernu, *J. Stat. Phys.* (in press).
- [4.17] J.P. Hansen and I.R. McDonald, *Phys. Rev. Lett.* 41 (1978) 1379.
- [4.18] H. Mori, *Progr. Theor. Phys.* 33 (1965) 423; 34 (1965) 399.
- [4.19] S.W. Lovesey, *J. Phys.* C4 (1971) 3057.
- [4.20] M.C. Abramo and M. Parrinello, *Lett. Nuovo Cim.* 12 (1975) 667.
- [4.21] S. Ichimaru and T. Tange, *Phys. Rev. Lett.* 32 (1974) 102.
- [4.22] M.C. Abramo and M.P. Tosi, *Nuov. Cim.* 21B (1974) 363.
- [4.23] S. Ichimaru, *Phys. Rev.* A2 (1970) 494.
- [4.24] S. Ichimaru, *Phys. Rev.* A15 (1977) 744 and [1.5].
- [4.25] A.A. Kugler, *J. Stat. Phys.* 12 (1975) 35.
- [4.26] K.I. Golden, G. Kalman and M.B. Silevich, *Phys. Rev. Lett.* 33 (1974) 1544.
- [4.27] K.I. Golden and G. Kalman, *Phys. Rev.* A19 (1979) 2112.
- [4.28] K.N. Pathak and K.S. Singwi, *Phys. Rev.* A2 (1970) 2427.
- [4.29] J. Bosse, W. Götzte and M. Lücke, *Phys. Rev.* A17 (1978) 434.
- [4.30] J. Bosse and K. Kubo, *Phys. Rev. Lett.* 40 (1978) 1660; *Phys. Rev.* A18 (1978) 2337.
- [4.31] H. Gould and G.F. Mazenko, *Phys. Rev. Lett.* 35 (1975) 1455; *Phys. Rev.* A15 (1977) 1274.
- [4.32] T. Gaskell and O. Chiakwelu, *J. Phys.* C10 (1977) 2021.
- [4.33] O. Chiakwelu, *J. Phys.* C11 (1978) 3743.
- [4.34] S. Sjödin and S.K. Mitra, *J. Phys.* A10 (1977) L163; *J. Phys.* C11 (1978) 2655.
- [4.35] J. Wallenborn and M. Baus, *Phys. Lett.* 61A (1977) 35; *Phys. Rev.* A18 (1978) 1737.

- [4.36] G.F. Mazenko, Phys. Rev. A9 (1974) 360.
- [4.37] M. Lindenfeld, Phys. Rev. A15 (1977) 1801.
- [4.38] L. Sjögren and A. Sjölander, Ann. Phys. 110 (1978) 122.
- [4.39] M. Baus and J. Wallenborn, Phys. Lett. 55A (1975) 90; J. Stat. Phys. 16 (1977) 91.
- [4.40] P.V. Giaquinta, M. Parrinello, M.P. Tosi and N.H. March, Phys. and Chem. Liq. 5 (1976) 197.
- [4.41] R.L. Varley, Phys. Lett. 62A (1977) 340.
- [5.1] E.E. Salpeter and H.M. Van Horn, Astrophys. J. 155 (1969) 183.
- [5.2] A. Alastuey and B. Jancovici, Astrophys. J. (in press).
- [5.3] E. Wigner, Phys. Rev. 40 (1932) 749;
- J.G. Kirkwood, Phys. Rev. 44 (1933) 31; 45 (1934) 116.
- [5.4] J.P. Hansen and P. Vieillefosse, Phys. Lett. 53A (1975) 187.
- [5.5] W.B. Hubbard and W.L. Slattery, Astrophys. J. 168 (1971) 131.
- [5.6] J. Hammerberg and N.W. Ashcroft, Phys. Rev. B9 (1974) 409.
- [5.7] H.E. De Witt and W.B. Hubbard, Astrophys. J. 205 (1976) 295.
- [5.8] J.P. Hansen, J. Phys. (Paris) 36 (1975) L133.
- [5.9] M. Ross and D. Seale, Phys. Rev. A9 (1974) 396.
- [5.10] D. Stroud and N.W. Ashcroft, Phys. Rev. A13 (1976) 1660.
- [5.11] See [3.26].
- [5.12] H. Minoo, C. Deutsch and J.P. Hansen, Phys. Rev. A14 (1976) 840;
H. Minoo, J.P. Hansen and C. Deutsch, J. Phys. (Paris) 38 (1977) L191.
- [5.13] A. Alastuey and B. Jancovici, to be published.
- [5.14] J.M. Ziman, Phil. Mag. 6 (1961) 1013.
- [5.15] C. Deutsch and M. Lavaud, Phys. Rev. A9 (1974) 2598.
- [5.16] C. Deutsch, J. Math. Phys. 17 (1976) 1404.
- [5.17] R.R. Sari, D. Merlini and R. Calinon, J. Phys. A9 (1976) 1539.
- [5.18] R. Calinon, K.I. Golden, G. Kalman and D. Merlini, Phys. Rev. A20 (1979) 329, 336.
- [5.19] C.C. Grimes and G. Adams, Phys. Rev. Lett. 36 (1976) 145.
- [5.20] C.L. Zipfel, T.R. Brown and C.C. Grimes, Phys. Rev. Lett. 37 (1976) 1760.
- [5.21] R.W. Hockney and T.R. Brown, J. Phys. C8 (1975) 1813.
- [5.22] H. Totsuji, Phys. Rev. A17 (1978) 399.
- [5.23] R.C. Gann, S. Chakravarty and G.V. Chester, Phys. Rev. B20 (1979) 326.
- [5.24] A.L. Fetter, Phys. Rev. B10 (1974) 3739.
- [5.25] P.M. Platzman and N. Tzoar, Phys. Rev. B13 (1976) 3197.
- [5.26] J. Chalupa, Phys. Rev. B12 (1975) 4; B13 (1976) 2243.
- [5.27] H. Totsuji, J. Phys. Soc. Japan 39 (1975) 253; 40 (1976) 857.
- [5.28] H. Totsuji, Memoirs of School of Engineering, Okayama University 12 (1978) 89.
- [5.29] N. Itoh, S. Ichimaru and S. Nagano, Phys. Rev. B17 (1978) 2862.
- [5.30] F. Lado, Phys. Rev. B17 (1978) 2827.
- [5.31] R.S. Crandall, Phys. Rev. A8 (1973) 2136.
- [5.32] D.J. Thouless, J. Phys. C11 (1978) L189.
- [5.33] T. Nagai and A. Onuki, J. Phys. C11 (1978) L681.
- [5.34] A. Onuki, J. Phys. Soc. Japan 43 (1977) 396.
- [5.35] M. Baus, J. Stat. Phys. 19 (1978) 163;
see also M. Baus, Annals Israel Phys. Soc. 2 (1978) 652.
- [5.36] See e.g. D.L. Bowers and E.E. Salpeter, Phys. Rev. 119 (1960) 1180.
- [5.37] N.D. Mermin, Phys. Rev. 176 (1968) 250.
- [5.38] M. Baus, J. Stat. Phys. (in press).
- [5.39] H. Kosterlitz and D.J. Thouless, J. Phys. C6 (1973) 1181.
- [5.40] A.P. Volodin, M.S. Khaikin and V.S. Edelman, JETP Lett. 26 (1977) 543.
- [5.41] S. Nagano, H. Totsuji, N. Itoh and S. Ichimaru, to be published.
- [5.42] T. Dunn and A.A. Broyles, Phys. Rev. 157 (1967) 156;
C. Deutsch and M.M. Gombert, J. Math. Phys. 17 (1976) 1077.
- [5.43] F.J. Dyson, Ann. Phys. (N.Y.) 63 (1971) 1.
- [5.44] M. Baus, Phys. Rev. A16 (1977) 2493.
- [5.45] J.P. Hansen and P. Vieillefosse, Phys. Rev. Lett. 37 (1976) 391.
- [5.46] J.P. Hansen, G.M. Torrie and P. Vieillefosse, Phys. Rev. A16 (1977) 2153.
- [5.47] B. Brami, J.P. Hansen and F. Joly, Physica 95A (1979) 505.
- [5.48] H.E. De Witt and F.J. Rodgers, UCRL report 50028-76-1 (1976).

- [5.49] E.L. Pollock and B.J. Alder, Phys. Rev. A15 (1977) 1263.
- [5.50] D.J. Stevenson, Phys. Rev. B12 (1975) 3999.
- [5.51] B. Firey and N.W. Ashcroft, Phys. Rev. A15 (1977) 2072.
- [5.52] D.J. Stevenson, Phys. Lett. 58A (1976) 282.
- [5.53] D.M. Straus, N.W. Ashcroft and H. Beck, Phys. Rev. B15 (1977) 1914.
- [5.54] D.J. Stevenson and E.E. Salpeter, Astrophys. J. Suppl. 35 (1977) 221.
- [5.55] E.L. Pollock and B.J. Alder, Nature 275 (1978) 41.
- [5.56] M. Baus, Physica 88A (1977) 319, 336 and 591.
- [5.57] I.R. McDonald, P. Vieillefosse and J.P. Hansen, Phys. Rev. Lett. 39 (1977) 271.
- [5.58] M. Baus, Phys. Rev. Lett. 40 (1978) 793.
- [5.59] M. Baus, in: [1.5].
- [5.60] J.P. Hansen, I.R. McDonald and P. Vieillefosse, Phys. Rev. A (in press).
- [5.61] J.P. Hansen and J.J. Weis, Mol. Phys. 33 (1977) 1379.
- [5.62] J.L. Lebowitz and J. Percus, Phys. Rev. 144 (1966) 251.
- [5.63] See e.g. chapter 5 of [1.2].
- [5.64] R.G. Palmer and J.D. Weeks, J. Chem. Phys. 58 (1973) 4171.
- [5.65] M.S. Wertheim, Phys. Rev. Lett. 10 (1963) 321; J. Math. Phys. 5 (1964) 643.
- [5.66] E. Thiele, J. Chem. Phys. 39 (1963) 474.
- [5.67] F. Lado, Phys. Rev. A8 (1973) 2548.
- [5.68] F. Lado, Mol. Phys. 31 (1976) 1117.
- [5.69] F. Lado, Phys. Rev. 135 (1964) A1013.
- [5.70] H.C. Andersen, D. Chandler and J.D. Weeks, J. Chem. Phys. 56 (1972) 3812; H.C. Andersen and D. Chandler, J. Chem. Phys. 57 (1972) 1918.
- [5.71] H.E. De Witt, in: [1.5].
- [5.72] Y. Rosenfeld and N.W. Ashcroft, to be published.
- [5.73] E. Waisman and J.L. Lebowitz, J. Chem. Phys. 56 (1972) 3086; 56 (1972) 3093.
- [5.74] D.N. Card and J.P. Valleau, J. Chem. Phys. 52 (1970) 6232.
- [5.75] P.N. Vorontsov-Vel'yaminov and M. El'yashevich, Elektrokhimiya 4 (1968) 1430; B.P. Chasovskikh and P.N. Vorontsov-Vel'yaminov, Teplofizika Vysokikh Temperatur 14 (1976) 199.
- [5.76] B. Larsen, J. Chem. Phys. 65 (1976) 3431.
- [5.77] L. Blum, Mol. Phys. 30 (1975) 1529.
- [5.78] J.S. Hoyer, J.L. Lebowitz and G. Stell, J. Chem. Phys. 61 (1974) 3253.
- [5.79] E. Waisman, Mol. Phys. 25 (1973) 45.
- [5.80] G. Stell and S.F. Sun, J. Chem. Phys. 63 (1975) 5333.
- [5.81] J.S. Hoyer and G. Stell, J. Chem. Phys. 67 (1977) 524; B. Larsen, G. Stell and K.C. Wu, J. Chem. Phys. 67 (1977) 530.
- [5.82] J.C. Rasaiah and H.L. Friedman, J. Chem. Phys. 48 (1968) 2742; 50 (1969) 3965.
- [5.83] B. Larsen, J. Chem. Phys. 68 (1978) 4511.
- [5.84] J.C. Rasaiah, D.V. Card and J.P. Valleau, J. Chem. Phys. 56 (1972) 248.
- [5.85] J.C. Rasaiah, J. Chem. Phys. 56 (1972) 3071.
- [5.86] D. Elkoubi, P. Turq and J.P. Hansen, Chem. Phys. Lett. 52 (1977) 493.
- [5.87] H.C. Andersen, D. Chandler and J.D. Weeks, J. Chem. Phys. 57 (1972) 2626.
- [5.88] P.N. Vorontsov-Vel'yaminov, A.M. El'yashevich, L.A. Morgenshtern and V.P. Chasovskikh, Teplofizika Vysokikh Temperatur 8 (1970) 277.
- [5.89] G. Stell, K.C. Wu and B. Larsen, Phys. Rev. Lett. 37 (1976) 1369.
- [5.90] M.J.L. Sangster and M. Dixon, Advances in Physics 25 (1976) 247.
- [5.91] L.V. Woodcock and K. Singer, Trans. Faraday Soc. 67 (1971) 12.
- [5.92] J.P. Hansen and I.R. McDonald, Phys. Rev. A11 (1975) 2111.
- [5.93] P.V. Giaquinta, M. Parrinello, W. Bouche and M.P. Tosi, Lett. Nuovo Cim. 19 (1977) 215.
- [5.94] P.V. Giaquinta, M. Parrinello and M.P. Tosi, Phys. Chem. Liquids 5 (1976) 305; Physica 92A (1978) 185.
- [5.95] P. Vieillefosse, J. de Physique Lettres 38 (1977) L43.
- [5.96] P.C. Martin, Phys. Rev. 161 (1967) 143.
- [5.97] G. Ciccotti, G. Jacucci and I.R. McDonald, Phys. Rev. A13 (1976) 426.
- [5.98] G. Jacucci, I.R. McDonald and A. Rahman, Phys. Rev. A13 (1976) 1581.
- [5.99] A. Rahman, J. Chem. Phys. 65 (1976) 4845.
- [5.100] P. Vashista and A. Rahman, Phys. Rev. Lett. 40 (1978) 1337.
- [5.101] See e.g. R.A. Grandey, in: [1.5].

- [5.102] T. Morita, Progr. Theor. Phys. 21 (1959) 501;
A.A. Barker, J. Chem. Phys. 55 (1971) 1751;
M. Pokrant, A.A. Broyles and T. Dunn, Phys. Rev. A10 (1974) 379;
C. Deutsch, Phys. Lett. 60A (1977) 317.
- [5.103] H. Gould, R.G. Palmer and G.E. Estévez, J. Stat. Phys. 21 (1979) 55.